Identification and Characterisation of the Type VI Secretion System in *Rhodobacter sphaeroides*



Kathryn E. Potter
St Hugh's College

A thesis submitted for the degree of *Doctor of Philosophy*
Trinity Term 2021

Dedication

To my Nanna

"If nothing is going well, call your Grandmother." - Italian Proverb

Abstract

The type VI secretion system (T6SS) is a versatile multi-component nanomachine found in 25% of Gram-negative bacteria. It translocates effector proteins into neighbouring eukaryotic or prokaryotic cells, and therefore it is important for bacterial virulence, as well as interbacterial competition. Although initially T6SSs were considered to be primarily contact-dependent weapons deployed during bacterial warfare, recently T6SSs that secrete effector proteins to sequester common goods from the environment have also been identified. Characterised examples of such systems play a role in the uptake of zinc, manganese, iron, copper and molybdate ions. The mechanism behind T6SS-dependent metal ion acquisition involves secretion of a metal-binding protein which sequesters metal ions from the extracellular milieu. The subsequent steps by which cells uptake the sequestered metal ions remain largely elusive, nonetheless it it is known that, in some cases, interaction of the secreted protein with a TonB-dependent outer membrane transporter is required.

Here we report the previously uncharacterised T6SS of *Rhodobacter sphaeroides* WS8N. By performing bioinformatic analyses on the putative T6SS cluster we find that it encodes all 13 core T6SS proteins along with four proteins known to be involved in T6SS regulation (TagE-H), the T6SS tip sharpening protein PAAR, the peptidoglycan-binding protein TagL and an additional seven hypothetical proteins. We also find the presence of a T6SS to be strain, and not species, specific in the Rhodobacteraceae family of proteobacteria.

Further, we investigated the conditions under which the the T6SS of *R. sphaeroides* WS8N is active and demonstrate that, its function is required for photoheterotrophic growth under iron-limited conditions. In particular, presence of this T6SS allows growth of *R. sphaeroides* WS8N in limited amounts of both Fe^{2+} and Fe^{3+}, but does not support growth in iron-depleted media supplemented with heme. Finally, we performed preliminary biochemical studies of the C-terminal extension of VgrG, which showed the potential to bind iron. This suggests that VgrG might be the secreted protein facilitating the T6SS-dependent uptake of iron.

The data presented in this study represents the first characterisation of a T6SS from the Rhodobacteraceae family of proteobacteria, informing us on the role of this system in a class of organisms that heavily depend on the use of iron for their growth.

Acknowledgements

Firstly, I would like to thank Dr Despoina Mavridou for providing the supervision, guidance and opportunities that were essential for the completion of this work. It was under her guidance that this project came into its own. I am endlessly grateful for her advice and support and it is not an exaggeration to say that I would not have gotten through this without her. Although the best remote supervisor a student could ask for, I very much look forward to working with her at the University of Texas at Austin.

I am indescribably grateful to Prof. Kevin Foster for his guidance and support. He adopted me into a welcoming and motivated lab environment when my original supervision became precarious. Thank you for the catch (climbing pun intended)! I'd also like to thank members of the Foster lab for occasional advice and frequent laughs, especially Olivier Cunrath, Sean Booth and Jacob Palmer for the former and Thomas Meiller-Legrand, Frances Spragge and Signe Lagercrantz for the latter.

I want to thank Dr George Wadhams and Prof. Judith Armitage for introducing me to my favourite pink critter, *Rhodobacter sphaeroides*, they provided me with the invaluable foundation upon which this thesis was built. I'd like to extend my thanks to Dr Chris Jones and Dr Nicolas Delalez whose constant presence during my first year in the lab made the transition from undergraduate to DPhil student less intimidating, a little too fun and whose initial centrifuge supervision avoided many a disaster. I'd also like to thank past and present members of the adjacent Berks lab, namely Dr Felicity Alcock, Dr Sam Hickman and Dr Jad Sassine, for lending a hand with all things protein related. I'd like to express my thanks to Dr Chris Furniss for his generous help with protein expression and purification.

I'd like to thank Prof. Gail Preston for her wisdom and making life much easier on multiple occasions; I am grateful to have been part of the Doctoral Training Centre. I'd also like to extend my thanks to the BBSRC and the EPSRC who so generously funded my DPhil studies.

I'd like to thank Hannah, Ellen, Jamie, Astrid and Kate, they know what for. Your friendship has known no bounds and I could not have asked for a better support network. It would not be right to submit this thesis without also mentioning Maisie R, Maisie V, Annie and Rachel. While I'm sure none of my friends could tell you what this thesis is about, their role in its eventual

submission is undeniable.

I am grateful to my family for their continued support, especially my Nanna who has been waiting patiently to tell anyone who will listen that her granddaughter has *finally* submitted her DPhil thesis. I'd like to extend my thanks and my apologies to my Nanna's neighbours, chiropodist, hair dresser, cleaner, window cleaners, gardener and even her MP for listening to the embarrassing praise-singing. The support of my Mum and Dad, while much quieter, was unwavering and wholly necessary, no one makes me better cups of tea. I love you all very much.

Lastly I'd like to express my eternal gratitude to the climbing wall, while it distracted me from my studies at times, it taught me balance, and without it, my sanity would be much less intact.

Abbreviations

BLAST	Basic Local Alignment Search Tool
cPCR	colony polymerase chain reaction
DMSO	dimethyl sulfoxide
DNA	deoxyribonucleic acid
h	hour
kb	kilobase
LB	Luria-Bertani
µ	micro
m	milli
min	minute
M	molar
n	nano
NCBI	National Center for Biotechnology Information
OD	optical density
PCR	polymerase chain reaction
rpm	revolutions per minute
s	second
SDS-PAGE	sodium dodecyl sulphate polyacrylamide gel electrophoresis
TBE	tris-borate-EDTA buffer
Tris	tris-(hydroxymethyl) aminomethane
V	Volt
wt	wild type

Contents

1 Introduction **1**

1.1 Bacterial secretion systems 2

1.1.1 Overview of the Type VI Secretion System 3

1.1.2 Structure and firing mechanism of the T6SS 4

1.2 Effector delivery by the T6SS 6

1.2.1 Anti-eukaryotic effectors 10

1.2.2 Anti-bacterial effectors 11

1.2.3 T6SS effectors involved in the acquisition of common goods 13

1.3 T6SS-dependent metal acquisition 13

1.4 The importance of T6SS-dependent metal ion acquisition for bacterial fitness 20

1.5 Bacterial iron acquisition 23

1.6 A brief introduction to *Rhodobacter sphaeroides* 25

1.7 Iron uptake in the *Rhodobacter* genus 27

1.7.1 Ferrous iron uptake 27

1.7.2 Ferric iron uptake 28

1.7.3 Regulation of iron metabolism in *R. sphaeroides* 29

1.8 Project aims 30

2 Materials and Methods **32**

2.1 Strains and plasmids . . . 33

2.2 Growth conditions . . . 33

2.2.1 Antibiotics . . . 33

2.2.2 Growing *E. coli* . . . 35

2.2.3 Growing *R. sphaeroides* . . . 35

2.2.4 Growing *R. sphaeroides* starter cultures for growth assays 35

2.2.5 *R. sphaeroides* growth assay . . . 36

2.2.6 Divalent transition metal-depleted growth assay media . 37

2.3 Genetic techniques . . . 39

2.3.1 Polymerase Chain Reaction (PCR) . . . 39

2.3.2 Purification of plasmid DNA and PCR products . . . 39

2.3.3 Agarose gel electrophoresis . . . 41

2.3.4 Restriction enzyme digests . . . 41

2.3.5 DNA ligation . . . 41

2.3.6 NEB HiFi DNA Assembly . . . 42

2.3.7 Primers used to generate the pET21a-VgrGCTer-twinStrepII protein expression vector . . . 42

2.3.8 Making chemically competent *E. coli* cells . . . 42

2.3.9 Transformation of plasmids into competent *E. coli* cells . 43

2.3.10 Conjugation of plasmids into *R. sphaeroides* . . . 44

2.3.11 Homologous recombination for the generation of *R. sphaeroides* insertion and deletion mutants . . . 44

2.3.12 DNA sequencing . . . 47

2.4 Protein characterisation . . . 48

2.4.1 FLAG-tagged proteins 48
2.4.1.1 Sample preparation for sodium dodecyl sulphate polyacrylamide gel electrophoresis (SDS-PAGE) 48
2.4.1.2 Western Blotting 49
2.4.2 StrepII-tagged proteins 49
2.4.2.1 Sample preparation for SDS-PAGE 49
2.4.2.2 Western Blotting 50
2.4.3 Protein Purification 51
2.5 Hcp Secretion Assay 52
2.5.1 Preparation of supernatant samples 52
2.5.2 Preparation of cell lysate samples 52
2.6 Fluorescence Microscopy 53

3 Bioinformatic analysis of *Rhodobacter sphaeroides* WS8N T6SS 55

3.1 Introduction 56
3.2 Identification of T6SS genetic loci in Rhodobacteraceae 56
3.3 *In silico* analysis of the structural components of 20 T6SS clusters from phylogenetic group i3 62
3.4 *in silico* analysis of the structural components of T6SS clusters across phylogenetic groups 63
3.5 Bioinformatic analysis of the *R. sphaeroides* WS8N VgrG protein 68
3.6 RSWS8N_RS18685 encodes a putative PAAR protein 72
3.7 Bioinformatic analysis of the putative regulatory proteins found in the *R. sphaeroides* WS8N T6SS cluster 72
3.8 RSWS8N_RS18675, RSWS8N_RS18680 and RSWS8N_RS18700 encode putative adaptor proteins 76

3.9 RSWS8N_RS18790 encodes a putative effector protein with peptidase activity 77

3.10 No putative function can be determined for the proteins encoded by RSWS8N_RS18670, RSWS8N_RS18690 and RSWS8N_RS18695 78

3.11 Discussion 80

4 Optimisation of the growth conditions used to assess the phenotypic consequences of deleting the T6SS cluster in *R. sphaeroides* WS8N 84

4.1 Introduction 85

4.2 Construction of *R. sphaeroides* ΔT6SS mutant strain 86

4.3 Optimisation of *R. sphaeroides* growth conditions to assess the phenotypic consequences of deleting the T6SS cluster 91

4.3.1 Testing growth of wild type *R. sphaeroides* WS8N and the ΔT6SS mutant strain in iron-depleted media 93

4.3.1.1 Growth in iron-depleted succinate media with chelated casamino acids, phosphate buffer, growth factor and MilliQ water 93

4.3.1.2 Growth in iron-free succinate media with chelated casamino acids 96

4.3.2 Optimisation of the culturing conditions of *R. sphaeroides* WS8N to reduce inter-replicate variability 101

4.3.2.1 Use of 72 h starter cultures grown directly from frozen glycerol stocks improves the inter-replicate variation 103

4.3.2.2 Use of 72 h starter cultures inoculated with multiple colonies grown on LB agar is best practice for the reduction of inter-replicate variation 105

4.3.2.3 Use of 72 h starter cultures inoculated with a single colony grown on LB agar does not improve the inter-replicate variability as compared to using multiple colonies for inoculation 109

4.3.3 Overview of the inter-replicate variability after the different optimisation steps taken in this chapter 111

4.3.4 Discussion 113

5 The T6SS of *R. sphaeroides* WS8N has a role in ferrous and ferric iron acquisition under iron limiting conditions 116

5.1 Introduction 117

5.2 Growth of wild-type *R. sphaeroides* WS8N and of its ΔT6SS mutant strain under normal laboratory conditions 119

5.2.1 There is no difference between the growth profiles of wild-type *R. sphaeroides* WS8N and its ΔT6SS mutant under standard laboratory conditions after 48 h of photoheterotrophic growth in regular succinate media 119

5.2.2 There is no difference between the growth profiles of wild-type *R. sphaeroides* WS8N and its ΔT6SS mutant when grown aerobically in regular succinate media 121

5.3 Testing the growth dependence of wild-type *R. sphaeroides* WS8N on divalent transition metal ions 123

5.4 Determining the phenotypic consequence of T6SS absence in divalent-transition-metal-depleted growth conditions 126

5.4.1 There is no difference in growth between wild-type *R. sphaeroides* and its ΔT6SS mutant when grown under zinc-, manganese-, copper- or cobalt-limited conditions 126

5.4.2 The ΔT6SS mutant exhibits a severe growth defect under iron-limited conditions 127

5.5 The T6SS is required for growth under limited iron conditions . 133

5.6 There is no significant difference between the aerobic growth of wild-type *R. sphaeroides* WS8N and its ΔT6SS mutant under iron limitation 139

5.7 The confinement of T6SS activity to photoheterotrophic conditions is supported by existing microarray data 140

5.8 Discussion 142

6 Further investigation of the T6SS apparatus of *R. sphaeroides* WS8N 147

6.1 Introduction 148

6.2 Hcp is expressed under both low- and high- iron conditions . . . 149

6.3 The T6SS hallmark protein Hcp can be detected in the cellular but not extracellular fraction of *R. sphaeroides* WS8N cultures . 150

6.4 T6SS could not be observed *in vivo* under low or high iron conditions 152

6.5 The C-terminus of VgrG shows preliminary evidence of iron-binding capacity 153

6.6 Discussion 158

7 Discussion **162**

8 Appendix **168**

8.1 Media and reagents 169

8.1.1 Luria broth 169

8.1.2 Succinate media 169

8.1.3 1 M Phosphate buffer 169

8.1.4 Concentrated base 169

8.1.5 Metals 44 solution 170

8.1.6 Growth factor 170

8.1.7 5X Amino Acid Supplement 170

8.1.8 M22 171

8.1.9 10X TBE 171

8.1.10 10X SDS Running Buffer 171

8.1.11 10X Vogel-Bonner Medium (VBM) 171

8.2 The complete nucleotide and amino acid sequences of PpFbFP . 171

8.2.1 Nucleotide sequence of PpFbFP (447 bp) 171

8.2.2 Amino acid sequence of PpFbFP(148 aa) 172

List of Figures

1.1 Structure and mechanism of the type VI secretion system. . . . 7

1.2 Modes of effector delivery by the T6SS. 8

1.3 Graphical summary of the mechanisms of the six currently described examples of T6SS-dependent metal ion acquisition. . . . 21

3.1 Genetic organisation of the T6SS operons of *R. sphaeroides* WS8N. 58

3.2 Genetic organisation of the T6SS gene clusters of sequenced Rhodobacteraceae family members 61

3.3 *In silico* analysis of the structural components of *R. sphaeroides* T6SS and comparison with 20 T6SS clusters from the i3 phylogenetic group i3. 64

3.4 Taxonomic distribution of *R. sphaeroides* and of the strains used in the analysis of T6SS clusters of the i3 classification. 65

3.5 *In silico* analysis of the structural components of *R. sphaeroides* T6SS and comparison with 5 T6SS clusters from each of the five phylogenetic groups. 66

3.6 Taxonomic distribution of *R. sphaeroides* and of the strains used in the analysis of T6SS clusters across all type i phylogenetic groups. 67

3.7 Amino acid sequence alignment of VgrG proteins from various organisms. 69
3.8 Graphic representation of the domains predicted to be present in VgrG proteins from various bacteria. 70
3.9 Conserved domain prediction for the VgrG protein of **a** *R. sphaeroides* WS8N and **b** *B. thailandensis* E264. 72
3.10 Conserved domain search for the T6SS regulatory proteins present in the *R. sphaeroides* WS8N T6SS cluster. 73
3.11 Amino acid sequence alignment of the T6SS regulatory protein TagE (PpkA) from various organisms. 74
3.12 Amino acid sequence alignment of the T6SS regulatory protein TagF from various organisms. 75
3.13 Amino acid sequence alignment of the T6SS regulatory protein TagG (PppA) from various organisms. 75
3.14 Amino acid sequence alignment of the T6SS regulatory protein TagH (Fha) from various organisms. 76
3.15 Amino acid sequence alignment of the putative adaptor protein encoded by RSWS8N_RS18700 against VgrG1a from *P. aeruginosa* PAO1. 77
3.16 Phyre2 hit report for homologs of the putative *R. sphaeroides* WS8N T6SS effector protein encoded by RSWS8N_RS18790. . . 79

4.1 DNA sequence of the 500 bp up and downstream flaking regions of the main structural T6SS operon of *R. sphaeroides* WS8N. . 89
4.2 1000 bp insert used for the generation of pK18mobsacB-ΔT6SS 90

4.3 Schematic outlining the overlap extension PCR workflow employed to generate a deletion construct 90
4.4 Genetic organisation of (**a**) *R. sphaeroides* WS8N T6SS and (**b**) *R. sphaeroides* ΔT6SS mutant 91
4.5 Growth of wild-type *R. sphaeroides* WS8N and the ΔT6SS mutant under various $FeCl_3.6H_2O$ concentrations in iron-depleted succinate media (-$FeSO_4.7H_2O$, chelated CAA, GF, PB, MilliQ) 95
4.6 Growth of wild-type *R. sphaeroides* WS8N under various $FeCl_3.6H_2O$ concentrations in iron-depleted succinate media (-$FeSO_4.7H_2O$, chelated CAA, GF, PB, MilliQ water) 97
4.7 Growth of wild-type *R. sphaeroides* WS8N and the ΔT6SS mutant under different $FeCl_3.6H_2O$ concentrations in iron-depleted succinate media (-$FeSO_4.7H_2O$, chelated CAA) 99
4.8 Growth of wild-type *R. sphaeroides* WS8N under various $FeCl_3.6H_2O$ concentrations in iron-depleted succinate media (-$FeSO_4.7H_2O$, chelated CAA) 100
4.9 Schematic of the three starter culture protocols tested in this research 102
4.10 Growth of wild-type *R. sphaeroides* WS8N and its ΔT6SS mutant after 48 h under different $FeCl_3.6H_2O$ concentrations in iron-depleted succinate media (-$FeSO_4.7H_2O$, chelated CAA) from 72 h starter cultures inoculated directly from frozen glycerol stock 104

4.11 Growth of wild-type *R. sphaeroides* WS8N and its ΔT6SS mutant under different $FeCl_3.6H_2O$ concentrations in iron-depleted succinate media (-$FeSO_4.7H_2O$, chelated CAA) from 72 h starter cultures grown from colonies 106

4.12 Growth of wild-type *R. sphaeroides* WS8N in iron-depleted succinate media 107

4.13 Growth of the ΔT6SS mutant under different $FeCl_3.6H_2O$ concentrations in iron-depleted succinate media (-$FeSO_4.7H_2O$, chelated CAA) from 72 h starter cultures grown from single or multiple colonies 110

4.14 Standard deviation of OD_{700} measurements of wild-type *R. sphaeroides* WS8N and of itsΔT6SS mutant after 48 h of growth in regular succinate media or iron-depleted media supplemented with the indicated $FeCl_3.6H_2O$ concentration for each optimisation protocol 112

5.1 Photoheterotrophic growth of wild-type *R. sphaeroides* and its ΔT6SS mutant in regular succinate media 120

5.2 Growth curves of wild-type *R. sphaeroides* WS8N and its ΔT6SS mutant grown aerobically in regular succinate media 122

5.3 Growth rates of wild-type *R. sphaeroides* WS8N and its ΔT6SS mutant when grown aerobically in regular succinate media . . . 123

5.4 The growth dependence of wild-type *R. sphaeroides* WS8N on divalent transition metals 125

5.5 Growth of wild-type *R. sphaeroides* WS8N and its ΔT6SS mutant under different $ZnSO_4.7H_2O$ concentrations in Zn-depleted succinate media 128
5.6 Growth of wild-type *R. sphaeroides* WS8N and its ΔT6SS mutant under different $MnSO_4.4H_2O$ concentrations in manganese-depleted succinate media 129
5.7 Growth of wild-type *R. sphaeroides* WS8N and its ΔT6SS mutant under different $CuSO_4.5H_2O$ concentrations in copper-depleted succinate media 130
5.8 Growth of wild-type *R. sphaeroides* WS8N and its ΔT6SS mutant under different $CoCl_2.6H_2O$ concentrations in cobalt-depleted succinate media 131
5.9 Growth of wild-type *R. sphaeroides* WS8N and itsΔT6SS mutant under different $FeSO_4.7H_2O$ concentrations in iron-depleted succinate media 133
5.10 The growth dependence of wild-type *R. sphaeroides* WS8N on hemin 135
5.11 Growth of wild-type *R. sphaeroides* WS8N and its ΔT6SS mutant in iron-depleted succinate media supplemented with hemin 136
5.12 The growth dependence of wild-type *R. sphaeroides* WS8N on Fe^{3+} 137
5.13 Growth of wild-type *R. sphaeroides* WS8N and its ΔT6SS mutant under different $FeCl_3.6H_2O$ concentrations in iron-depleted succinate media 138

5.14 There is a phenotypic difference between wild-type *R. sphaeroides* and its ΔT6SS mutant when grown in iron-depleted media supplemented with iron in its ferrous and ferric forms, but not in its bound form 139

5.15 Aerobic growth of wild-type *R. sphaeroides* WS8N and its ΔT6SS mutant in iron-depleted media supplemented with $FeCl_3.6H_2O$. 141

5.16 T6SS gene expression during the transition from anaerobic photosynthesis to aerobic respiration in *R. sphaeroides* 2.4.1 142

6.1 Detection of HcpFLAG in whole-cell lysates of *R. sphaeroides* grown under low- and high-iron conditions 150

6.2 Anti-TlpT Western blot 151

6.3 Hcp cannot be detected in culture supernatants after photoheterotrophic growth 152

6.4 *R. sphaeroides* WS8N T6SS sheaths could not be observed under low- or high-iron conditions 154

6.5 Expression and purification of VgrGCTer-StrepII 155

6.6 The C-terminal domain of VgrG has putative iron-binding capacity 157

List of Tables

2.1 Strains 33

2.2 Plasmids 34

2.3 Antibiotic concentrations 35

2.4 Concentrated base for iron-depleted succinate media 38

2.5 Divalent transition metal-depleted Metals 44 38

2.6 PCR mixture composition 39

2.7 Thermocycling conditions for PCR 40

2.8 Colony PCR mixture composition 40

2.9 Thermocycling conditions for colony PCR 40

2.10 Restriction enzyme digest reaction mixture composition 41

2.11 DNA ligation reaction mixture composition 42

2.12 NEB HiFi DNA assembly reaction mixture composition 42

2.13 Oligonucleotides used for the generation of the pET21a-VgrGCTer-twinStrepII protein expression construct 43

2.14 Oligonucleotides used for the generation of *R. sphaeroides* mutants 46

2.15 Oligonucleotides used for the sequencing of pK18*mobsacB* suicide vector constructs 47

2.16 Oligonucleotides used for the sequencing of pET21a protein expression constructs 47

2.17 Oligonucleotides used for the sequencing of genomic mutant constructs 48

3.1 List of core gene and accessory components of *R. sphaeroides* WS8N T6SS and their putative function and COG classification. T6SS homologues were identified using NCBI, BLASTp and Phyre2. 59

4.1 Primers used in the construction of *R. sphaeroides* ΔT6SS . . . 88

Chapter 1

Introduction

1.1 Bacterial secretion systems

Bacteria produce a plethora of macromolecular nanomachines that secrete a variety of substrates, from small molecules to proteins, enabling them to respond to their ever changing environment. These specialised protein secretion systems are critical for niche survival as the secreted substrates play important roles in fundamental bacterial processes, such as adhesion, motility, antibiotic resistance and virulence. Secreted substrates can remain associated with the bacterial outer membrane, be released into the extracellular space, or injected into a target cell[1].

In Gram-negative bacteria, which the scope of this introduction is limited to, the secretory process can occur in one of two ways: 1) in a one-step pathway, via a secretory apparatus spanning both the inner and outer membranes; 2) in a two-step pathway that involves a stopover in the periplasm and relies on different secretory apparatuses to traverse the inner and outer membranes. In particular, substrates that are secreted in a two-step manner are first delivered across the inner membrane into the periplasm through the Sec or Tat secretion systems, and then transferred across the outer membrane by a second secretory apparatus. Hence this two-step mode of protein secretion is known as Sec- or Tat-dependent protein secretion[2]. By contrast, one-step protein secretion is referred to as Sec- or Tat-independent secretion. Nine Gram-negative protein secretion systems have been described. The Type II Secretion System (T2SS), T5SS, T8SS, T9SS and T10SS secrete proteins in a Sec- or Tat-dependent manner[3–5], whereas the T1SS, T3SS, T4SS and T6SS span both membranes and transport their substrates in a Sec- or Tat-independent manner[2]. Ad-

ditionally, T3SS, T4SS and T6SS can traverse a third membrane, since they deliver their substrates directly into neighbouring cells[2].

The first report of the type VI secretion system (T6SS) dates back to 1996 when Williams *et al.* identified the secreted protein, Hcp, in *Vibrio cholerae* [6]. A further decade of research facilitated the initial characterisation of T6SS function in 2006, when two seminal papers from the Mekalanos lab were published[7, 8]. The former presented the prototype of a new secretion system that involves the extracellular translocation of proteins in *V. cholerae*, designating it the Type VI Secretion System[7]. The latter then provided the biochemical and genetic evidence that a virulence-associated genetic locus of *Pseudomonas aeruginosa* encodes a protein secretion apparatus[8].

1.1.1 Overview of the Type VI Secretion System

The T6SS is a versatile, multi-component protein export apparatus present in more than 25% of Gram-negative bacteria[9]. It functions as an inverted bacteriophage tail, and uses a contractile sheath to propel an inner tube associated with an effector spike out of the firing cell and into the target cell or the extracellular milieu[10]. Indeed, the T6SS apparatus and phage tail-associated protein complexes share a common evolutionary origin and are structurally and mechanistically related[11]. All T6SSs are encoded by large gene clusters that vary in genetic organisation and can be divided into six sub-families, i1, i2, i3, i4a, i4b and i5[12, 13]. Two additional evolutionarily divergent T6SS-like systems which share a common mode of action with canonical T6SS have been designated T6SS^{ii} and T6SS^{ii}[14, 15]. While T6SS clusters are found both in

pathogenic and non-pathogenic bacteria[12], all but two of the bacterial species harbouring at least one T6SS gene cluster belong to Proteobacteria[12]. Bacterial genomes encode between one and six evolutionarily distinct T6SS clusters along with the effector arsenal, which varies between strains[12, 16]. There are a handful of examples of T6SS that function as virulence factors against eukaryotic cells, however, the T6SS is primarily considered a contact-dependent, anti-bacterial weapon. T6SS-producing bacteria deploy their apparatus to translocate antibacterial proteins into neighbouring bacterial cells; the latter will die if they lack cognate immunity proteins against the toxins of the T6SS attacker. Alternative non-combative functions of the T6SS besides their well documented role in warfare, have also been proposed, especially in the acquisition of common goods. This is perhaps unsurprising given that one of the first documented T6SSs was involved in a mutualistic relationship between *Rhizobium leguminosarum* and its plant host[17]. In the interest of a concise thesis, this introduction will be limited to a brief overview of the T6SS, followed by an in depth review of the six currently described T6SS-dependent metal uptake systems.

1.1.2 Structure and firing mechanism of the T6SS

The T6SS forms a multi-protein complex that comprises 14 core proteins (TssA-M and PAAR), while also containing varying numbers of accessory components[12]. Biochemical and structural studies support a general model across all species studied thus far[18]. The apparatus is made up of three main parts: the trans-membrane complex, the cytoplasmic baseplate, and the tail structure. Assembly of the apparatus begins with the formation of the trans-

membrane complex that spans the cell envelope and consists of ten or twelve copies of TssJ and TssL/TssM that localise in the outer and inner membrane, respectively[19–21]. The baseplate is made up of six $TssEF_2G(K_3)_2$ wedges and is recruited to the cytosolic face of the membrane complex, serving as an assembly platform for tail polymerisation[22–24]. Effector loading onto its cognate VgrG, which itself is included in the baseplate structure, activates assembly of the TssBC contractile sheath and formation of the tail[25]. On the tail, the TssBC sheath encases an inner tube of stacked hexameric rings of Hcp (TssD) sharpened with a $VgrG(TssI)_3PAAR$ spike[8]. Whilst found in all T6SSs, TssA is a diverse component of the apparatus in that it exists in two major forms: a long 55- to 60- kDa protein ($TssA_L$) and a shorter 40 kDa version ($TssA_S$)[26]. Phylogenetic clusters, reflecting those generated using TssB as per the literature[12], can be mapped using TssA protein sequences. $TssA_L$ proteins belong predominantly to phylogenetic groups i1 and i2, whilst $TssA_S$ proteins map to phylogenetic groups i3, i4 and i5[26]. In both forms TssA is a core structural component essential for T6SS function[27, 28]. It promotes priming and polymerization of the sheath, whereby after recruiting the remaining baseplate proteins, it is displaced by the growing sheath and migrates at its distal end, eventually reaching the other side of the cell[28]. TssA is also involved in stabilising the extended sheath, although the two forms of the protein do this in different ways. $TssA_L$ proteins anchor the distal end of the extended sheath through their association with the accessory protein TagA, when they reach the other side of the cell[29, 30]. By contrast, $TssA_S$ proteins, before migrating with the extending sheath, recruit the accessory protein TagB to the baseplate; the latter accumulates at the baseplate and

is proposed to form a collar-like structure that prevents the T6SS from firing before the sheath reaches all the way to the other side of the cell[26].

When fully assembled, the T6SS spans the width of the cell in its extended form[10]. Contraction of the sheath propels the Hcp inner tube and the VgrG/PAAR tip along with any associated effectors from the inside of the producing cell into a neighbouring target cell or the environment. The mechanics of this propulsion event, which occurs in less than two seconds, are reminiscent of a coiled-spring-like mechanism [16, 31]. Hcp, VgrG and PAAR are unusual components of the T6SS in that whilst they are integral structural elements of the system that are essential for its functional assembly, they also function as effectors, contributing to type VI activity. Following the firing of the T6SS apparatus, the sheath undergoes ClpV(TssH)-dependent disassembly and recycling of its TssB and TssC components[32, 33]. Figure 1.1 summarises the structure, assembly and mechanism of firing of a typical contractile T6SS.

1.2 Effector delivery by the T6SS

It is through the enzymatic activity of the secreted effector proteins that T6SS exerts its effects on target cells. T6SS-delivered effector proteins can be categorised into one of two groups: specialised effectors or cargo effectors. Specialised effectors are composed of an effector domain covalently attached to a structural subunit of the T6SS apparatus (VgrG, PAAR or Hcp), whereas cargo effectors interact non-covalently with the same structural T6SS components[34]. These different modes of effector delivery are depicted in figure 1.2.

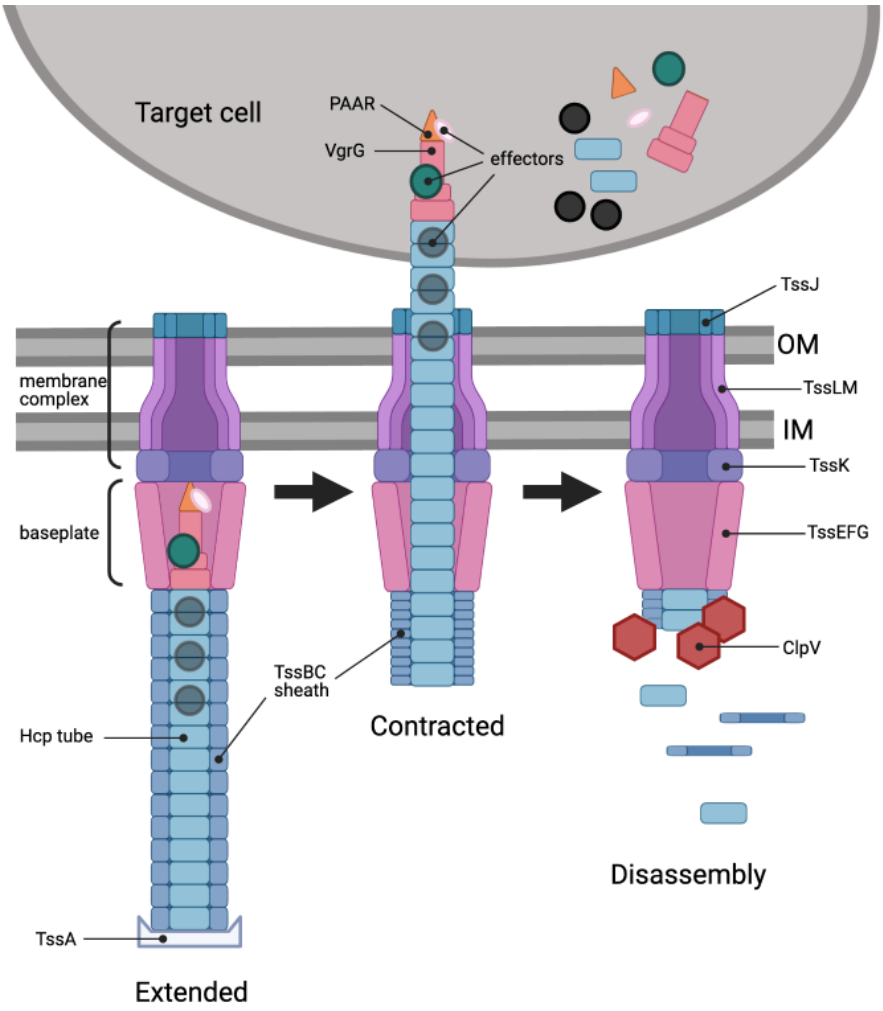


Figure 1.1: **Structure and mechanism of the type VI secretion system.** Schematic illustration of the T6SS assembly and firing mechanism. In addition to these core components, T6SS gene clusters usually encode accessory proteins, the function of most of which remains unknown. Accessory proteins are not included in the general model. The T6SS comprises three main components: the trans-membrane complex, the cytoplasmic baseplate and the tail, which is made up of the contractile sheath and the cell-puncturing inner tube. The envelope-spanning membrane complex (TssJLM) provides a docking station for TssA, which orchestrates the assembly of the cytoplasmic baseplate (TssEFGK). Formation of the baseplate, in turn, initiates polymerisation of the sheath (TssBC), which encases an inner tube (Hcp), sharpened with a VgrG/PAAR spike. While the sheath elongates, TssA that is located at the end of the sheath structure, moves aways from the baseplate, and when the sheath is fully extended, it ends up at the other side of the cell as compared to its original location in the apparatus. Contraction of the sheath propels the Hcp inner tube and the VgrG/PAAR tip along with associated effectors from the inside of the secreting cell into a neighbouring target cell. The sheath subsequently undergoes ClpV-dependent disassembly and its TssBC, baseplate and trans-membrane complex components are recycled. Created with BioRender.com

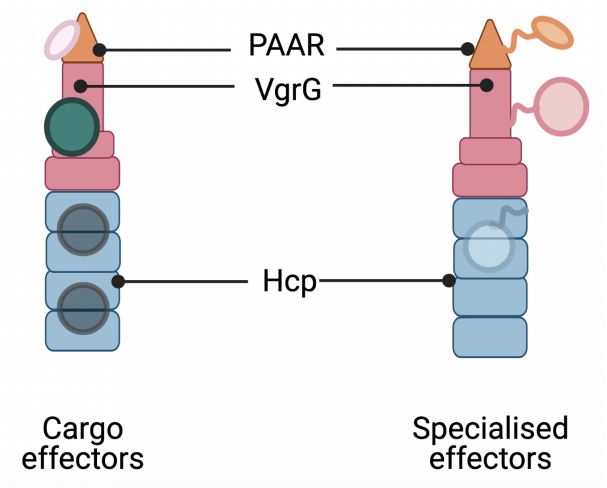


Figure 1.2: **Modes of effector delivery by the T6SS.** Schematic illustration of the different mechanisms of T6SS effector delivery. Cargo effectors interact non-covalently with Hcp, PAAR or VgrG, whereas specialised effectors are C-terminal extension domains of Hcp, PAAR or VgrG. Figure reproduced from Hernandez *et al.*[35]. Created with BioRender.com

Recognition of cargo effectors by the T6SS machinery remains poorly understood, with no universal secretion signals identified at the time of writing[35]. The T6SS-harbouring bacteria is protected from self intoxication by the possession of immunity proteins often encoded in effector/immunity protein pairs on the bacterial genome[36]. Immunity proteins specifically bind their cognate effector protein in order to neutralise it by obstructing the active site[16]. There is evidence to suggest bacteria employ a 'bet-hedging' approach by using their T6SS to deploy a cocktail of effector proteins with different modes of action[37]. Studies in *P. aeruginosa* revealed the concomitant delivery of multiple effectors by the T6SS. These effectors demonstrated conditional efficacy, whereby effector deployment is dependent on environmental conditions, and were shown to behave synergistically, that is the sum of their effects was greater than the individual effect of one effector protein[37].

In some cases an adaptor protein is required for stabilisation and/or loading

of cargo effectors onto the VgrG-PAAR spike and subsequent secretion by the T6SS[35]. DUF4123, DUF2169, DUF2875 and DUF1795 domain-containing proteins have been identified as T6SS adaptor proteins. DUF4123 domain-containing proteins have been demonstrated to facilitate effector loading onto the tip of the apparatus by interacting directly with their cognate effector protein and the C-terminal extension of their cognate VgrG protein[38–40]. Similarly, DUF2169 domain-containing proteins have been shown to be essential for Tde2 translocation and antibacterial activity in *Agrobacterium tumefaciens*, by facilitating binding of of this effector to VgrG[38] . A DUF2875 domain-containing protein has also been shown to function as an adaptor necessary for the loading of a cargo effector, Tle2, onto a VgrG protein, VgrG2b, of *P. aeruginosa* [41]. Along with VgrG adaptor proteins, one example of an adaptor required for the delivery of specialised PAAR effectors has also been described[42]. Adaptor protein EagT6 is necessary for the stability and loading of Tse6, a specialised PAAR effector of *P. aeruginosa*. It has been proposed that adaptor proteins allow the evolution of a wider range of cargo effectors that otherwise could not interact with the T6SS machinery[40].

Effectors are often toxins which promote the survival of the producing bacterium by killing competing strains and species, or are implicated in virulence and host infection by subverting host cells. More recently, effector proteins which are secreted to sequester common goods have been identified[43–47]. Anti-bacterial, anti-eukaryotic will be discussed in brief, while effectors implicated in the acquisition of common goods will be presented in more detail in the sections to follow.

1.2.1 Anti-eukaryotic effectors

There are many examples of bacterial virulence phenotypes dependent on the action of the T6SS. Often the anti-eukaryotic function of the T6SS is linked to specialised effectors located at the C-terminus of VgrG, although some cargo effectors with activity in eukaryotic cells have also been identified[48]. So far, the anti-eukaryotic effectors that have been characterised, function by protecting the T6SS producer from host defence mechanisms, manipulating the host cytoskeleton or membrane, or modulating the inflammatory response of the host[48]. T6SS-4 of *Yersinia* protects this pathogen from host-mediated oxidative stress by scavenging Zn^{2+} via the secretion of a Zn^{2+}-binding protein, YezP[43]. Deletion of YezP results in mutants with significantly diminished virulence in mice. VgrG1 from *V. cholerae* possesses an actin crosslinking domain at its C-terminus which when injected into host cells crosslinks G-actin, causing the accumulation of toxic actin oligomers and, consequently eukaryotic cell death[49]. T6SS-5 of *Burkholderia* species contributes to virulence by inducing the fusion of host cell membranes resulting in multinucleated cells[50]. Finally, the T6SS effector EvpP of *Edwardsiella tarda* inhibits the Ca^{2+}-dependent MAPK-Jnk pathway, and as a result blocks the activation of the NLRP3 imflammasome, which allows bacterial colonisation[51].

In addition to their role in bacterial virulence, there are some anti-eukaryotic T6SS that are deployed against eukaryotic microbes. For example, *V. cholerae* uses its T6SS to avoid *Dictyostelium discoideum* predation by secreting VgrG1, TseL and VasX[52]. VgrG1, as mentioned above, promotes actin crosslinking,

TseL is a lipase and VasX disrupts the eukaryotic membrane. More recently anti-fungal T6SS effectors have also been identified in *Serratia*. These toxins are secreted by a T6SS previously thought to be solely anti-bacterial, highlighting the multiplicity of functions of this nanoweapon[53]. In particular, Tfe1 lead to loss of plasma membrane potential in fungal cells, while Tfe2 hinders nutrient uptake and amino acid metabolism, consequently inducing autophagy; both effectors ultimately cause fungal cell death.

1.2.2 Anti-bacterial effectors

Bacteria often exist in densely populated polymicrobial communities, where they reside in close proximity to one another and have finite access to resources. This inevitably results in competition between species and strains of bacteria through the use of molecular weapons that directly contribute to their fitness during antagonism. The T6SS is one such weapon through which bacteria can translocate proteins that disrupt essential biochemical processes for the growth of neighbouring cells. Anti-bacterial effector proteins induce cell lysis or growth inhibition by disrupting conserved bacterial structures such as the cell wall or membrane or by interrupting key metabolic processes through the degradation of critical molecules.

Many anti-bacterial effectors act on the bacterial cell envelope. The peptidoglycan cell wall is a common target for specialised and cargo effectors alike, with many examples described in the literature to date. Such effectors either target specific peptide bonds within the peptide crossbridges of the cell wall or attack the backbone glycan chains[16]. These bonds are cleaved by

effectors that are peptidoglycan amidases and peptidoglycan glycoside hydrolases, respectively. The membrane of recipient cells is also a common target for anti-bacterial effectors, which compromise the inner membrane via lipase/phospholipase activity or through the formation of pores that quench the proton motive force[37, 54].

Anti-bacterial toxins targeting cytoplasmic processes of prey cells are another well-studied class of T6SS effector proteins. These effectors target conserved molecules and interrupt bacterial growth. Nucleic acids are one such target affected by a variety of effector proteins with nuclease activity. Rhs1 and Rhs2 from *Dickeya dadantii* encode C-terminal endonucelase domains which degrade recipient cell DNA[55], while Tse7 from *P. aeruginosa* is an evolved PAAR domains with DNase activity[56]. Recently an effector from *Burkholderia gladioli*, TseTBg, was shown to have both DNase and RNase activity[57]. Other essential cytoplasmic processes are also inhibited by T6SS toxins. For example, ADP-ribosyltransferase effectors target FtsZ, a critical protein for cell division[58], and glycohydrolase effectors (Tse6 of *P. aeruginosa* and Tse2 of *Pseudomonas*) deplete the crucial electron carriers NAD^+ and $NADP^+$, causing cell death[42, 59]. Finally, the first T6SS toxin to inhibit protein synthesis was recently identified in *P. aeruginosa*, further expanding the repertoire of antibacterial effector activities; Tse8 hampers the function of the transamisome complex, blocking the incorporation of asparagine during translation[60].

1.2.3 T6SS effectors involved in the acquisition of common goods

More recently, in addition to anti-bacterial and anti-eukaryotic effectors, which are delivered in a contact dependent manner into recipient cells, effectors which are secreted by the T6SS into the extracellular environment have also been discovered. All currently known examples of such proteins have roles in metal ion acquisition. The Zn^{2+}-binding effector proteins YezP and TseZ are secreted by *Y. pseudotuberculosis* T6SS-4 and *Burkholderia* T6SS-4, respectively[43, 46]. Additionally, a Mn^{2+}-binding protein, TseM, secreted by *B. thailandensis* T6SS-4 has also been identified[44]. The H2-T6SS of *P. aeruginosa* is used to secrete the Cu_{2+}-binding protein Azu and the molybdate-binding protein ModA, while the H3-T6SS is secretes the iron-binding protein TseF[45, 47, 61]. The ability to sequester essential metal ions from environments that are nutrient depleted offers a competitive a advantage to the T6SS producers and is fitting for a secretion systems that has such central role in interbacterial competition. T6SS-dependent metal acquisition will be discussed in more detail in the sections to follow.

1.3 T6SS-dependent metal acquisition

Upon its discovery, the function of the T6SS was proposed to be primarily anti-eukaryotic. As more T6SSs were identified and their effectors characterised, it became apparent that the principal function of this apparatus was contact-dependent inter-bacterial competition. At the same time, besides its well-documented contributions in bacterial warfare and host-pathogen inter-

actions, it became clear that the T6SS has alternative, non-combative roles in bacterial ecology. One such alternative function of particular interest to this thesis is the scavenging and sequestration of metal ions, which has implications for bacterial survival in adverse conditions, whereby any means available can be used to obtain essential nutrients.

The first report of this unconventional role for the T6SS was in *Y. pseudotuberculosis*, whose genome encodes four distinct T6SS clusters that are likely to be functionally distinct and their deployment niche dependent. In 2015, Wang and colleagues[43] demonstrated that the T6SS-4 functions to mitigate oxidative-stress-induced hydroxyl radicals by acquiring zinc ions (Zn2+) from the environment through T6SS-mediated translocation of a zinc binding protein.

Metal ion homeostasis has been shown to regulate cellular levels of hydroxyl radicals[62], and more specifically it has been demonstrated that elevated intracellular zinc levels increase resistance to oxidative stress[63]. Wang *et al.* found that expression of T6SS-4 is activated by both oxidative stress itself, and by OxyR, the primary regulatory protein involved in the bacterial oxidative stress response. Mutants lacking essential T6SS components, such as Hcp, ClpV or IcmF, showed increased sensitivity to oxidative stress compared to the wild-type strain, while failing to accumulate intracellular zinc ions. Instead, oxidative stress led to hydroxyl radical accumulation in the T6SS mutants, an effect that was only alleviated upon *hcp*, *clpV*, or *icmF* complementation. Furthermore, T6SS-4 was shown to be responsive not only to oxidative stress,

but also to the levels of environmental zinc ions; removal of zinc ions from the medium led to increased T6SS-4 expression, and addition of exogenous zinc repressed the expression of the apparatus. These results, along with the phenotype of T6SS-4 mutants described above, link the expression of this T6SS with zinc acquisition. In the same study it was shown that zinc sequestration is accomplished by T6SS-4-mediated translocation of YezP (Yersinia extracellular zinc-binding protein). The gene for this protein is located at the end of the T6SS-4 gene cluster, and it encodes an effector that contains a putative zinc finger motif and is able to bind zinc ions. The T6SS-4 dependent mechanism through which *Y. pseudotuberculosis* acquires Zn^{2+} and overcomes oxidative stress is depicted in figure 1.3. This paper is the first to consider the T6SS as a novel mechanism for bacterial metal ion uptake and discusses the role of this system in host immunity resistance and bacterial survival in challenging environments.

T6SS-4 of *B. thailandensis* is another example of a T6SS deployed to scavenge Zn^{2+} ions[46]. This T6SS secretes a proteinaceous zincophore, TseZ, to sequester Zn^{2+} ions from the extracellular environment. Deletion of *clpV4* abrogates the secretion of TseZ, a defect which is restored upon complementation. In a similar manner to the T6SS-4 of *Y. pseudotuberculosis*, when extracellular Zn^{2+} is present, T6SS-4 expression is repressed; regulation of this cluster is controlled by the zinc uptake regulator, Zur. After T6SS firing, the producer can uptake zinc through the direct interaction of zinc-loaded TseZ with HmuR, a TonB-dependent outer membrane transporter that is generally responsible for the uptake of Zn^{2+} ions. The mechanism behind T6SS-dependent

Zn^{2+} uptake in *B. thailandensis* is depicted in figure 1.3. Like with the secretion of YezP in *Y. pseudotuberculosis*, Si *et al.* demonstrated the secretion of TseZ to be upregulated by severe oxidative stress. HmuR possesses dual substrate specificity for heme and zinc, preferentially transporting heme under normal conditions and zinc under oxidative stress conditions. The substrate specificity of HmuR is regulated at the post-translational level by the formation of an intramolecular disulfide bond upon sensing extracellular oxidative stress. Interestingly, this study highlighted the graduated nature of bacterial oxidative stress response. Under mild oxidative stress intramolecular disulfide bond formation occurs switching the specificity of HmuR to zinc, however, in this instance HmuR-mediated zinc uptake alone is sufficient to mitigate oxidative stress, which saves the cell from activating the energetically costly T6SS-dependent zinc uptake. Si *et al* postulate that severe oxidative stress induces a master regulator such as OxyR, which subsequently upregulates the T6SS-4.

In addition to T6SS-dependent zinc uptake, a manganese uptake function for T6SS-4 of *B. thailandensis* has also been described. Like Zn^{2+}, Mn^{2+} is an essential micronutrient transition metal, necessary for many cellular processes, and especially resistance to oxidative stress. Manganese has a central role in mitigating oxidative stress because it is a cofactor for manganese superoxide dismutase and for non-proteinaceous manganese antioxidants[64]. Si and colleagues discovered that *B. thailandensis* T6SS-4 counteracts oxidative stress by importing Mn^{2+}[44]. TseM (type VI secretion system effector for $Mn^{2}+$ binding), a Mn^{2+}-binding effector encoded by a gene located at the

end of the T6SS cluster, is secreted by T6SS-4 into the extracellular milieu to scavenge Mn^{2+}. Mn^{2+}-bound TseM then interacts with a $\underline{Mn}^{2+}$-specific TonB-dependent outer membrane transporter, MnoT, which Si *et al.* suggest actively transports environmental Mn^{2+} across the outer membrane (see figure 1.3). When Si and colleagues subjected a $\Delta clpV4$ mutant to Mn^{2+} starvation under oxidative stress conditions growth was markedly impaired in contrast to the wild type. The addition of exogenous Mn^{2+} had no effect on the $\Delta clpV4$ mutant under oxidative stress but it did increase the survival of the wild type and the complemented $\Delta clpV4$ mutant suggesting that secretion of TseM is required for manganese uptake. Like with zinc-scavenging T6SSs, T6SS-4 genes were repressed by the addition of exogenous Mn^{2+} in a dose dependent manner.

In *P. aeruginosa* both the H2-T6SS and H3-T6SS have been implicated in T6SS-dependent metal ion uptake. H2-T6SS functions in both copper and molybdate uptake while H3-T6SS plays a role in the uptake of iron. As previously discussed for zinc and manganese, copper is an essential transition metal for bacterial growth since it is a redox cofactor in the catalytic centres of many enzymes[65]. H2-T6SS of *P. aeruginosa* was demonstrated to secrete a copper-binding effector, Azu, to scavenge Cu^{2+} ions in times of scarcity[47]. Also in this case, a TonB-dependent outer membrane transporter was recognised as a binding partner for Azu; OprC, is a Cu^{2+}-specific TonB-dependent outer membrane (see figure 1.3). Han *et al.* demonstrated that *azu*, H2-T6SS and *oprC* gene expression is repressed by the Cu^{2+}-sensing transcriptional regulator, CueR and induced by low concentrations of Cu^{2+}.

Molybdenum, a trace metal element, is a necessary component of molybdoenzymes that are required for bacterial nitrate metabolism [66]. Nitrate reductase, one such molybdoenzyme, is, in turn, critical for anaerobic bacterial growth[67]. In nature, molybdenum exists as the oxyanion, molybdate (MoO_4^{2-}). A high-affinity molybdate uptake system, ModABC, has been described in *P. aeruginosa*, as have non-specific anion importers[68, 69]. In addition to the role of H2-T6SS of *P. aeruginosa* in copper uptake, H2-T6SS-dependent acquisition of molybdate has also been described[61]. Under anaerobic conditions, where molybdenum is required for the function of nitrate reductase, the expression of H2-T6SS genes is activated by the master regulator, Anr, while exogenous addition of molybdate has the opposite effects. Wang *et al.* found that in de-repressed conditions and in the absence of molybdate, H2-T6SS secretes the effector ModA, a molybdate-binding protein. ModA was demonstrated to interact with VgrG2b, whereas (MoO_4^{2-})-bound ModA was also shown to interact with IcmP, an insulin-cleaving metalloproteinase located in the outer membrane. This is demonstrative that firstly, ModA is secreted in a H2-T6SS dependent manner, and secondly that ModA delivers (MoO_4^{2-}) into the periplasm by IcmP (see figure 1.3). The means by which (MoO_4^{2-}) is then translocated into the cytoplasm remains to be experimentally verified, though the authors hypothesise that translocation across the inner membrane occurs via ModABC or other inner membrane channels. Finally, Wang *et al.* showed H2-T6SS to be critical for the survival of *P. aeruginosa* under anaerobic conditions, suggesting molybdate is an essential cofactor for nitrate reductase which reduces nitrate into nitrite during anaerobic respiration where nitrate is reduced to nitrite by nitrate reductase. Taken together with the observation

that *modA* and *clpV2* mutants are less competitive against *Escherichia coli* when compared to the wild-type strain, one can conclude that the function of H2-T6SS in acquiring MoO_4^{2-} confers a competitive edge for *P. aeruginosa*, promoting its survival under anaerobic conditions.

Thus far, the proposed mechanisms by which bacteria perform T6SS-dependent metal ion uptake are similar, starting with the secretion of a proteinaceous metallophore that binds a particular metal ion, and subsequently relying on the uptake of the metal-bound effector by the bacterial cell through a TonB-dependent outer membrane transporter or ABC transporter. However, the last example that will be described here is more complex than that. The H3-T6SS of *P. aeruginosa* was shown to be involved in iron acquisition. Owing to its unique redox potential and role as a cofactor in many enzymes, iron is essential for a variety of cellular processes and bacterial lifestyles (bacterial iron usage and uptake will be discussed in more detail in sections 1.5 and 1.7). Lin *et al.* demonstrated the H3-T6SS-dependent secretion of TseF and its subsequent incorporation into outer membrane vesicles (OMVs) by direct interaction with the iron-binding *Pseudomonas* quinolone signal (PQS). High-affinity binding between TseF, PQS and Fe^{3+} suggest that these molecules form a complex. The mechanism by which the sequestered iron is taken up by the cell remains elusive, nonetheless Lin and colleagues did manage to identify receptors that are involved in this process, OprF and FptA. Only when these receptors were expressed could *P. aeruginosa* utilise PQS-Fe^{3+} to sustain growth (see figure 1.3). FptA is a known *P. aeruginosa* siderophore receptor and OprF is a porin that permits the slow, non-specific transport of solutes [70, 71]. TseF was

described by the authors as the bridge between PQS-Fe^{3+} and OprF and/or FptA and the integrator of three distinct systems, the T6SS, PQS and OMVs. In contrast to the other effectors of T6SS involved in metal ion acquisition described thus far, TseF has not been shown to bind iron directly.

1.4 The importance of T6SS-dependent metal ion acquisition for bacterial fitness

Within the repertoire of vertebrate host defence mechanisms against pathogens, are strategies that exploit the fastidious nature of bacteria when it comes to their dependency on trace metals[72]. These processes are referred to as nutritional immunity and either exploit the toxicity of these metals to pathogenic bacteria, or aim to decrease the availability of essential metal ions such as iron, zinc, manganese and copper, thereby necessitating the deployment of high-affinity metal uptake systems. This explains why five of the six examples of T6SS-mediated metal ion uptake described to date have been demonstrated to be critical for virulence. *Y. pseudotuberculosis* mutants lacking T6SS-4 or the Zn^{2+}-binding secreted protein YezP are defective in virulence in mice[43]. *B. thailandensis* mutants lacking clpV4, the Mn^{2+}-binding protein, TseM, or the Mn^{2+}-specific TonB-dependent outer membrane transporter, MnoT, are defective in virulence in the *Galleria mellonella* larvae infection model. Likewise, *B. thailandensis* mutants lacking the Zn^{2+}-binding protein, TseZ, or the TonB-dependent outer membrane transporter, HmuR are significantly less virulent in insect models[44, 46]. The H2-T6SS-dependent Cu^{2+} transport system of *P. aeruginosa* is necessary for virulence in a mouse model of acute pneumonia, while mutants lacking ClpV2, the Cu^{2+}-binding protein, Azu, or the

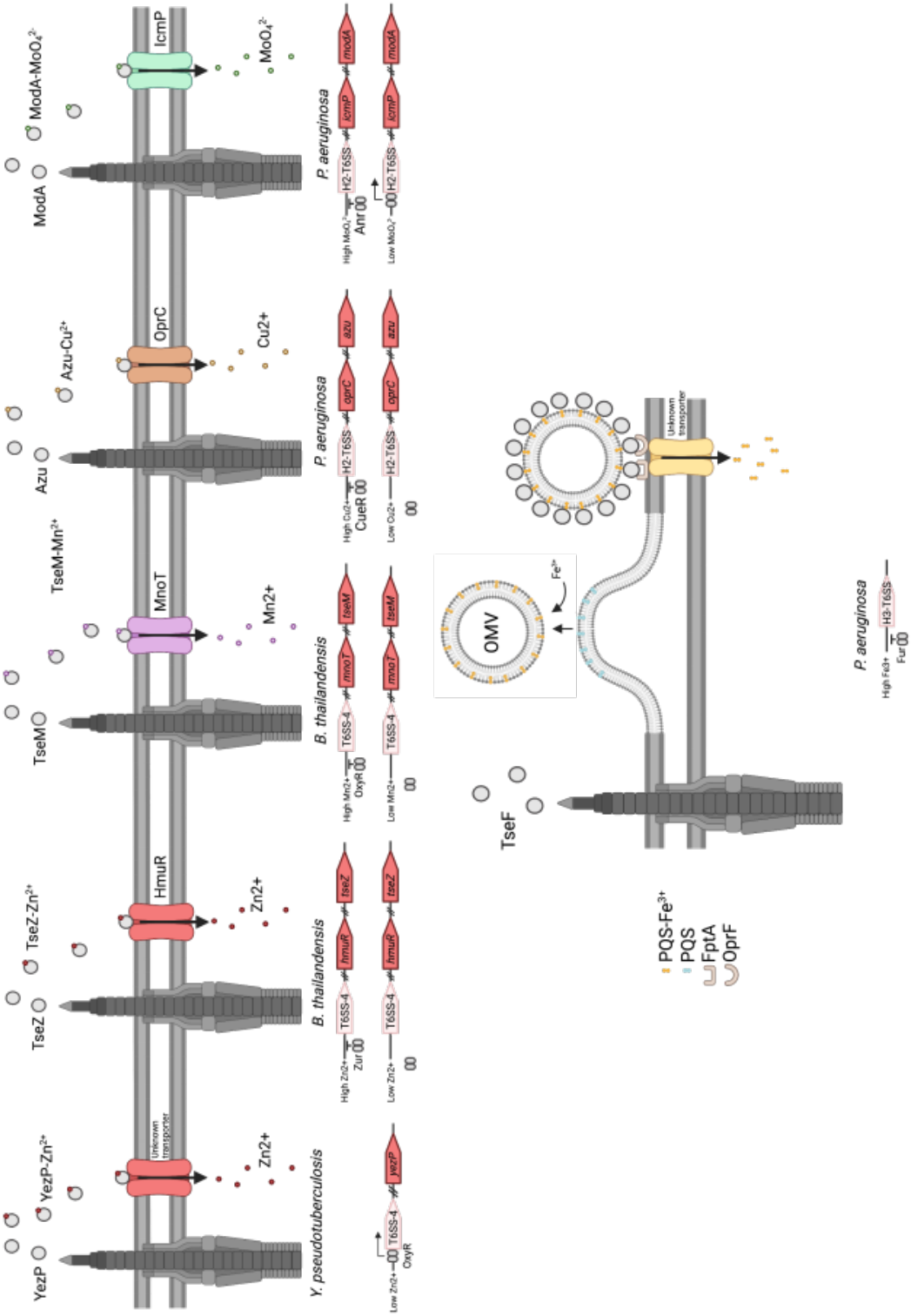


Figure 1.3: **Graphical summary of the mechanisms of the six currently described examples of T6SS-dependent metal ion acquisition.** Created with BioRender.com

transcriptional regulator, CueR, show significantly increased mouse survival compared to mice infected with wild-type *P. aeruginosa* PAO1[47]. Similarly, the H2-T6SS-dependent MoO_4^{2-} transport system is also critical for virulence of *P. aeruginosa*. Mutant strains lacking ClpV2, the MoO_4^{2-}-binding protein, ModA, or the master regulator, Anr, permitted greater mouse survival in a mouse model of acute pneumonia[61].

Three of the six examples of T6SSs used for metal ion uptake described to date have been shown to have a role in the mitigation of oxidative stress, which is critical to bacterial persistence within a host. *Y. pseudotuberculosis* circumvents oxidative stress via T6SS-4-dependent uptake of Zn^{2+}[43], while *B. thailandensis* employs its T6SS to detoxify hydroxyl radicals via T6SS-4-dependent uptake of Zn^{2+} or Mn^{2+} ions[44, 46]. That being said, oxidative stress resistance and the ability to outcompete neighbouring bacteria in a metal-scarce environment is equally as critical for inter-bacterial competition. T6SS-4-dependent uptake of both Mn^{2+} and Zn^{2+} in *B. thailandensis* has been shown to be critical for interbacterial competition, with wild-type strains demonstrating a competitive advantage against *E. coli* K12 in manganese- and zinc-depleted conditions[44, 46]. This was further validated by the fact that any competitive advantage for the wild-type *B. thailandensis* strain in these settings was largely abrogated in mutants lacking ClpV4, TseM or MnoT and mutants lacking Clpv4, TseZ or HmuR under low concentrations of manganese and zinc, respectively. Similarly, H2-T6SS-dependent uptake of Cu^{2+} conferred a competitive advantage for wild-type *P. aeruginosa* when competing with*E. coli* under copper-limiting conditions, an advantage which was lost in

mutants lacking the Cu^{2+}-binding protein, Azu, or the Cu^{2+}-specific TonB-dependent outer membrane transporter, OprC[47]. That was also observed for H2-T6SS-dependent uptake of MoO_4^{2-}, when *P. aeruginosa* was pitted against *E. coli* under, while absence ClpV2 or ModA abolished this competitive advantage when molybdenum was scarce[61].

Even though metal ions can traverse across the outer membrane via passive diffusion, in order to meet cellular demands, bacteria must actively acquire metals from the environment. This is usually achieved through high-affinity metal ion binding molecules such as siderophores, or specific ion transporters when the extracellular concentration of metals is too low for diffusion to be effective [73–75]. The discovery of T6SS effectors with a role in metal ion acquisition expanded our knowledge both on the repertoire of T6SS functions and the means by which bacteria can take up scarce essential metal ions from their surroundings in order to survive under harsh conditions, such as host nutritional immunity. Wang *et al.* postulate that the role of T6SS in mitigating non-biological stress could provide an explanation for the widespread nature of T6SS among bacteria.

1.5 Bacterial iron acquisition

Metals are required for many cellular processes and, therefore, are essential for bacterial survival. However, they do become toxic if present in excess, thus metal homeostasis must be carefully maintained. Since metals are acquired from the environment they must pass through the membranous interface of

bacterial cells. Membranes are the molecular gatekeepers of bacteria; they control the passage of molecules into and out of cells and, therefore play a critical role in maintaining homeostasis. Gram-negative bacteria possess both an inner and outer membrane. Inner-membrane permeability is highly selective as passage of molecules is governed by highly specific transporters. By contrast, the outer membrane is permeable to most small solutes, as it possesses pores with limited selectivity that permit diffusion of molecules from the environment into the intermembrane space based primarily on their size[76]. Inner-membrane transporters of free metal ions are well characterised in bacteria, however, translocation of metals across the outer membrane and into the periplasm is poorly described beyond the porin hypothesis, i.e., that metals cross the outer membrane though pores with little selectivity that readily accommodate the diffusion of solutes.

Iron poses the biggest challenge for bacteria in terms of supply and demand, because it is predominantly present as ferric iron in any oxygenated environment, in contrast to other biologically relevant transition metals like manganese, copper, cobalt and zinc, which are available as soluble, divalent cations[76]. Iron is of critical importance to almost all organisms and is involved in a multitude of biochemical processes including photosynthesis, N_2 fixation, methanogenesis, H_2 production and consumption, respiration, the trichloroacetic acid cycle, oxygen transport, gene regulation, DNA biosynthesis, virulence, biofilm formation and quorum sensing[77]. The redox potentials of Fe^{2+} and Fe^{3+} range from -300 to +700 mV, making these ions suitable electron donors and acceptors in the electron transport chains of both respiration

and photosynthesis[78].

Prior to the photosynthetic oxidation of the Earth, ~2.9 billion years ago, most iron was in a reduced ferrous state (soluble at 0.1 M, at pH 7). However, the Great Oxidizing Event, which led to an oxygened atmosphere, resulted in surface and oceanic iron being predominantly oxidised to a Fe^{3+} state (soluble at 10^{-18} M, at pH 7)[77]. Due to its poor solubility at neutral pH, iron's bioavailability is severely limited. This scarcity has driven the evolution of a repertoire of iron uptake systems in bacteria. This includes uptake systems to harvest environmental elemental iron in both the ferrous and ferric state, iron chelating siderophores that bacteria secrete to scavenge iron, and heme transport systems to salvage iron bound to proteins.

1.6 A brief introduction to *Rhodobacter sphaeroides*

R. sphaeroides is a purple nonsulfur photosynthetic bacterium of the α-subclass of proteobacteria. The metabolic versatility of *R. sphaeroides* permits its growth using aerobic or anaerobic respiration, photosynthesis or fermentation[79]. *R. sphaeroides* utilises organic compounds as both a carbon source and a reductant during photoheterotrophic and chemoheterotrophic growth, while it is also capable of fixing carbon dioxide and dinitrogen[80]. This bacterium particularly thrives under microaerophilic conditions where it can easily transition between chemoheterotrophic and photoheterotrophic growth. This is because under low oxygen tension the formation of photosynthetic complexes in the membrane is readily induced. The membrane is subsequently

invaginated forming specialised intracytoplasmic membrane vesicles allowing the microbe to photosynthesise[79].

R. sphaeroides carries out photosynthesis via three membrane-bound pigment-protein complexes: light-harvesting complexes 1 (LHI) and 2 (LHII), and the re- action centre, along with the associated components required for subsequent electron transport[81]. Owing to clustering of the genes encoding the pigment-binding proteins of LHI and the reaction centre, along with genes for bacteriochlorophyll and carotenoid synthesiss into a 46 kb photosynthesis gene cluster and the availability of the DNA sequence for this cluster, *R. sphaeroides* became a model organism for the characterisation of the photosynthetic apparatus[81, 82]. The photosynthetic capability of *R. sphaeroides* prompted interest in its use as a synthetic biology chassis for use in the production of biofuels and bioplastics, thus *R. sphaeroides* is largely studied in the context of biotechnology[83–85].

R. sphaeroides has been used as a model organism for the study of bacterial chemotactic system. The characterisation of the chemotactic system of *R. sphaeroides* revealed the existence of a system fundamentally different to that of *E. coli* [86–88]. Chemotaxis is the directed motion of a bacterium toward favourable environmental conditions or away from unfavourable environmental conditions. In the case of *R. sphaeroides*, this movement is generated via the rotation of a single flagellum which rotates counterclockwise. The bacterium changes direction by stopping the rotation periodically, and reorienting before recommencing counterclockwise rotation and movement in a different

direction [89].

1.7 Iron uptake in the *Rhodobacter* genus

The numerous ways purple nonsulfur bacteria use iron highlight its metabolic versatility. Heme is used as a cofactor by terminal cytochrome oxidases during aerobic respiration, and by cytochromes c^y, c_2 and bc_1, which shuttle electrons to photosystem reaction centres and respiratory terminal oxidases, during photosynthetic and respiratory electron transport, respectively[77]. Iron is also essential for the production of Fe-S clusters which are required by enzymes that execute diverse biological processes including heme synthesis, bacteriochlorophyll synthesis and anoxygenic photosynthesis[77, 90]. With this list being far from exhaustive, it suffices to say that purple nonsulfur bacteria rely heavily on iron for growth and bacterial fitness. The multiple uptake systems for iron encoded by *R. sphaeroides* are described below.

1.7.1 Ferrous iron uptake

Under anaerobic conditions, iron predominantly exists in the ferrous ($Fe2^+$) form[91]. The Feo iron transport system is widespread among bacterial genomes and is, thus considered to be the major ferrous iron uptake system. *R. sphaeroides* 2.4.1 harbours one four-gene *feo* cluster consisting of two *feoA* genes followed by *feoB* and *feoC* ($feoA_1A_2BC$),but there is no experimental evidence for the role of *feo* gene products in this organism[77]. Nonetheless, the general model for the Feo system is assumed to apply. If this is the case, then FeoB encodes a membrane bound ferrous iron permease, FeoA has a SH3 domain thought

to be involved in protein-protein interactions, and FeoC is considered to be a transcription factor which controls the entire $feoA_1A_2BC$ operon[77].

1.7.2 Ferric iron uptake

Under aerobic conditions iron predominantly exists in the ferric ($Fe3^+$) state[91]. Siderophores are the primary mediator of ferric iron uptake. These are small molecules secreted by bacteria during iron starvation. Since siderophores have a high binding affinity for Fe^{3+} (10^{-20} M), they can solubilize and sequester ferric iron even from rust, which is how ferric iron is commonly found in nature[77]. Siderophore transporters comprise a TonB-dependent outer membrane ferrisiderophore receptor and an ABC transporter cassette (consisting of a periplasmic siderophore binding protein, a membrane permease and an ATPase). The organisation of siderophore transporters is well conserved among bacteria with similar systems used to also import heme and vitamin B_{12}[92].

R. sphaeroides harbours an *exbB-exbD-tonB* operon and four siderophore uptake systems[77]. The ExbB-ExbD-TonB complex acts as a molecular motor which harnesses the proton motive force across the inner membrane in order to import the ferrisiderophore from the outer membrane receptor into the periplasm[93]. The ferrisiderophore is then transported from the periplasm into the cytoplasm by an ABC transporter[77]. Interestingly, *R. sphaeroides* does not possess the genes required for siderophore synthesis and, therefore likely scavenges siderophores produced by other species (xenosiderophores). This is not an uncommon occurrence for environmental organisms, with previously unculturable bacteria exhibiting a dependency on xenosiderophores for

growth[94].

Another means of ferric iron uptake is via iron-ABC transporters. Iron-ABC transporters function similarly to siderophore uptake systems, without the requirement of an outer membrane receptor for translocation of iron into the periplasm. Encoded within the *R. sphaeroides* genome are putative homologues of the best studied iron-ABC transporter,FbpABC.

1.7.3 Regulation of iron metabolism in *R. sphaeroides*

The Irr and Fur proteins have been identified as global regulators of iron homeostasis in several α-proteobacteria [77]. These two proteins share strong sequence homology and belong to the same family of metal regulators, albeit with different modes of action, with Fur directly binding iron and Irr acting indirectly. In particular, the binding of elemental iron to Fur affects its ability to activate or repress downstream gene expression, while Irr indirectly monitors iron levels by sensing the activity of the enzyme involved in the final step of heme biosynthesis.

Bioinformatic analysis revealed four putative iron responsive regulators in *R. sphaeroides*; *irr*, *fur/mur*, *fur/zur* and *iscR*[95]. *fur/mur* deletion mutants show reduced growth under iron limitation, demonstrative of a role for Fur/Mur in the regulation of iron metabolism in *R. sphaeroides*. By contrast, Irr does not appear to be a master regulator of iron homeostasis; an *irr* deletion has little effect on bacterial growth under iron-limiting conditions, but leads to an increase in resistance to oxidative stress[96]. Complementation of the *irr*

gene restores the oxidative stress sensitive phenotype. Moreover, despite lacking any motifs associated with heme binding, the Irr protein of *R. sphaeroides* has been shown to bind heme[96]. IscR is a known transcriptional regulator of Fe-S cluster biogenesis genes in *E. coli*, and a role for IscR as a major regulator of iron homeostasis in *R. sphaeroides* has been proposed, but remains to be experimentally determined[95]. Finally, no experimental evidence exists to suggest the involvement of Zur in *R. sphaeroides* iron regulation; it is proposed that it is more likely to be involved in zinc uptake[77]. As is clear from the above analysis, iron-mediated gene regulation in *R. sphaeroides* remains largely elusive.

1.8 Project aims

The general aim of this thesis is to characterise the T6SS of *R. sphaeroides* WS8N and attempt to identify its role in the lifestyle of this bacterium. This will be the first experimentally characterised T6SS of the Rhodobacter genus, which encompasses bacterial organisms that are both fascinating and challenging to perform experiments on. Subsequent chapters will address the following specific aims:

- Perform bioinformatic analyses on the T6SS cluster of *R. sphaeroides* WS8N to determine its putative core components and secreted effector proteins
- Construct a *R. sphaeroides* WS8N mutant strain entirely lacking the T6SS gene cluster and optimise a robust growth assay in order to assess

the phenotypic consequences of T6SS absence

- Use the optimised growth assay to interrogate the phenotypic consequences of the ΔT6SS strain for a range of growth conditions, in order to assign a central function to the T6SS of *R. sphaeroides* WS8N
- Verify the role of *R. sphaeroides* WS8N T6SS in iron acquisition using biochemical and biophysical methods

Chapter 2

Materials and Methods

2.1 Strains and plasmids

Bacterial strains and plasmids used in this study are listed in tables 2.1 and 2.2, respectively.

Strain	Description	Reference
R. sphaeroides WS8N	Wild-type strain of *R. sphaeroides*, spontaneous WS8 mutant conferring nalidixic acid resistance	[97]
R. sphaeroides WS8N *ΔT6SS*	Deletion of the WS8N T6SS cluster	this study
R. sphaeroides WS8N *tssB::gfp*	*sfgfp* inserted upstream of the stop codon of *tssB* in WS8N	this study
R. sphaeroides WS8N *tssB::ppfbfp*	*ppfbfp* inserted upstream of the stop codon of *tssB* in WS8N	this study
R. sphaeroides WS8N *ΔvgrG*	deletion of the *vgrG* gene	this study
R. sphaeroides WS8N *Δhcp*	deletion of the *hcp* gene	this study
R. sphaeroides WS8N *tssB::flag*	FLAG tag inserted upstream of the stop codon of *tssB*	this study
R. sphaeroides WS8N *hcp::flag*	FLAG tag inserted upstream of the stop codon of *hcp*	this study
E. coli DH5α	Cloning strain	lab collection
E. coli S17-λpir	Plasmid mobilising strain, used to introduce plasmids into *R. sphaeroides* WS8N	[98]
E. coli BL21 (DE3)	Protein expression strain	lab collection

Table 2.1: Strains

2.2 Growth conditions

2.2.1 Antibiotics

Antibiotics used in this study and their concentrations during *E. coli* and *R. sphaeroides* growth are shown in table 2.3.

Plasmid	Description	Reference
pK18*mobsacB*	Kanamycin-resistant, sucrose-sensitive suicide plasmid	[98]
pK18*mobsacB*Δ*T6SS*	Kanamycin-resistant, sucrose-sensitive suicide plasmid for the generation of *R. sphaeroides* WS8N *ΔT6SS*	this study
pK18*mobsacB*Δ*vgrG*	Kanamycin-resistant, sucrose-sensitive suicide plasmid for the generation of *R. sphaeroides* WS8N *ΔvgrG*	this study
pK18*mobsacB*Δ*hcp*	Kanamycin-resistant, sucrose-sensitive suicide plasmid for the generation of *R. sphaeroides* WS8N *Δhcp*	this study
pK18*mobsacBtssB::gfp*	Kanamycin-resistant, sucrose-sensitive suicide plasmid for the generation of *R. sphaeroides* WS8N *tssB::gfp*	this study
pK18*mobsacBtssB::ppfbfp*	Kanamycin-resistant, sucrose-sensitive suicide plasmid for the generation of *R. sphaeroides* WS8N *tssB::ppfbfp*	this study
pK18*mobsacBtssB::flag*	Kanamycin-resistant, sucrose-sensitive suicide plasmid for the generation of *R. sphaeroides* WS8N *tssB::flag*	this study
pK18*mobsacBhcp::flag*	Kanamycin-resistant, sucrose-sensitive suicide plasmid for the generation of *R. sphaeroides* WS8N *hcp::flag*	this study
pET21a	Ampicillin-resistant, T7-based expression plasmid	Novagen
pET21a-*hud* TwinStrepII	pET21a with putative 'heme utilisation domain' (*hud*) of *vgrG* with a twin Strep-Tag II tag upstream of the stop codon, cloned into the *Nde*I and *Hind*III restriction sites	this study

Table 2.2: Plasmids

Antibiotic	Concentration for *E. coli*	Concentration for *R. sphaeroides*
Kanamycin	25 µg mL $^{-1}$	25 µg mL $^{-1}$
Nalidixic acid	25 µg mL $^{-1}$	25 µg mL $^{-1}$
Ampicillin	100 µg mL	-

Table 2.3: Antibiotic concentrations

2.2.2 Growing *E. coli*

Liquid cultures of *E. coli* were grown in LB (see 8.1.1) containing appropriate antibiotics at 37°C with shaking at 225 rpm. Solid growth for *E. coli* was performed on LB agar (2%) with incubation at 37°C.

2.2.3 Growing *R. sphaeroides*

R. sphaeroides was grown aerobically in succinate media (8.1.2) containing the appropriate antibiotics at 30°C with shaking at 225 rpm. For photo-heterotrophic growth, experiments were carried out in succinate media containing the appropriate antibiotics; cell suspensions were incubated in 1.5 mL tubes with minimal air space at 30°C under white light.

Solid growth for *R. sphaeroides* was performed on LB agar (2%) with incubation at 30 °C. When sucrose selection had to be applied, bacteria were grown using M22 minimal media (see 8.1.8), 10 % sucrose and 2 % agar.

2.2.4 Growing *R. sphaeroides* starter cultures for growth assays

R. sphaeroides WS8N strains to be tested were streaked from frozen glycerol stocks onto LB agar plates containing appropriate antibiotics. Plates were

then incubated at 30 °C for up to 72 h, until colonies were visible. Five single colonies were inoculated into 1.5 mL Eppendorf tubes containing succinate media and the appropriate antibiotic(s). Tubes were filled with cell suspension so that cells had minimal aeration and incubated under constant illumination (light intensity of ˜10 W/m^2) at 30°C for 72 h. Starter cultures were then normalised to OD_{700} 1.5 and diluted 1:1000 into the growth assay media.

2.2.5 *R. sphaeroides* growth assay

Growth assays were performed in 1.5 mL Eppendorf tubes containing the growth media and appropriate antibiotics with minimal aeration. Tubes were incubated under constant illumination (light intensity of ˜10 W/m^2) at 30°C for 96 h. At 24 h intervals (24, 48, 72 and 96 h) 150 µL of bacterial cell suspension were dispensed into a 96-well microtiter plate and OD_{700} was measured using a CLARIOstar plate reader (BMG LABTECH). 3 - 6 OD_{700} measurements were recorded for each well.

Growth assays were repeated on two different occasions. On both occasions the experiment was performed in biological triplicate, with each biological replicate performed in technical triplicate. All 18 points are plotted on the graphs presented in chapters 4 and 5. Whether the mean value of the technical and biological replicates was taken before plotting, thereby reducing the number of points on each graph, or by averaging all 18 values does not affect the position of the box plot components nor the statistics, thus all 18 points are plotted throughout this thesis.

2.2.6 Divalent transition metal-depleted growth assay media

Growth assays were performed in succinate media lacking each of the divalent transition metals required for the "metals 44" solution (see 8.1.5). Metal-depleted succinate media was prepared as described in 8.1.2 with the following modifications:

- 20% casamino acids were dissolved in MilliQ and cation-chelated using Chelex 100 resin (BIO-RAD). 5 mL of the chelated casamino acids were added per 1 litre of succinate media.

- For iron-depleted succinate media, the concentrated base was prepared as described in table 2.4, using the appropriate modified "metals 44" solution described in table 2.5.

- For zinc-, manganese-, copper- and cobalt-depleted succinate media, the concentrated base was prepared as described in 8.1.4, using the appropriate modified "metals 44" solution described in table 2.5.

For divalent transition metal-depleted growth assays, metal-depleted media was supplemented with the following concentrations of divalent transition metals:

- Zinc-depleted media was supplemented with 0 µM, 0.15 µM, 1.5 µM or 15 µM $ZnSO_4.7H_2O$.

- Iron-depleted media was supplemented with 0 µM, 0.1 µM, 1 µM or 10 µM $FeSO_4.7H_2O$.
- Manganese-depleted media was supplemented with 0 µM, 0.04 µM, 0.4 µM or 4 µM $ZnSO_4.7H_2O$.
- Copper-depleted media was supplemented with 0 nM, 6.5 nM, 65 nM or 650 nM $CuSO_4.5H_2O$.
- Cobalt-depleted media was supplemented with 0 nM, 3.5 nM, 35 nM or 350 nM $CoCl_2.6H_2O$.

The above concentrations of divalent transition metal solutions used to complement metal-depleted media were chosen to be ˜0 %, 0.8 %, 8 % and 80 % of the concentration used for the preparation of succinate media.

Ingredient	Quantity per litre
Nitrilotriacetic acid (diNa salt)	5.94 g
Metals 44 solution	25 mL
MgSO4.7H2O	14.5 g
CaCl2.2H2O	1.67 g
Ammonium molybdate 4H2O	4.6 mg

Table 2.4: Concentrated base for iron-depleted succinate media

Ingredient	Quantity per litre				
	-Zn	-Fe	-Mn	-Cu	-Co
EDTA	2.5 g	2.5 g	2.5 g	2.5 g	2.5 g
$ZnSO_4.7H_2O$	-	11 g	11 g	11 g	11 g
$FeSO_4.7H_2O$	5 g	-	5 g	5 g	5 g
3 M H_2SO_4	1.5 mL	1.5 mL	1.5 mL	1.5 mL	1.5 mL
$MnSO_4.4H_2O$	3 g	3	-	3 g	3 g
$CuSO_4.5H_2O$	0.39 g	0.39	0.39 g	-	0.39 g
$CoCl_2.6H_2O$	0.2 g	0.2	0.2 g	0.2	-

Table 2.5: Divalent transition metal-depleted Metals 44

Component	50 µL Reaction
5X Q5 Reaction Buffer	10 µL
10 mM dNTPs	1 µL
10 µM Forward Primer	2.5 µL
10 µM Reverse Primer	2.5 µL
DMSO	2.5 µL
Template DNA	variable
Q5 High-Fidelity DNA Polymerase	0.5 µL
5X Q5 High GC Enhancer	10 µL
Nuclease-Free Water	to 50 µL

Table 2.6: PCR mixture composition

2.3 Genetic techniques

2.3.1 Polymerase Chain Reaction (PCR)

All polymerase chain reactions (PCR) conducted to obtain DNA for cloning were carried out using Q5 High-Fidelity DNA polymerase (NEB) according to the manufacturers' instructions. The reaction mixture composition is outlined in table 2.6 and the thermocycling conditions can be found in table 2.7. Colony PCRs (cPCR) were used to confirm successfully cloned plasmids in *E. coli* and to determine successfully generated strains in *R. sphaeroides*. GoTaq G2 Green Master Mix (Promega) was used for all cPCR according to the manufacturers' instructions. The reaction mixture composition for cPCR is outlined in table 2.8 and the thermocycling conditions can be found in table 2.9. Oligonucleotides were synthesised by Sigma Aldrich or Integrated DNA Technologies.

2.3.2 Purification of plasmid DNA and PCR products

Purification of plasmid DNA was carried out using the QIAprep Spin Miniprep Kit (Qiagen). Purification of PCR products was carried out using the Monarch PCR & DNA Cleanup Kit (NEB). When necessary, any plasmids or PCR prod-

Step	Temperature	Time
Initial denaturation	98 °C	30 s
25 - 35 cycles	98 °C	10 s
	*50 - 70 °C	30 s
	72 °C	20 - 30 s/kb
Final extension	72 °C	2 min
Hold	4 - 10 °C	

* Optimal annealing temperature was determined for each set of primers using the NEB Tm Calculator.

Table 2.7: Thermocycling conditions for PCR

Component	25 µL Reaction
GoTaq G2 Green Master Mix, 2X	12.5 µL
10 µM Forward Primer	1 µL
10 µM Reverse Primer	1 µL
DMSO	1 µL
Template DNA	variable
Nuclease-Free Water	to 25 µL

Table 2.8: Colony PCR mixture composition

Step	Temperature	Time
Initial denaturation	96 °C	5 min
25 - 35 cycles	95 °C	30 s
	60 °C	30 s
	72 °C	2 min
Final extension	72 °C	5 min
Hold	4 - 10 °C	

Table 2.9: Thermocycling conditions for colony PCR

Component	50 µL reaction
Restriction enzyme 1	1 µL
Restriction enzyme 2	1 µL
DNA	1 µg
10X NEBuffer	5 µL
Nuclease-Free Water	to 50 µL

Table 2.10: Restriction enzyme digest reaction mixture composition

ucts subject to agarose gel electrophoresis were purified using the Monarch DNA Gel Extraction Kit (NEB).

2.3.3 Agarose gel electrophoresis

Gels were made using 1 % agarose in 0.5 x TBE (see 8.1.9); Invitrogen SYBR Safe DNA Gel Stain (Thermo Fisher Scientific) was added according to the according to the manufacturers' instructions. Fragments were subjected to electrophoresis at 120 V and gels were visualised under UV light.

2.3.4 Restriction enzyme digests

Restriction enzyme digests were carried out using High-Fidelity restriction endonucleases (NEB) for 1 h at 37 °C. The reaction mixture is outlined in table 2.10.

2.3.5 DNA ligation

Ligations were carried out as described in table 2.11. A molar ratio of 1:3 vector to insert was used in all cases. Ligations were incubated overnight at 16 °C and heat inactivated at 65 °C for 10 minutes.

Component	20 µL Reaction
T4 DNA Ligase Buffer (10X) (NEB)	2 µL
Vector DNA (5 kb)	50 ng
Insert DNA (1 kb)	30 ng
Nuclease-free water	to 20 µL
T4 DNA Ligase (NEB)	1 µL

Table 2.11: DNA ligation reaction mixture composition

Component	20 µL Reaction
Total amount of fragments	0.03-0.2 pmols, X µL
NEBuilder HiFi DNA Assembly Master Mix	10 µL
Deionized H2O	to 20 µL

Table 2.12: NEB HiFi DNA assembly reaction mixture composition

2.3.6 NEB HiFi DNA Assembly

Assembly of plasmid vectors and inserts was carried out as per the instructions supplied with NEBuilder HiFi DNA Assembly Master Mix (NEB), using the reaction mixture outlined in table 2.12. This reaction is for 2-3 fragment assembly, with a 1:2 vector to insert molar ratio.

2.3.7 Primers used to generate the pET21a-VgrGCTer-twinStrepII protein expression vector

The primers used to generate the pET21a-VgrGCTer-twinStrepII protein expression vector are displayed in table 2.13.

2.3.8 Making chemically competent *E. coli* cells

A 5 mL culture of each *E. coli* strain of interest was grown overnight. 100 µL was then sub-cultured in 40 mL LB and grown for 3 hours to an OD_{600} of 0.3-0.5. The subculture was divided into two 50 mL Falcon tubes and incubated on ice for 15 minutes. The cell suspension was then centrifuged at 1500 rpm x g at 4 °C for 10 minutes. Cells were gently re-suspended in 20 mL of

Name	Sequence
pET21a-VgrGCTer-twinStrepII P1	TGGATCGGGAGGTGGATCGTGGAGC CACCCGCAGTTCGAAAAATGAAAGC TTGCGGCCGCACTC
pET21a-VgrGCTer-twinStrepII P2	CCTCCGGAACCTCCACCTTTCTCGA ACTGCGG
pET21a-VgrGCTer-twinStrepII P3	CACACATATGCATACCGAGCTCATC AAGAACGAC
pET21a-VgrGCTer-twinStrepII P4	CACAGGATCCGTTCAGGTTGATCTT CGAGC

Table 2.13: Oligonucleotides used for the generation of the pET21a-VgrGCTer-twinStrepII protein expression construct

pre-chilled 0.1 M $CaCl_2$, incubated on ice for 1 hour, and centrifuged at 1500 rpm x g at 4 °C for 10 minutes. Finally, cells were gently re-suspended in 3 mL 0.1 M $CaCl_2$ and 15 % glycerol, transferred into pre-frozen 1.5 mL tubes, and stored at -80 °C in aliquots of 50 or 100 µL.

2.3.9 Transformation of plasmids into competent *E. coli* cells

Competent cells were thawed on ice. 1 µL of purified plasmid was mixed with 50 or 100 µL of competent cells by gently pipetting up and down and incubated on ice for 30 minutes. Cells were then heat shocked at 42 °C for 45 seconds and put back on ice for a further 2 minutes. 900 µL SOC media (NEB) was added to the cells, and the suspension was incubated at 37 °C with shaking at 225 rpm for 90 minutes, before plating 100 µL onto pre-warmed LB plates containing appropriate antibiotics.

2.3.10 Conjugation of plasmids into *R. sphaeroides*

As it is not possible to make *R. sphaeroides* chemically competent, plasmids were introduced to *R. sphaeroides* WS8N via conjugation using *E. coli* S17-1λ*pir* as the donor strain. *E. coli* S17-1λ*pir* was made chemically competent as described in section 2.3.8 and plasmids of interest were transformed into competent *E. coli* S17-1λ*pir* as described in section 2.3.9. Subsequently, 1 mL of early log phase *E. coli* S17-1λ*pir* culture and 1 mL of early stationary phase *R. sphaeroides* WS8N culture were each centrifuged at 6000 rpm in a tabletop centrifuge. Pellets were then re-suspended in 1 mL LB and centrifuged again at 6000 rpm before finally re-suspending in 100 µL LB; re-suspension of the S17-1λ*pir* cells was carried out gently to avoid shearing the pili.

10 µL of washed *E. coli* S17-1λ*pir* suspension was gently mixed with 100 µL of washed *R. sphaeroides* WS8N suspension. The mixture was then transferred onto a sterile nitrocellulose filter (Millipore), placed on an antibiotic-free LB agar plate, and incubated at 30 °C overnight. The filter was subsequently transferred to a 1.5 ml tube tube containing 800 µL LB and vortexed vigorously. 100 µL of cell suspension were spread on LB agar plates containing nalidixic acid as well as appropriate antibiotics for plasmid selection, and incubated at 30 °C for two days.

2.3.11 Homologous recombination for the generation of *R. sphaeroides* insertion and deletion mutants

The kanamycin-resistant, sucrose-sensitive suicide plasmid pK18*mobsacB* was used to introduce mutations into *R. sphaeroides* by homologous recombina-

tion. For genomic deletion mutants, the DNA fragment that was cloned into pK18*mobsacB* contained the 500 bp up-stream (P1 and P2) and down-stream (P3 and P4) regions directly flanking the gene to be deleted. For the generation of genomic insertion at the C-terminus of the gene of interest, the DNA fragment that was cloned into pK18*mobsacB* contained the ultimate 500 bp of the gene (P1 and P2), the tag of interest (P3 and P4) and the 500 bp region directly downstream (P5 and P6) the gene to be altered. Primers used for the generation of genomic mutants are displayed in table 2.14.

The generated mutator plasmid was introduced into *R. sphaeroides* as described in section (2.3.10). The last conjugation step, whereby transconjugants were plated on LB agar plates containing two antibiotics, nalidixic acid and, in the case of pK18*mobsacB* constructs, kanamycin, drives two events: i) the killing of the *E. coli* donor strain, which is sensitive to nalidixic acid, and ii) the first homologous recombination event. The origin of replication of pK18*mobsacB* is cannot be recognised by the *R. sphaeroides* recipient strain and, thus cannot be replicated. *R. sphaeroides* must therefore integrate the plasmid into its genome by homologous recombination in order to acquire kanamycin resistance and survive on the LB agar plates containing the antibiotic.

Single colonies from the first recombination event were grown on succinate media containing nalidixic acid for 48 hours at 30 °C. During this growth step a second spontaneous recombination event occurs, which excises the vector backbone from the *R. sphaeroides* genome, including the genes conferring sucrose

Strain	Name	Sequence (restriction site, FLAG tag, linker)	Restriction site
ΔT6SS	ΔT6SSP1	CACAGAATTCCACCCGCAGCGCGCC	EcoRI
	ΔT6SSP2	CGGGTCCCGAGGAGCCTCTCCTGTTCCCCGATCATGCCCG	
	ΔT6SSP3	CGGGCATGATCGGGGAACAGGAGAGGCTCCTCGGGACCCG	
	ΔT6SSP4	CACAAAGCTTCGGCCAGCCGGTCG	HindIII
hcp::flag	hcp::flagP1	CGCGGGATCCTTCAGGACATGGCATTCACAGGC	BamHI
	hcp::flagP2	TCA CTTGTCGTCATCGTCTTTGTAGTC GCCGG	
		AGGAGCCGCGGGCGGCGACGACGTTATATTCG	
	hcp::flagP3	GGCTCCTCCGGC GACTACAAAGACGATGACGA	
		CAAG TGAGCGCGGCGGCCCCGCTGGCGCGGAG	
	hcp::flagP4	CGCGAAGCTTCCGGCCCGAAAAGGCGGGAACG	HindIII
tssB::ppfbfp	tssB::ppfbfpP1	CGCGGGATCCAACGCAACCGCGCTCC	BamHI
	tssB::ppfbfpP2	GCCGCCGCCCGCCGCCGCTTCCTCCGGCTGGCGCGACT	
	tssB::ppfbfpP3	GCGGCGGCGGGCGGCGGCATCAACGCAAAACTCCTGC	
	tssB::ppfbfpP4	CATTCCTCCGGCTGGCGCGAGTGCTTGGCCTGGCCC	
	tssB::ppfbfpP5	GGGCCAGGCCAAGCACTCGCGCCAGCCGGAGGAATG	
	tssB::ppfbfpP6	CGCGAAGCTTTGGTGGCTGAACTCATAGGC	HindIII

Table 2.14: Oligonucleotides used for the generation of *R. sphaeroides* mutants

sensitivity and kanamycin resistance. The second recombination event was selected for by plating onto sucrose selection plates (see section 2.2.3). These plates were then incubated at 30 °C for three to five days, and replica plating was used to confirm the loss of the *kan*^{r} gene. Since the second recombination event occurs at either the wild-type or mutant locus, it can result in either a reversion to the wild-type strain or in the generation of the desired mutant; successful mutants were differentiated by colony PCR (see section 2.3.1).

2.3.12 DNA sequencing

All plasmid constructs and genomic mutations were confirmed by Sanger sequencing (performed by Source BioScience, Oxford) on the purified plasmid or a cPCR amplicon, respectively. All pK18*mobsacB* constructs, pET21a protein expression constructs, and genomic mutant strains were confirmed using the oligonucleotides shown in tables 2.15, 2.16, and 2.17, respectively.

Primer	Sequence
M13F	TGTAAAACGACGGCCAGT
30nt_M13R	AGCGGATAACAATTTCACACAGGA

Table 2.15: Oligonucleotides used for the sequencing of pK18*mobsacB* suicide vector constructs

Primer	Sequence
T7 promoter (F)	TAATACGACTCACTATAGGG
T7 terminator (R)	GCTAGTTATTGCTCAGCGG

Table 2.16: Oligonucleotides used for the sequencing of pET21a protein expression constructs

Strain	Name	Sequence
ΔT6SS	ΔT6SSCPF	CGTCAGATCGGTCGCATAGCGGGCGAG
	ΔT6SSCPR	CGACAAGGACACGAGCGTGGGCCGGAAC
hcp::flag	hcp::flagCPF	CTGATCGCTCCTCTCCGCTT
	hcp::flagCPR	CGCAGATCGCGCGCCA
tssB::ppfbfp	tssB::ppfbfpCPF	CGTGGAGCATTACGGCAGC
	tssB::ppfbfpCPR	GAGCTGGTCGGCCAGT

Table 2.17: Oligonucleotides used for the sequencing of genomic mutant constructs

2.4 Protein characterisation

2.4.1 FLAG-tagged proteins

2.4.1.1 Sample preparation for sodium dodecyl sulphate polyacrylamide gel electrophoresis (SDS-PAGE)

R. sphaeroides cell lysates were obtained by re-suspending 1 mL of cultures at OD_{700} 10 in 200 µL 2X Laemmli sample buffer (Merck). Samples were boiled for 10 minutes at 95 °C. *E. coli* cell lysates were obtained by re-suspending 1 mL of cultures at OD_{600} 0.5 in 50 µL 2X Laemmli sample buffer Samples were boiled for 10 minutes at 95 °C.

SDS-PAGE analysis was performed on 4-20 % Mini-PROTEAN TGX precast gels (Bio-Rad), using 1X SDS Running Buffer (8.1.10). 12 µL of sample was loaded per well. Gels were run at a constant current of 35 mA for 40 min at room temperature. Precision Plus Protein Dual Color Standard (Bio-Rad) was used for molecular weight estimation. Samples were standardised by OD_{700} prior to loading and equivalent volumes were loaded per lane.

2.4.1.2 Western Blotting

After SDS-PAGE, proteins were transferred onto 0.2 µM nitrocellulose membranes using the semi-dry Trans-Blot Turbo Transfer System (Bio-Rad). Following transfer, transfer was confirmed by staining for total protein with Ponceau S straining solution (0.1 % Ponceau S (w/v) in 5 % acetic acid). Membranes were then de-stained in water and blocked with 2 % (w/v) milk powder in TBST (20 mM Tris-Hcl pH 7.6, 137 mM NaCl, 0.02 % Tween-20) for 30 min at room temperature. Membranes were then probed with 10 µg μL^{-1} (diluted 1:400) monoclonal ANTI-FLAG M2 primary antibody (Sigma-Aldrich) in 2% (w/v) milk powder solution in TBST for 1 h at room temperature. The membranes were then washed three times (5 min each) with TBST before being incubated with polyclonal anti-mouse antibody-peroxidase conjugate (goat; Sigma) diluted 1:10,000 for 30 min at room temperature. The membranes were washed again three times with TBST (5 min each). Western blots were visualised with the Westar Supernova HRP substrate (Cyanagen) and the film was developed in an X-ray film processor (Optimax).

2.4.2 StrepII-tagged proteins

2.4.2.1 Sample preparation for SDS-PAGE

E. coli BL21(DE3) cells harbouring the pET21a-VgrGCTer-StrepII plasmid were grown in LB supplemented with the appropriate antibiotics at 37 °C with shaking at 200 RPM to an OD_{600} of 0.8. Protein expression was subsequently induced by addition of IPTG at a final concentration of 1 mM for 16 hours at 30 °C. 1 mL of culture was harvested, and the cell pellet was re-suspended in 600 µL BugBuster Master Mix (Millipore) and incubated with gentle agitation

at room temperature for 15 min. 4X Laemmli sample buffer was added and the sample was boiled at 95 °C for 5 min.

SDS-PAGE analysis was performed on 10 % NuPAGE Bis-Tris mini protein gels (Invitrogen), using 1X MES-SDS Running Buffer (Invitrogen), prepared according to the manufacturers' instructions. Gels were run at a constant voltage of 180 V for 10 min, before the voltage was increased to 200 V for a further 40 min at room temperature. SeeBlue Plus2 Pre-Stained Standard (Invitrogen) was used for molecular weight estimation and to determine transfer efficiency during Western blotting.

2.4.2.2 Western Blotting

Protein samples obtained by SDS-PAGE were transferred onto 0.2 µM nitrocellulose membranes using the semi-dry Trans-Blot Turbo Transfer System (Bio-Rad). Membranes were blocked with 3 % (w/v) bovine serum albumin in TBST (20 mM Tris-Hcl pH 7.6, 137 mM NaCl, 0.02 % Tween-20) for 1 h at room temperature, before incubation in the primary antibody suspension (1:3000 dilution of Strep-Tactin AP conjugate (IBA) in TBST). The membranes were then washed three times (5 min each) with TBST before being incubated with polyclonal anti-mouse antibody-peroxidase conjugate (goat; Sigma) diluted 1:10,000 for 30 min at room temperature. The membranes were washed a again three times with TBST (5 min each). Western blots were developed with the Immobilon Crescendo chemiluminescent reagent (Merck) using a Gel Doc XR+ Imager (Bio-Rad)

2.4.3 Protein Purification

E. coli BL21(DE3) cells harbouring the pET21a-HUD-StrepII plasmid were obtained through transformation as described in section 2.3.9 and were growth in 5 mL LB supplemented with the appropriate antibiotics at 37 °C with shaking at 200 RPM overnight. This culture was used to inoculate (at 1:500) four 2 L flasks, each containing 500 mL of LB along with appropriate antibiotics. Cells were then grown to an OD_{600} of 0.8 at 37 °C with shaking at 200 RPM, and protein expression was induced with IPTG at 1 mM final concentration for 16 hours at 30 °C with shaking at 200 RPM. Cells were harvested by centrifugation at 8000 x g for 15 min at 4 °C, re-suspended in 20 mL 50 mM Tris-HCl pH 7.5, 150 mM NaCl, and lysed by sonnication (10 cycles at 60 % amplitude, with 10 s on and 50 s off), after the addition of cOmplete EDTA-free Protease Inhibitors (Roche) according to the manufacturers' specifications. Cell lysates were clarified by centrifugation at 35,000 x g for 30 min at 4 °C and the supernatant was applied to StrepTactin Sepharose (IBA) resin that had been pre-equilibrated with 50 mM Tris-HCl pH 7.5, 150 mM NaCl. The resin was then washed with 50 mM Tris-HCl pH 7.5, 1 M NaCl until protein could no longer be detected using Bradford reagent (Bio-Rad) and HUD-StrepII was eluted with 50 mM Tris-HCl pH 7.5, 150 mM NaCl, 2.5 mM D-desthiobiotin (IBA). The eluate was concentrated using a Vivaspin 20 concentration device (Vivascience) with a 5 kDA cut-off membrane, and buffer exchanged by serial concentration and re-dilution in 50 mM Tris-Hcl pH 7.5, 150 mM NaCl. The final protein amount obtained was 3.8 mg.

2.5 Hcp Secretion Assay

2.5.1 Preparation of supernatant samples

For detecting Hcp secreted into culture supernatant, *R. sphaeroides* WS8N wild type and Hcp-FLAG mutant strains were grown as described in sections 2.2.4 and 2.2.5. Thereafter, 13 mL of culture at OD_{700} were centrifuged for 15 minutes at 1500 x g and 4°C. After centrifugation, supernatants were transferred into a fresh tube and centrifuged again for 20 minutes at 1500 x g and 4°C. This step was repeated once more until the supernatants were clear. The supernatants were then collected and protein was precipitated by adding 1.45 mL ice-cold 100 % trichloroacetic acid (Sigma-Aldrich). The samples were inverted briefly to mix and incubated on ice overnight. Samples were then centrifuged for 30 minutes at 16,000 x g and 4°C. The precipitated protein pellets were washed with 1 mL ice-cold 90 % acetone (Sigma-Aldrich) by gentle agitation for 15 minutes and centrifuged again for 30 minutes at 16,000 x g and 4°C. Supernatants were discarded and the precipitated protein pellet were allowed to dry at room temperature before being re-suspended in 20 µL 2 X Laemmli sample buffer. Samples were denatured for 10 minutes at 95 °C.

2.5.2 Preparation of cell lysate samples

R. sphaeroides cell lysates were obtained by re-suspending 1 mL of cultures at OD_{700} 10 in 200 µL 2X Laemmli sample buffer (Merck). Samples were boiled for 10 minutes at 95 °C. *E. coli* cell lysates were obtained by re-suspending 1 mL of cultures at OD_{600} 0.5 in 50 µL 2X Laemmli sample buffer Samples were boiled for 10 minutes at 95 °C.

Samples were subjected to SDS-PAGE analysis and Western blotting using an anti-FLAG antibody, as described in section 2.4.1. An additional Western blot was performed to assess the efficiency of cell lysis using using a polyclonal antibody against TlpT, a cytoplasmic chemosensory receptor. Anti-TlpT Western blots were performed as descibed for anti-FLAG blots with the following modifications: Membranes were probed with 0.75 µg/mL anti-TlpT antibody produced in rabbit (Abgent) diluted in 5 % milk powder in TBST overnight at 4 °C. The secondary antibody used was anti-rabbit IgG (whole molecule)–peroxidase antibody produced in goat (Merck) diluted 1:10,000 in 5 % milk powder in TBST. Immobilon Forte Western HRP substrate (Millipore) was applied to the membranes and Western blots were developed using Amersham Hyperfilm ECL (GE) in an X-ray film processor (Optimax).

2.6 Fluorescence Microscopy

5 cm diameter Petri dishes with a 3 cm diameter glass window were used to visualise *R. sphaeroides* WS8N cells expressing TssB-PpFbFP. 6 µL of bacterial culture was placed onto a 1X Vogel-Bonner medium agar (2 % w/v) pad, which was then inverted in order to sandwich the cells between the agar pad and the glass bottom of the Petri dish. Samples were imaged using a Zeiss Axio Observer inverted widefield microscope equipped with a 63X Plan Apochromat oil-immersion objective, Zeiss HXP 120 illuminator for excitation, Zeiss MRm camera, Definite Focus system, Zeiss 90 HE LED filter set, and Zeiss Zen software. Fluorescence images were acquired every 2 s for a total of 120

s using an exposure time of 150 ms. Acquired data was processed using the Zeiss-associated ZEN software (ZEN Blue) and FIJI.

Chapter 3

Bioinformatic analysis of *Rhodobacter sphaeroides* WS8N T6SS

3.1 Introduction

To date, the T6SS in the Rhodobacter genus remains uncharacterised, despite its presence in *R. sphaeroides* WS8N being noticed following the publication of the DNA sequence of its genome in 2011[99]. This chapter aims to provide a tentative bioinformatic analysis of the *R. sphaeroides* WS8N T6SS and compare it to experimentally studied T6SSs described in the literature. For proteins that bear no homology to any structural components of characterised T6SSs, T6SS-associated genes, effectors or immunity proteins, a more thorough bioinformatic analysis was conducted.

3.2 Identification of T6SS genetic loci in Rhodobacteraceae

The genes encoding the core components of the T6SS (*tss*) are usually organised within one genetic cluster alongside various accessory genes (T6SS-associated genes; *tag*), the function of many of which remains unknown[100]. A bioinformatic analysis of the genome of *R. sphaeroides* WS8N[99] revealed the presence of genes encoding homologues of the 13 core T6SS proteins, TssA-M, an additional four proteins known to be involved in T6SS regulation TagE, TagF, TagG and TagH, the T6SS tip sharpening protein PAAR, the peptidoglycan-binding protein TagL and seven more hypothetical proteins. This ensemble represents the only T6SS cluster of *R. sphaeroides* WS8N, it is located on chromosome 2 and is divided into what appears to be five operons (figure 3.1). No T6SS protein homologs were identified outside of the T6SS cluster by HMMER and BLASTp searches using the SecReT6 database[101].

The first operon of the identified T6SS cluster contains six largely uncharacterised genes, RSWS8N_RS18670, RSWS8N_RS18675, RSWS8N_RS18680, RSWS8N_RS18685, RSWS8N_RS18690 and RSWS8N_RS18695. Of these, RSWS8N_RS18685 is the only gene encoding a protein homologous to a known T6SS protein, PAAR. The second operon comprises two genes, RSWS8N_RS18700 and *tssH* (*clpV*). The third operon contains three genes known to be involved in T6SS regulation, *tagE* (*ppkA*), *tagH* (*fha*) and *tagF* along with genes for structural components, *tssA-M*; At 37.9 kDa, the protein encoded by *tssA* represents the shorter form of this protein[26]. Finally, the fourth operon consists of *tssI* (*vgrG*), a second *tssM* analogue, RSWS8N_RS18790 and *tagG* (*pppA*), also involved in T6SS regulation, while the fifth one just contains a putative *tagL* gene. Table 3.1 shows each gene, the corresponding COG[12] and its putative function.

Along with the genome of *R. sphaeroides* WS8N, HMMER and BLASTp searches were conducted on all currently available Rhodobacteraceae genome sequences using SecReT6[101]. It is worth noting that there are no experimentally verified T6SS clusters in the Rhodobacteraceae family of alphaproteobacteria to date. A single T6SS cluster with identical organisation as described above was found in nine of the eleven sequenced *R. sphaeroides* strains (WS8N, 2.4.1, ATCC 17029, CH10, DSM 158, KD131, MBTLJ-8, MBTLJ-13, MBTLJ-20). Interestingly a near-identical cluster, yet to be experimentally verified, was also identified in *Paracoccus* strain ATCC 19367, suggesting that this T6SS is likely strain, and not species, specific (figure 3.2).

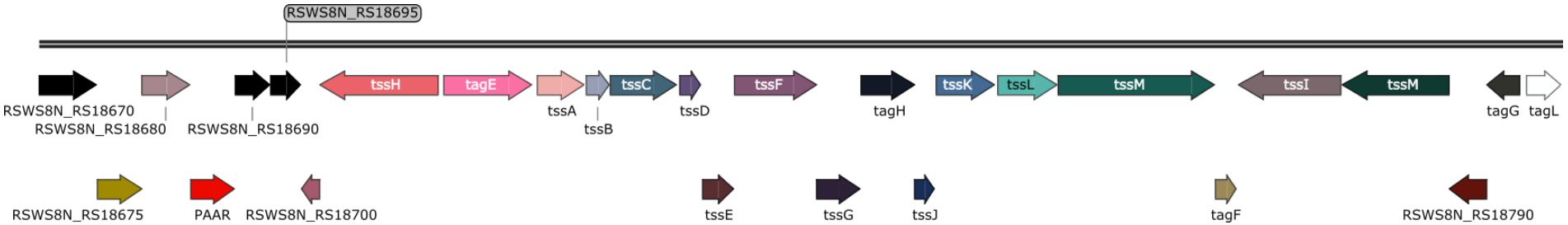
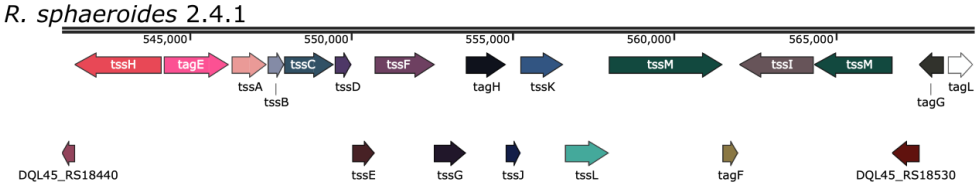


Figure 3.1: **Genetic organisation of the T6SS operons of *R. sphaeroides* WS8N.** The genes are indicated by the annotated locus tag or designated name as per the standardised nomenclature for T6SS[102].

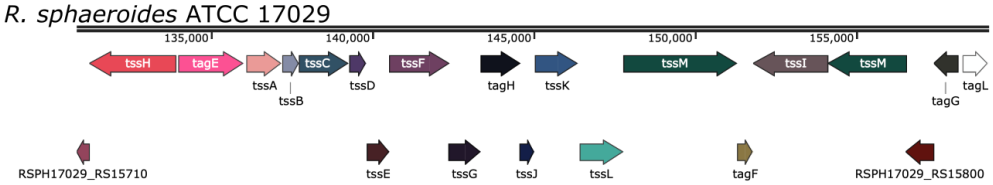
Locus tag	COG	Gene name	Protein description
RSWS8N_RS18670			Hypothetical protein
RSWS8N_RS18675			DUF2169 domain-containing protein
RSWS8N_RS18680			3-oxoacyl-ACP synthase
RSWS8N_RS18685	COG4104	PAAR	Type VI secretion system tip sharpening PAAR protein
RSWS8N_RS18690			Hypothetical protein
RSWS8N_RS18695			Hypothetical protein
RSWS8N_RS18700			Hypothetical protein
RSWS8N_RS18705	COG0542	tssH (clpV)	Type VI secretion system ATPase
RSWS8N_RS18710	COG0515	tagE (ppkA)	Serine/threonine protein kinase
RSWS8N_RS18715	COG3515	tssA	Type VI secretion system ImpA family N-terminal domain-containing protein
RSWS8N_RS18720	COG3516	tssB (vipA)	Type VI secretion system contractile sheath small subunit
RSWS8N_RS18725	COG3517	tssC (vipB)	Type VI secretion system contractile sheath large subunit
RSWS8N_RS18730	COG3157	tssD (hcp)	Type VI secretion system tube protein Hcp
RSWS8N_RS18735	COG3518	tssE	Type VI secretion system baseplate subunit TssE
RSWS8N_RS18740	COG3519	tssF	Type VI secretion system baseplate subunit TssF
RSWS8N_RS18745	COG3520	tssG	Type VI secretion system baseplate subunit TssG
RSWS8N_RS18750	COG3456	tagH (fha)	Type VI secretion system-associated Fha domain protein
RSWS8N_RS18755	COG3521	tssJ	Type VI secretion system membrane complex lipoprotein, tssJ
RSWS8N_RS18760	COG3522	tssK	Type VI secretion system baseplate subunit TssK
RSWS8N_RS18765	COG3455	tssL	Type VI secretion system membrane complex protein TssL, long form
RSWS8N_RS18770	COG3523	tssM	Type VI secretion system membrane complex protein TssM
RSWS8N_RS18775	COG3913	tagF	DUF2094 domain-containing protein
RSWS8N_RS18780	COG3501	tssI (vgrG)	Type VI secretion system tip protein VgrG
RSWS8N_RS18785	COG3523	tssM	Type VI secretion system membrane complex protein TssM
RSWS8N_RS18790			M15 family metallopeptidase
RSWS8N_RS18795	COG0631	tagG (pppA)	Serine/threonine protein phosphatase
RSWS8N_RS18800	COG2885	tagL	OmpA family protein

Table 3.1: List of core gene and accessory components of *R. sphaeroides* WS8N T6SS and their putative function and COG classification. T6SS homologues were identified using NCBI, BLASTp and Phyre2.

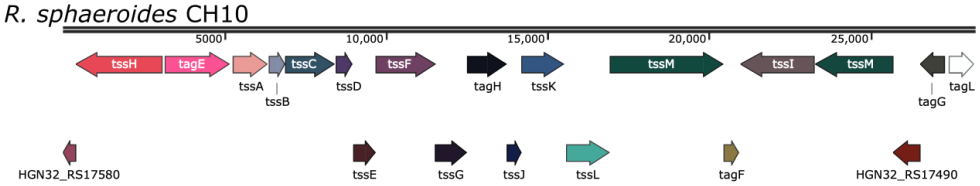
R. sphaeroides 2.4.1



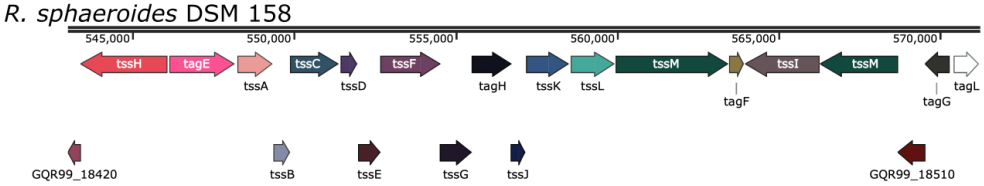
R. sphaeroides ATCC 17029



R. sphaeroides CH10



R. sphaeroides DSM 158



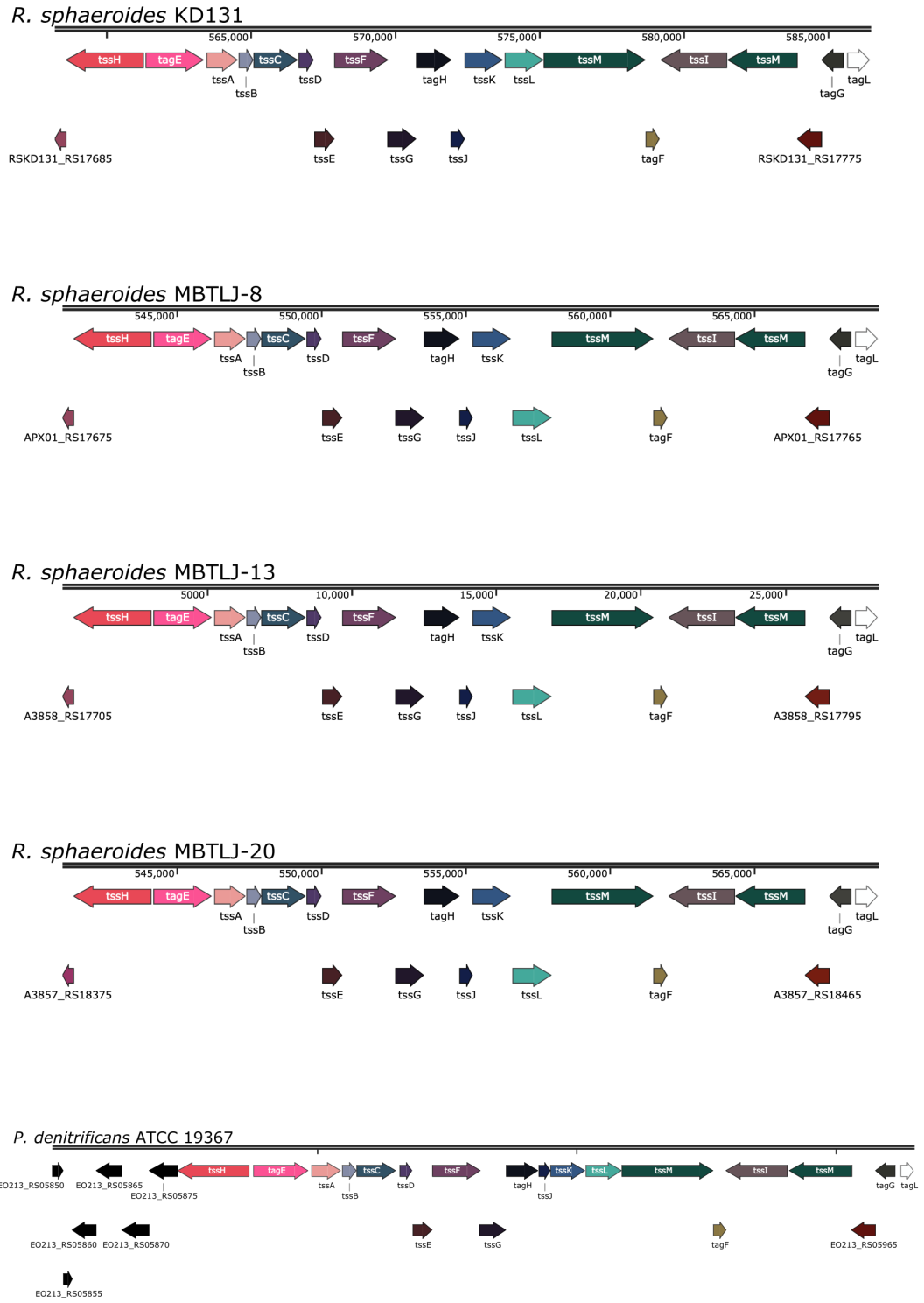


Figure 3.2: **Genetic organisation of the T6SS gene clusters of sequenced Rhodobacteraceae family members.** The near-identical, also experimentally uncharacterised, T6SS cluster identified in *P. denitrificans* is also shown. The genes are indicated by the annotated locus tag or designated name as per the standardised nomenclature for T6SS[102].

3.3 *In silico* analysis of the structural components of 20 T6SS clusters from phylogenetic group i3

More than 25% of proteobacteria encode at least one T6SS in their genome[9]. T6SSs are encoded by large gene clusters that vary in genetic organisation and can be divided into six sub-families, i1, i2, i3, i4a, i4b and i5[12, 13]. Two additional evolutionarily divergent T6SS-like systems, which share a common mode of action with canonical T6SS have been designated T6SS^{ii} and T6SS^{iii}[14, 15]. Bioinformatic analysis using the SecRet6 database predicts the *R. sphaeroides* T6SS to belong to the i3 sub-family [13, 14, 101, 103]. An *in silico* analysis comparing the structural components (TssA-M) of twenty T6SS clusters from the i3 phylogenetic group and the corresponding *R. sphaeroides* T6SS structural proteins (figure 3.3) was carried out, whereby the percentage identity and coverage for each relevant protein from each T6SS cluster was calculated in relation to the corresponding protein from *R. sphaeroides* WS8N. This was assessed using bit score, denoted by coloured cells as indicated in the figure legend, which is an indicator of sequence similarity that is independent of query sequence length and database size and that is normalised based on the raw pairwise alignment score. Where possible, experimentally verified T6SS were included in this analysis; for alphaproteobacteria like *R. sphaeroides*, there were no experimentally verified i3 T6SSs at the time this thesis was written. To get a better sense of the organisms with i3 T6SSs, a taxonomic distribution analysis was also carried out and shown in Figure 3.4. Unsurprisingly, of the i3 T6SS clusters analysed here, those most similar to *R. sphaeroides* are clusters belonging to other alphaproteobacteria (figures 3.3 and 3.4); notably

T6SS clusters known to be involved in metal ion acquisition do not bear more homology to the *R. sphaeroides* T6SS cluster than clusters that perform other functions.

3.4 *in silico* analysis of the structural components of T6SS clusters across phylogenetic groups

An *in silico* analysis of the structural components of *R. sphaeroides* T6SS was also carried out against T6SS clusters across phylogenetic groups [12] (figure 3.5); five T6SS clusters per phylogenetic group were included. As in section 3.3, the percentage identity, percentage coverage and bit score for each protein from each T6SS cluster was calculated in relation to the corresponding protein from *R. sphaeroides* WS8N. Similarly to before, a taxonomy of the analysed strains was also performed (see Figure 3.6). As expected, the *R. sphaeroides* T6SS cluster bears most homology to clusters of the i3 classification (figure 3.5 and, like with the i3 analysis, T6SSs involved in metal ion acquisition are not more related to the T6SS of *R. sphaeroides* than systems that have other roles. Beyond clusters that belong to the i3 group, the *R. sphaeroides* T6SS does not seem to be a close relative to T6SSs from any of the other phylogenetic groups, with bit scores for most of these pairwise comparisons being in the same range.

Strain	SecReT6 Identifier		TssA	TssB	TssC	TssD	TssE	TssF	TssG	TssH	TssI	TssJ	TssK	TssL	TssM
Acidovorax citrulli AAC00-1	T6SS00164	Identity (%)	31.67	46.01	57.67	23.87	27.03	33.33	33.33	52.55		29.69	31.84	32.26	30.74
		Coverage (%	48	85	96	93	76	99	75	99		68	98	82	99
Azoarcus olearius sp. BH72	T6SS00161	Identity (%)	27.17	46.02	56.65	38.19	33.33	35.45	34.49	56.57	38.55	24.68	33.64	33.58	30.43
		Coverage (%	96	100	96	85	75	98	87	99	100	88	95	86	99
Bordetella bronchiseptica RB50	T6SS00009	Identity (%)	47.37	49.38	58.52	27.67	30.5	35.42	31.16	58.1	38.97	27.44	34.25	34.62	33.01
		Coverage (%	21	82	96	95	73	100	73	99	88	91	95	91	99
Bradyrhizobium japonicum J5	T6SS01063	Identity (%)		45.98	54	31.9	29.71	30.25	30.19	51.97	34.98		27.15	33.52	30.81
		Coverage (%)		96	96	97	67	99	80	96	98		96	67	92
Burkholderia pseudomallei K96243	T6SS01292	Identity (%)	33.09	45.66	55.16	26.42	28.17	36.82	27.75	54.31	39.79	29.14	29.64	33.08	32.82
		Coverage (%	36	83	98	96	70	100	70	99	98	87	93	85	98
Burkholderia pseudomallei K96243	T6SS01293	Identity (%)	31.62	46.67	56.09	33.1	31.18	33.28	30.06	49.66	35.56	25.93	30.28	28.68	30.46
		Coverage (%	39	88	99	88	89	98	85	97	79	75	95	86	97
Burkholderia pseudomallei K96243	T6SS01294	Identity (%)	33.81	47.88	54.37	34.48	26.03	35	32.17	49.52	39.33	29.1	29.56	31.18	28.73
		Coverage (%	44	81	99	86	67	99	81	96	71	80	95	76	96
Burkholderia pseudomallei K96243	T6SS01295	Identity (%)	36.23	42.37	49.69	26.14	35.29	33.51	26.07	43.19	37.81		29.08	26.69	24.13
		Coverage (%	22	93	94	86	41	59	91	90	57		94	49	54
Burkholderia thailandensis E264	T6SS00114	Identity (%)	36.23	43.02	49.69	25.31	30	33.78	25.38	43.6	355.39	31.37	29.08	26.85	24.17
		Coverage (%	37	93	94	92	77	59	91	89	68	25	99.4	49	54
Citrobacter rodentium DBS100	T6SS01013	Identity (%)	33.33	49.7	55.89	32.87	21.62	30.25	27.82	50.45	34.67	26.53	29.64	26.79	
		Coverage (%	39	93	99	86	40.8	99	77	97	83	26	96	76	
Enterobacter cloacae subsp. cloacae ATCC 13047	T6SS00395	Identity (%)	30.53	50.91	57.38	23.9	34.27	32.01	31.48	55.43	38.98	27.78	25.86	28.11	29.62
		Coverage (%	36	90	96	96	67	98	85	99	93	73	95	92	99
Mesorhizobium loti MAFF303099	T6SS00007	Identity (%)	43.04	69.32	82.27	37.67	50.22	58.59	47.67	64.65	52	42.57	63.64	52.98	55.27
		Coverage (%	97	98	100	86	91	99	96	99	100	98	99	100	99
Paracoccus denitrificans PD1222	T6SS00159	Identity (%)	51.86	83.68	84.29	66.87	60	62.12	48.82	72.11	59.77	53.42	71.2	59.91	63.68
		Coverage (%	99	95	99	100	95	99	97	98	100	92	99	98	98
Pseudomonas aeruginosa PAO1	T6SS00003	Identity (%)	38.71	46.55	59.23	35.67	37.24	35.68	31.63	56.98	41.07	28.78	34.03	35.1	33.03
		Coverage (%	18	96	97	93	76	100	86	99	94	90	33.6	84	97
Pseudomonas fluorescens F113	T6SS00540	Identity (%)	40.32	47.56	58.93	32.5	36.84	35.74	33.23	55.46	41.46	29.05	33.03	34.17	33.46
		Coverage (%	17	93	96	96	68	100	90	99	94	88	96	86	91
Pseudomonas protegens Pf-5	T6SS00035	Identity (%)	26.82	46.95	59.71	30.14	34.33	35.27	33.23	55.7	39.65	32.82	33.57	34.76	33.24
		Coverage (%	96	91	96	87	69	100	86	99	97	77	96	85	91
Rhodobacter sphaeroides 2.4.1	T6SS00099	Identity (%)	99.72	100	99.4	100	98.3	99.03	98.49	98.2	98.31	97.33	99.32	98.23	97.87
		Coverage (%	100	100	99	100	100	100	100	100	100	100	100	100	100
Rhodobacter sphaeroides WS8N	NA	Identity (%)	100	100	100	100	100	100	100	100	100	100	100	100	100
		Coverage (%	100	100	100	100	100	100	100	100	100	100	100	100	100
Serratia marcescens RM66262	T6SS01264	Identity (%)	30.3	50.3	57.67	23.93	34.04	32.4	33.23	57.38	35.64		26.4	29.97	29.79
		Coverage (%	19	88	96	98	65	100	86	96	88		95	93	99
Sinorhizobium fredii USDA 257	T6SS00669	Identity (%)	42.36	74.71	82.04	34.97	49.57	55.59	45.24	65.42	51.04	41.61	65.91	53.22	56.98
		Coverage (%	96	95	99	100	90	100	94	99	100	98	99	99	99
Yersinia pseudotuberculosis YPIII	T6SS00260	Identity (%)	31.75	45.78	51.45	28.12	29.73	27.87	24.25	45.75	34.2	47.37	28.15	24.51	21.91
		Coverage (%	31	85	95	92	63	91	92	93	67	11	95	59	79

Figure 3.3: ***In silico* analysis of the structural components of *R. sphaeroides* T6SS and comparison with 20 T6SS clusters from the i3 phylogenetic group.**. *R. sphaeroides* WS8N (highlighted in grey) is the reference cluster for analysis. T6SS clusters known to function in metal ion acquisition are highlighted in pink. The SecReT6 identifier [101] is given for each cluster. Cells containing identity and coverage metrics are colour coded according to their maximum bit score provided by the NCBI blastp search tool[104]. Bit score is an indicator of sequence similarity that is independent of query sequence length and database size and that is normalised based on the raw pairwise alignment score; red cells indicate the most similar alignment (score $>$ 200), followed by magenta (score = 80-200), green (score = 50-80), blue (score = 40-50) and black cells (score $<$ 40). Grey cells indicate proteins for which no significant similarity was detected when aligned with the corresponding *R. sphaeroides* protein. White cells indicate proteins that could not be found in a given T6SS cluster. In cases where more than one analogue of a specific T6SS structural component was found in a given cluster the analogue most similar to that of *R. sphaeroides* was included in the table.

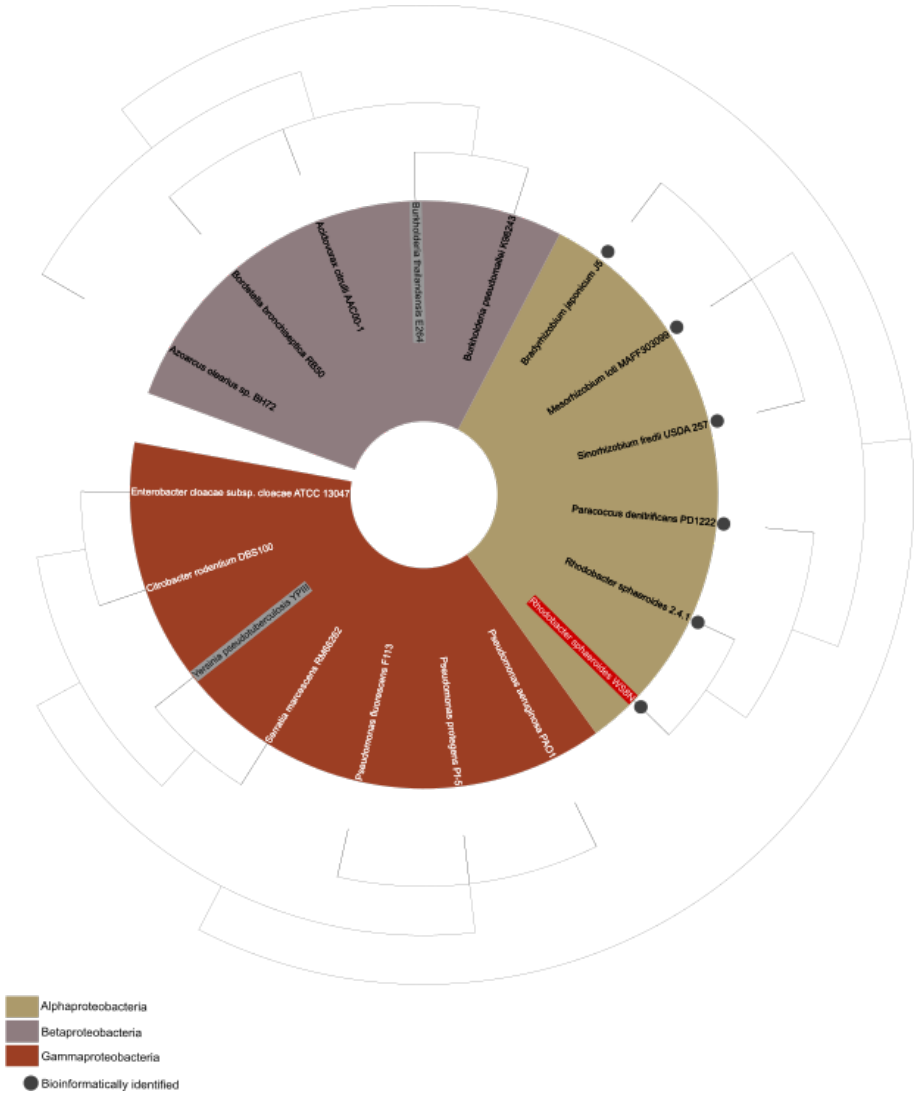
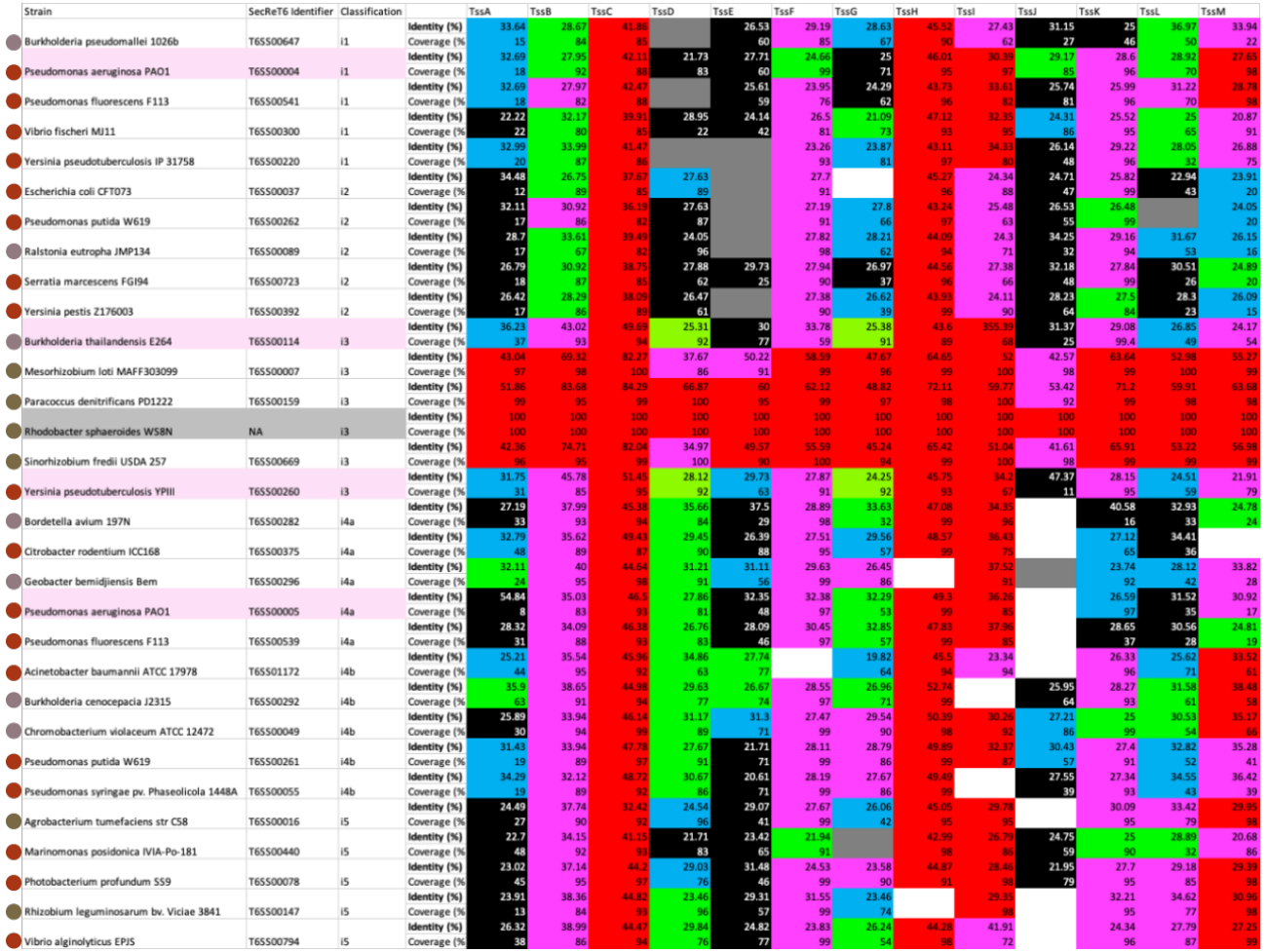


Figure 3.4: **Taxonomic distribution of *R. sphaeroides* and of the strains used in the analysis of T6SS clusters of the i3 classification.** *R. sphaeroides* is highlighted in red. Strains possessing an i3 T6SS cluster demonstrated to be involved in metal ion acquisition are highlighted in grey. A grey dot indicates a strain encoding an i3 T6SS cluster that has not been experimentally verified.



Strain	SecReT6 identifier	Classification		TssA	TssB	TssC	TssD	TssE	TssF	TssG	TssH	TssI	TssJ	TssK	TssL	TssM
Burkholderia pseudomallei 1026b	T6SS00647	i1	Identity (%)	33.64	28.67	41.86		26.53	29.19	28.63	45.52	27.43	31.15	25	36.97	33.94
			Coverage (%	15	84	85		60	85	67	90	62	27	46	50	22
Pseudomonas aeruginosa PAO1	T6SS00004	i1	Identity (%)	32.69	27.95	42.11	21.73	27.71	24.66	25	46.01	30.39	29.17	28.6	28.92	27.65
			Coverage (%	18	92	88	83	60	99	71	95	97	85	96	70	98
Pseudomonas fluorescens F113	T6SS00541	i1	Identity (%)	32.69	27.97	42.47		25.61	23.95	24.29	43.73	33.61	25.74	25.99	31.22	28.78
			Coverage (%	18	82	88		59	76	62	96	82	81	96	70	98
Vibrio fischeri MJ11	T6SS00300	i1	Identity (%)	22.22	32.17	39.91	28.95	24.14	26.5	21.09	47.12	32.35	24.31	25.52	25	20.87
			Coverage (%	22	80	85	22	42	81	73	93	95	86	95	65	91
Yersinia pseudotuberculosis IP 31758	T6SS00220	i1	Identity (%)	32.99	33.99	41.47			23.26	23.87	43.11	34.33	26.14	29.22	28.05	26.88
			Coverage (%	20	87	86			93	81	97	80	48	96	32	75
Escherichia coli CFT073	T6SS00037	i2	Identity (%)	34.48	26.75	37.67	27.63		27.7		45.27	24.34	24.71	25.82	22.94	23.91
			Coverage (%	12	89	85	89		91		96	88	47	99	43	20
Pseudomonas putida W619	T6SS00262	i2	Identity (%)	32.11	30.92	36.19	27.63		27.19	27.8	43.24	25.48	26.53	26.48		24.05
			Coverage (%	17	86	82	87		91	66	97	63	55	99		20
Ralstonia eutropha JMP134	T6SS00089	i2	Identity (%)	28.7	33.61	39.49	24.05		27.82	28.21	44.09	24.3	34.25	29.16	31.67	26.15
			Coverage (%	17	67	82	96		98	62	94	71	32	94	53	16
Serratia marcescens FGI94	T6SS00723	i2	Identity (%)	26.79	30.92	38.75	27.88	29.73	27.94	26.97	44.56	27.38	32.18	27.84	30.51	24.89
			Coverage (%	18	87	85	62	25	90	37	96	66	48	99	26	20
Yersinia pestis Z176003	T6SS00392	i2	Identity (%)	26.42	28.29	38.09	26.47		27.38	26.62	43.93	24.11	28.23	27.5	28.3	26.09
			Coverage (%	17	86	89	61		90	39	99	90	64	84	23	15
Burkholderia thailandensis E264	T6SS00114	i3	Identity (%)	36.23	43.02	49.69	25.31	30	33.78	25.38	43.6	355.39	31.37	29.08	26.85	24.17
			Coverage (%	37	93	94	92	77	59	91	89	68	25	99.4	49	54
Mesorhizobium loti MAFF303099	T6SS00007	i3	Identity (%)	43.04	69.32	82.27	37.67	50.22	58.59	47.67	64.65	52	42.57	63.64	52.98	55.27
			Coverage (%	97	98	100	86	91	99	96	99	100	98	99	100	99
Paracoccus denitrificans PD1222	T6SS00159	i3	Identity (%)	51.86	83.68	84.29	66.87	60	62.12	48.82	72.11	59.77	53.42	71.2	59.91	63.68
			Coverage (%	99	95	99	100	95	99	97	98	100	92	99	98	98
Rhodobacter sphaeroides WS8N	NA	i3	Identity (%)	100	100	100	100	100	100	100	100	100	100	100	100	100
			Coverage (%	100	100	100	100	100	100	100	100	100	100	100	100	100
Sinorhizobium fredii USDA 257	T6SS00669	i3	Identity (%)	42.36	74.71	82.04	34.97	49.57	55.59	45.24	65.42	51.04	41.61	65.91	53.22	56.98
			Coverage (%	96	95	99	100	90	100	94	99	100	98	99	99	99
Yersinia pseudotuberculosis YPIII	T6SS00260	i3	Identity (%)	31.75	45.78	51.45	28.12	29.73	27.87	24.25	45.75	34.2	47.37	28.15	24.51	21.91
			Coverage (%	31	85	95	92	63	91	92	93	67	11	95	59	79
Bordetella avium 197N	T6SS00282	i4a	Identity (%)	27.19	37.99	45.38	35.66	37.5	28.89	33.63	47.08	34.35		40.58	32.93	24.78
			Coverage (%	33	93	94	84	29	98	32	99	96		16	33	24
Citrobacter rodentium ICC168	T6SS00375	i4a	Identity (%)	32.79	35.62	49.43	29.45	26.39	27.51	29.56	48.57	36.43		27.12	34.41	
			Coverage (%	48	89	87	90	88	95	57	99	75		65	36	
Geobacter bemidjiensis Bem	T6SS00296	i4a	Identity (%)	32.11	40	44.64	31.21	31.11	29.63	26.45		37.52		23.74	28.12	33.82
			Coverage (%	24	95	98	91	56	99	86		91		92	42	28
Pseudomonas aeruginosa PAO1	T6SS00005	i4a	Identity (%)	54.84	35.03	46.5	27.86	32.35	32.38	32.29	49.3	36.26		26.59	31.52	30.92
			Coverage (%	8	83	93	81	48	97	53	99	85		97	35	17
Pseudomonas fluorescens F113	T6SS00539	i4a	Identity (%)	28.32	34.09	46.38	26.76	28.09	30.45	32.85	47.83	37.96		28.65	30.56	24.81
			Coverage (%	31	88	93	83	46	97	57	99	85		37	28	19
Acinetobacter baumannii ATCC 17978	T6SS01172	i4b	Identity (%)	25.21	35.54	45.96	34.86	27.74		19.82	45.5	23.34		26.33	25.62	33.52
			Coverage (%	44	95	92	63	77		64	94	94		96	71	61
Burkholderia cenocepacia J2315	T6SS00292	i4b	Identity (%)	35.9	38.65	44.98	29.63	26.67	28.55	26.96	52.74		25.95	28.27	31.58	38.48
			Coverage (%	63	91	94	77	74	97	71	95		64	93	61	58
Chromobacterium violaceum ATCC 12472	T6SS00049	i4b	Identity (%)	25.89	33.94	46.14	31.17	31.3	27.47	29.54	50.39	30.26	27.21	25	30.53	35.17
			Coverage (%	30	94	99	89	71	99	90	98	92	86	99	54	66
Pseudomonas putida W619	T6SS00261	i4b	Identity (%)	31.43	33.94	47.78	27.67	21.71	28.11	28.79	49.89	32.37	30.43	27.4	32.82	35.28
			Coverage (%	19	89	97	91	71	99	86	99	87	57	91	52	41
Pseudomonas syringae pv. Phaseolicola 1448A	T6SS00055	i4b	Identity (%)	34.29	32.12	48.72	30.67	20.61	28.19	27.67	49.49		27.55	27.34	34.55	36.42
			Coverage (%	19	89	92	86	71	99	86	99		39	93	43	39
Agrobacterium tumefaciens str C58	T6SS00016	i5	Identity (%)	24.49	37.74	32.42	24.54	29.07	27.67	26.06	45.05	29.78		30.09	33.42	29.95
			Coverage (%	27	90	92	96	41	99	42	95	95		95	79	98
Marinomonas posidonica IVIA-Po-181	T6SS00440	i5	Identity (%)	22.7	34.15	41.15	21.71	23.42	21.94		42.99	26.79	24.75	25	28.89	20.68
			Coverage (%	48	92	93	83	65	91		98	86	59	90	32	86
Photobacterium profundum SS9	T6SS00078	i5	Identity (%)	23.02	37.14	44.2	29.03	31.48	24.53	23.58	44.87	28.46	21.95	27.7	29.18	29.39
			Coverage (%	45	95	97	76	46	99	90	91	98	79	95	85	98
Rhizobium leguminosarum bv. Viciae 3841	T6SS00147	i5	Identity (%)	23.91	38.36	44.82	23.46	29.31	31.55	23.46		29.35		32.21	34.62	30.96
			Coverage (%	13	84	93	96	57	99	74		98		95	77	98
Vibrio alginolyticus EPJS	T6SS00794	i5	Identity (%)	26.32	38.99	44.47	29.84	24.82	23.83	26.24	44.28	41.91		24.34	27.79	27.25
			Coverage (%	38	86	94	76	77	99	54	98	72		96	87	99

Figure 3.5: ***In silico* analysis of the structural components of *R. sphaeroides* T6SS and comparison with 5 T6SS clusters from each of the five phylogenetic groups.**. *R. sphaeroides* WS8N (highlighted in grey) is the reference cluster for analysis. T6SS clusters known to function in metal ion acquisition are highlighted in pink. The SecReT6 identifier [101] is given for each cluster. Cells containing identity and coverage metrics are colour coded according to their maximum bit score provided by the NCBI blastp search tool[104]. Bit score is an indicator of sequence similarity that is independent of query sequence length and database size and that is normalised based on the raw pairwise alignment score; red cells indicate the most similar alignment (score $>$ 200), followed by magenta (score = 80-200), green (score = 50-80), blue (score = 40-50) and black cells (score $<$ 40). Grey cells indicate proteins for which no significant similarity was detected when aligned with the corresponding *R. sphaeroides* protein. White cells indicate proteins that could not be found in a given T6SS cluster. Strains appearing in multiple phylogenetic groups have multiple T6SS. In cases where more than one analogue of a specific T6SS structural component was found in a given cluster the analogue most similar to that of *R. sphaeroides* was included in the table.

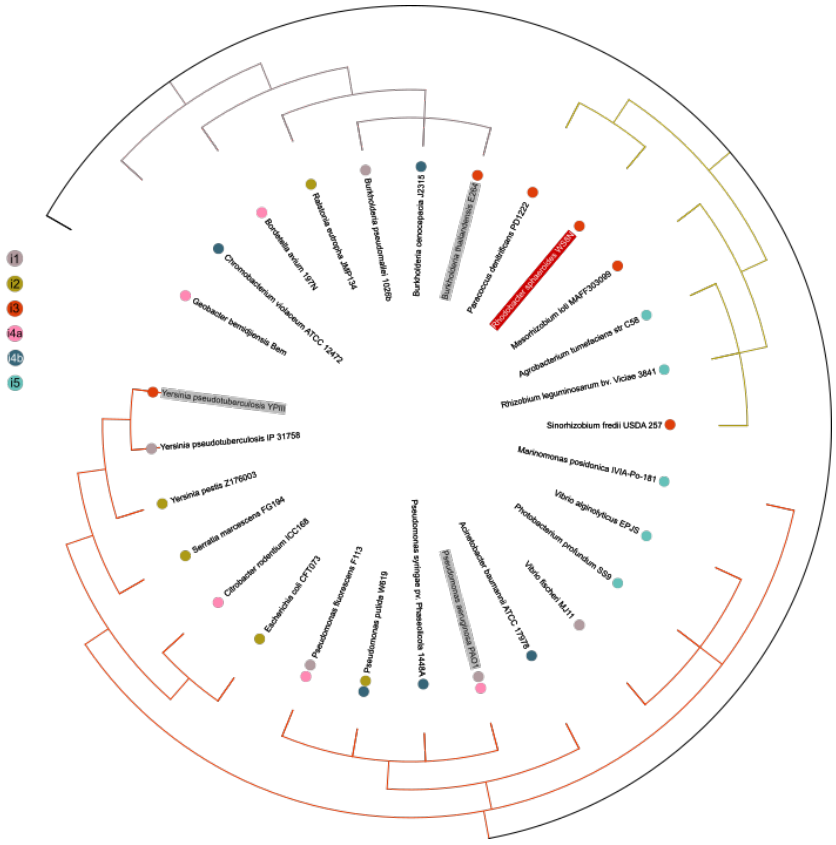


Figure 3.6: **Taxonomic distribution of *R. sphaeroides* and of the strains used in the analysis of T6SS clusters across all type i phylogenetic groups.** *R. sphaeroides* is highlighted in red. Strains possessing a T6SS cluster demonstrated to be involved in metal ion acquisition are highlighted in grey. This figure is not representative of each strain's complete arsenal of T6SS clusters, only the ones included in the analysis. T6SS cluster phylogenetic classification is designated by the coloured dot next to each strain as per the key. Alphaproteobacteria are shown in yellow branches, betaproteobacteria in grey and gammaproteobacteria in red.

3.5 Bioinformatic analysis of the *R. sphaeroides* WS8N VgrG protein

R. sphaeroides WS8N encodes one VgrG (TssI) protein (figure 3.7). VgrG proteins fall into one of two categories, canonical or evolved. While the former are solely composed of the gp5- and gp27-like domains which comprise the cell puncturing part of the T6SS apparatus, the latter can also carry out effector functions. It is through the C-terminal extension, which usually encodes a domain with enzymatic activity, that evolved VgrGs perform their effector function. The VgrG protein of *R. sphaeroides* WS8N was compared to characterised VgrG proteins as well as VgrG proteins of T6SS clusters known to be involved in metal ion acquisition (figure 3.8). The domains shown in figure 3.8 were obtained using both a conserved domain search (NCBI) and comparison with studies reported in the literature[105–108]; only C-terminal domains with enzymatic activity are shown.

Of the characterised VgrG proteins known to be evolved VgrGs included in figure 3.8, the C-terminal domain of VgrG1 from *V. cholerae* is known to induce actin cross-linking in host cells[111], and the C-terminal domain of VgrG3 from the same organisms was shown to target peptidoglycan[106]. The C-terminal domain of VgrG2b from *P. aeruginosa* encodes a metallopeptidase proposed to interfere with enzymes involved in peptidoglycan remodelling[107], the C-terminal domain of VgrG1 from *Aeromonas* has actin-disrupting ADP-ribosyltransferase activity[108], and the C-terminal domain of VgrG5 from *Burkholderia* has been shown to facilitate membrane fusion during intarcellular spread by *B. pseudomallei* during infection[112]. By contrast VgrG1

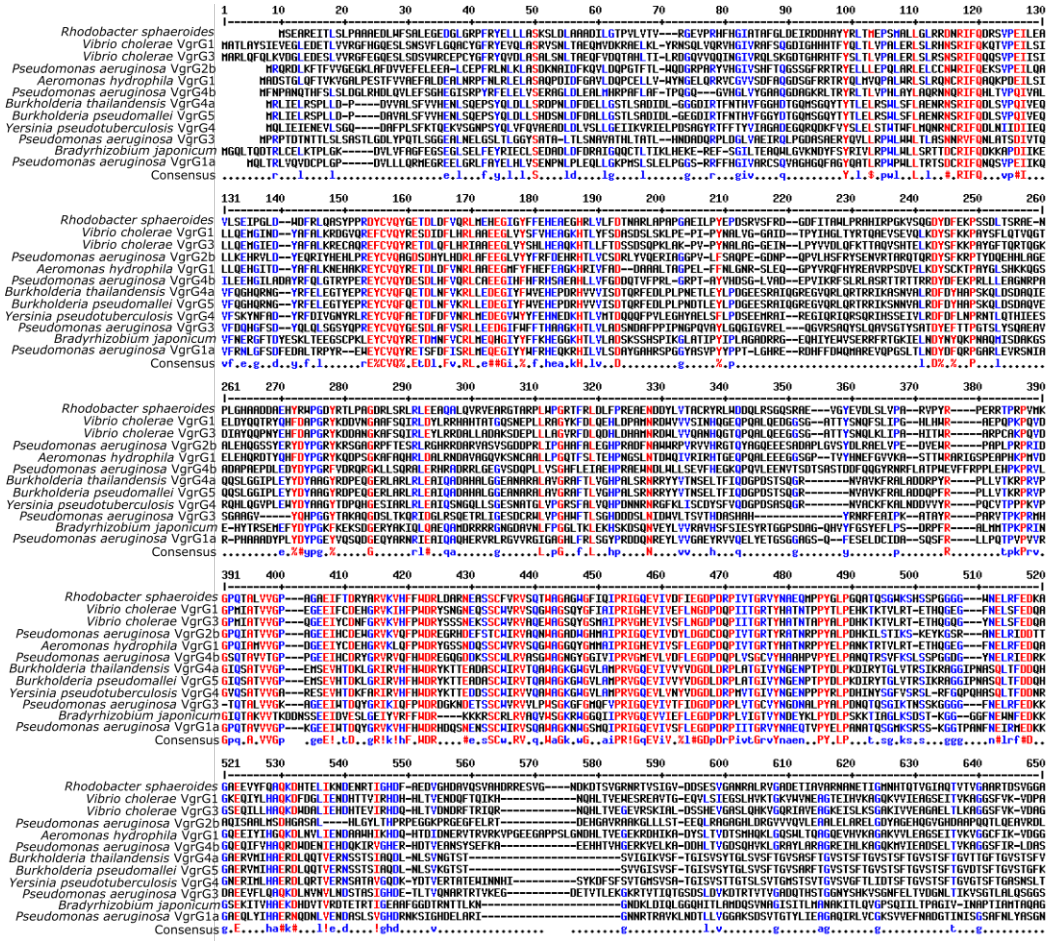


Figure 3.7: **Amino acid sequence alignment of VgrG proteins from various organisms.** The amino acid sequence of the core VgrG domain of the *R. sphaeroides* VgrG protein was aligned with experimentally verified VgrG proteins from several bacterial species. Amino acid sequences were aligned using Multalin[109], which uses the BLOSUM62 symbol comparison table. For the consensus sequence ! is either an I or V amino acid, $ is L or M, % is F or Y, and # is any one of NDQEBZ.

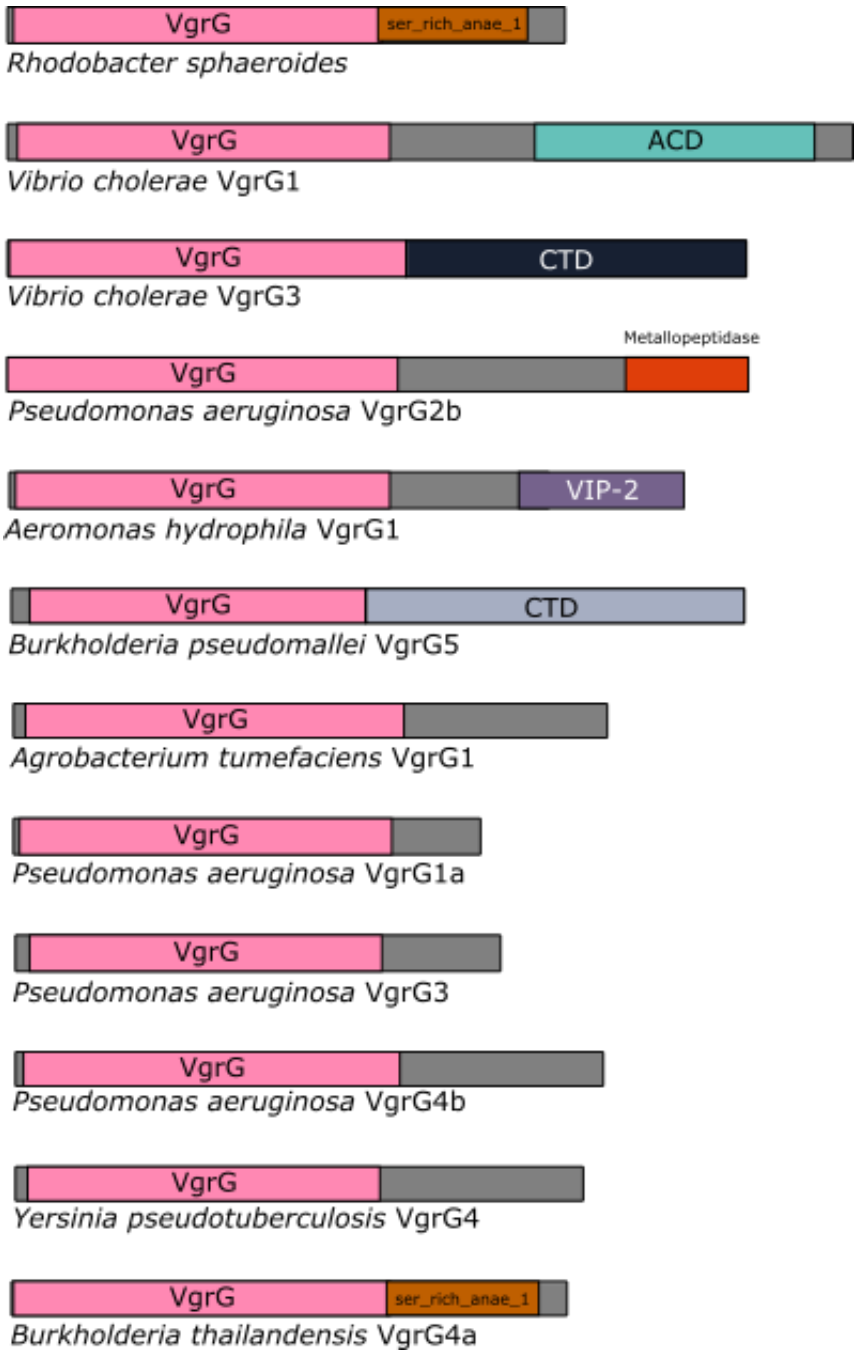


Figure 3.8: **Graphic representation of the domains predicted to be present in VgrG proteins from various bacteria.** The pink domain labelled VgrG represents the gp5/gp27 core which comprises the VgrG superfamily domain of canonical VgrG proteins. Domains labelled CTD (C-terminal domain) have been shown to possess enzymatic effector activity experimentally, but bioinformatic analysis has failed to identify the specific region of the C-terminus responsible. Other abbreviations are as follows: ACD, actin cross-linking domain; VIP, vegetative insecticidal protein. The figure was prepared using Illustrator for Biological Sequences[110].

from *A. tumefaciens*, and VgrG1a, VgrG3 and VgrG4b from *P. aeruginosa* are canonical VgrG proteins[38, 113]. VgrG4 from *Y. pseudotuberculosis* and VgrG4a from *B. thailandensis*, also included in figure 3.8 , are encoded in T6SS clusters experimentally demonstrated to be involved in metal acquisition.

Based on the analysis presented in figure 3.8, no recognisable effector domain could be identified in the C-terminal region of VgrG of *R. sphaeroides* WS8N using sequence similarity or structure similarity criteria (through use of conserved domain search (NCBI)[114] and Phyre2[115], respectively). This suggests that the *R. sphaeroides* WS8N VgrG protein belongs to the group of canonical VgrG proteins. Although no enzymatic effector domain was identified, a serine-rich region in the C-terminus of the *R. sphaeroides* WS8N VgrG protein was detected using NCBI conserved domain search (figure 3.9). Species encoding such domains are often capable of anaerobic metabolism[116]. Interestingly, the VgrG4a protein of *B. thailandensis* also possesses a C-terminal serine-rich domain (figure 3.9). Deletion of VgrG4a from *B. thailandensis* abrogates secretion of TseM by T6SS-4 which functions to sequester Mn^{2+} ions from the environment[44]. The *R. sphaeroides* WS8N VgrG protein shares an amino acid identity of 31.20 % with the *B. thailandensis* VgrG4a protein. The C-terminal regions share an amino acid identity of 34.85 %, whilst the N-terminal serine rich regions in these VgrG proteins share an amino acid identity of 25.57 %. Amino acid sequences were aligned using Clustal Omega[117].

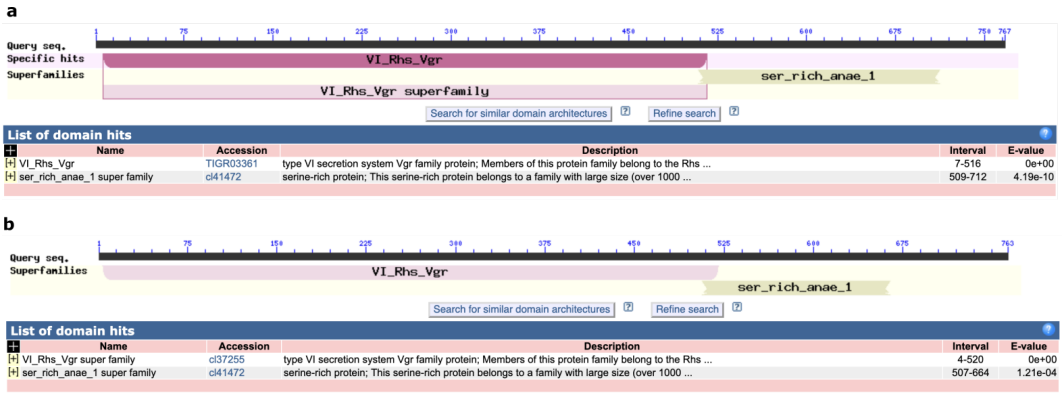


Figure 3.9: **Conserved domain prediction for the VgrG protein of (a) *R. sphaeroides* WS8N and (b) *B. thailandensis* E264.** Conserved domains were predicted using CD-search (NCBI)[114].

3.6 RSWS8N_RS18685 encodes a putative PAAR protein

An NCBI conserved domain search of the protein encoded by RSWS8N_RS18685 revealed a DUF4150-domain-containing protein. Members of the DUF4150 family are part of a diverse superfamily of PAAR-repeat proteins, known to be involved in type VI secretion[118]. At the start of this research no gene was annotated as encoding a PAAR protein in the *R. sphaeroides* WS8N genome and this agreed with the T6SS protein prediction analysis provided for Rhodobacteraceae by the SecReT6 database. Our prediction that RSWS8N_RS18685 encodes a PAAR protein was recently corroborated by the addition of *R. sphaeroides* WS8N to the SecReT6 database, where RSWS8N_RS18685 is indeed annotated as a PAAR component.

3.7 Bioinformatic analysis of the putative regulatory proteins found in the *R. sphaeroides* WS8N T6SS cluster

Genes encoding analogues of four proteins that are known to be involved in T6SS regulation are present in the *R. sphaeroides* WS8N T6SS cluster, *tagE*

(*ppkA*), *tagF*, *tagG* (*pppA*) and *tagH* (*fhA*). Each of these protein sequences was analysed using the NCBI Conserved Domain Search[114] (figure 3.10), and aligned with sequences from experimentally verified T6SS clusters (figures 3.11, 3.12, 3.13 and 3.14). All *R. sphaeroides* WS8N putative regulatory T6SS components were found to be very similar to experimentally verified proteins, something that suggests that they have similar roles in the regulation of T6SS of *R. sphaeroides* WS8N T6SS as in other bacterial species.



Figure 3.10: **Conserved domain search for the T6SS regulatory proteins present in the *R. sphaeroides* WS8N T6SS cluster.** (**a**) TagE (PpkA), (**b**) TagF, (**c**) TagG (PppA) and (**d**) TagH (Fha). Conserved domains were predicted using CD-search (NCBI)[114].

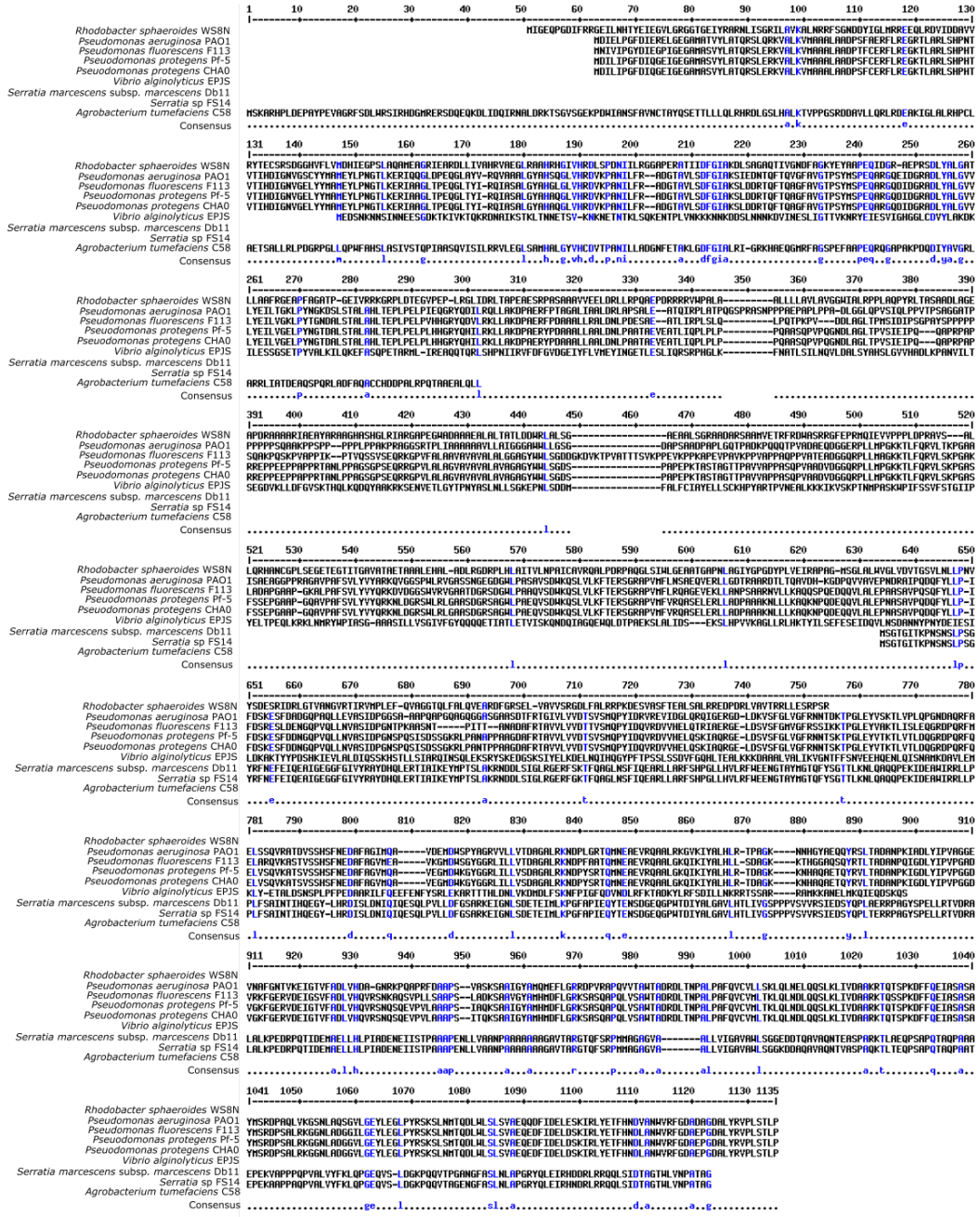


Figure 3.11: **Amino acid sequence alignment of the T6SS regulatory protein TagE (PpkA) from various organisms.** Amino acid sequences were aligned using Multalin[109] which uses the BLOSUM62 symbol comparison table. For the consensus sequence ! is either an I or V amino acid, $ is L or M, % is F or Y, and # is any one of NDQEBZ.

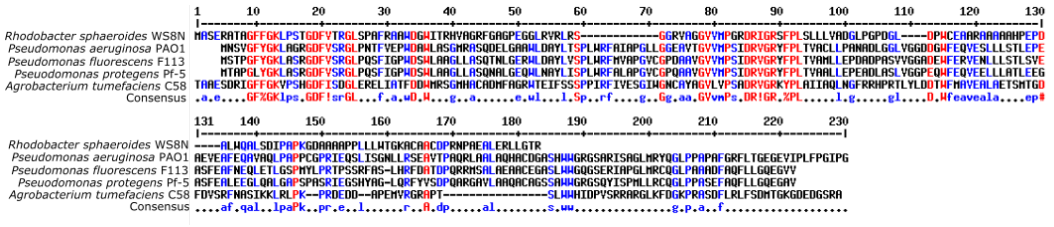


Figure 3.12: **Amino acid sequence alignment of the T6SS regulatory protein TagF from various organisms.** Amino acid sequences were aligned using Multalin[109] which uses the BLOSUM62 symbol comparison table. For the consensus sequence ! is either an I or V amino acid, $ is L or M, % is F or Y, and # is any one of NDQEBZ.

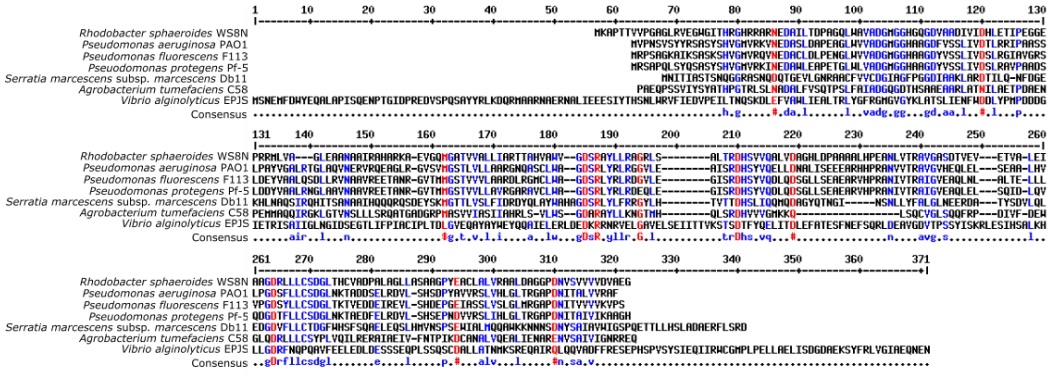


Figure 3.13: **Amino acid sequence alignment of the T6SS regulatory protein TagG (PppA) from various organisms.** Amino acid sequences were aligned using Multalin[109] which uses the BLOSUM62 symbol comparison table. For the consensus sequence ! is either an I or V amino acid, $ is L or M, % is F or Y, and # is any one of NDQEBZ.

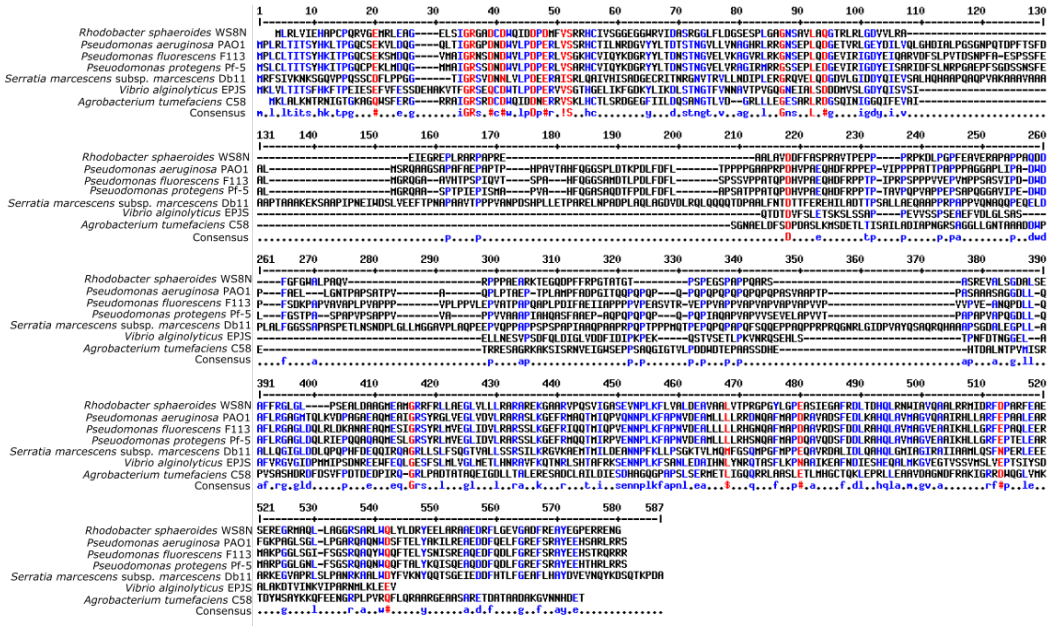


Figure 3.14: **Amino acid sequence alignment of the T6SS regulatory protein TagH (Fha) from various organisms.** Amino acid sequences were aligned using Multalin[109] which uses the BLOSUM62 symbol comparison table. For the consensus sequence ! is either an I or V amino acid, $ is L or M, % is F or Y, and # is any one of NDQEBZ.

3.8 RSWS8N_RS18675, RSWS8N_RS18680 and RSWS8N_RS18700 encode putative adaptor proteins

Bioinformatic analysis using the NCBI conserved domain search revealed that RSWS8N_RS18675 encodes a DUF2169 domain-containing protein. Adaptor proteins containing such domains have been shown to be necessary for T6SS effector secretion in *A. tumefaciens* [38]. RSWS8N_RS18680 encodes a protein with a PRK06147 domain. Genes encoding PRK06147 homologs are often found to be adjacent to T6SS genes and have recently been proposed to be a novel type of T6SS adaptor protein[119] .

Analysis of the protein encoded by RSWS8N_RS18700 with the NCBI conserved domain search predicted it to have long-chain-fatty-acid-CoA synthetase activity, based on its sequence similarity to the PRK07768 protein superfam-

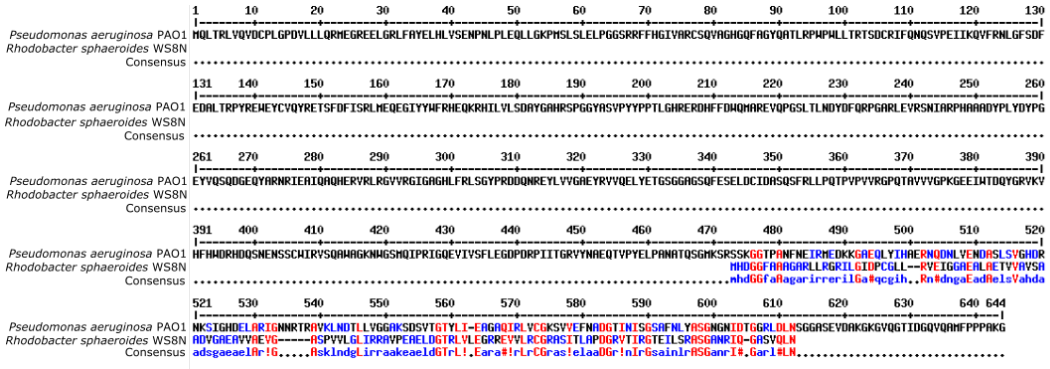


Figure 3.15: **Amino acid sequence alignment of the putative adaptor protein encoded by RSWS8N_RS18700 against VgrG1a from *P. aeruginosa* PAO1.** Amino acid sequences were aligned using Multalin[109] which uses the BLOSUM62 symbol comparison table. For the consensus sequence ! is either an I or V amino acid, $ is L or M, % is F or Y, and # is any one of NDQEBZ.

ily. There is no evidence in the current T6SS literature of PRK07768 homologs being involved in type six secretion, nonetheless further analysis using Phyre2 shed some light to this gene product. Phyre2 predicted with high confidence (97%) that this protein is a structural homolog of VgrG1a from *P. aeruginosa* PAO1; a sequence alignment of the protein encoded by RSWS8N_RS18700 and VgrG1a from *P. aeruginosa* PAO1 is shown in figure 3.15. Given that RSWS8N_RS18700 encodes a 132 amino acid polypeptide homologous only to the C terminus of VgrG1a from *P. aeruginosa* PAO1, it is conceivable that RSWS8N_RS18700 is another T6SS adaptor gene.

3.9 RSWS8N_RS18790 encodes a putative effector protein with peptidase activity

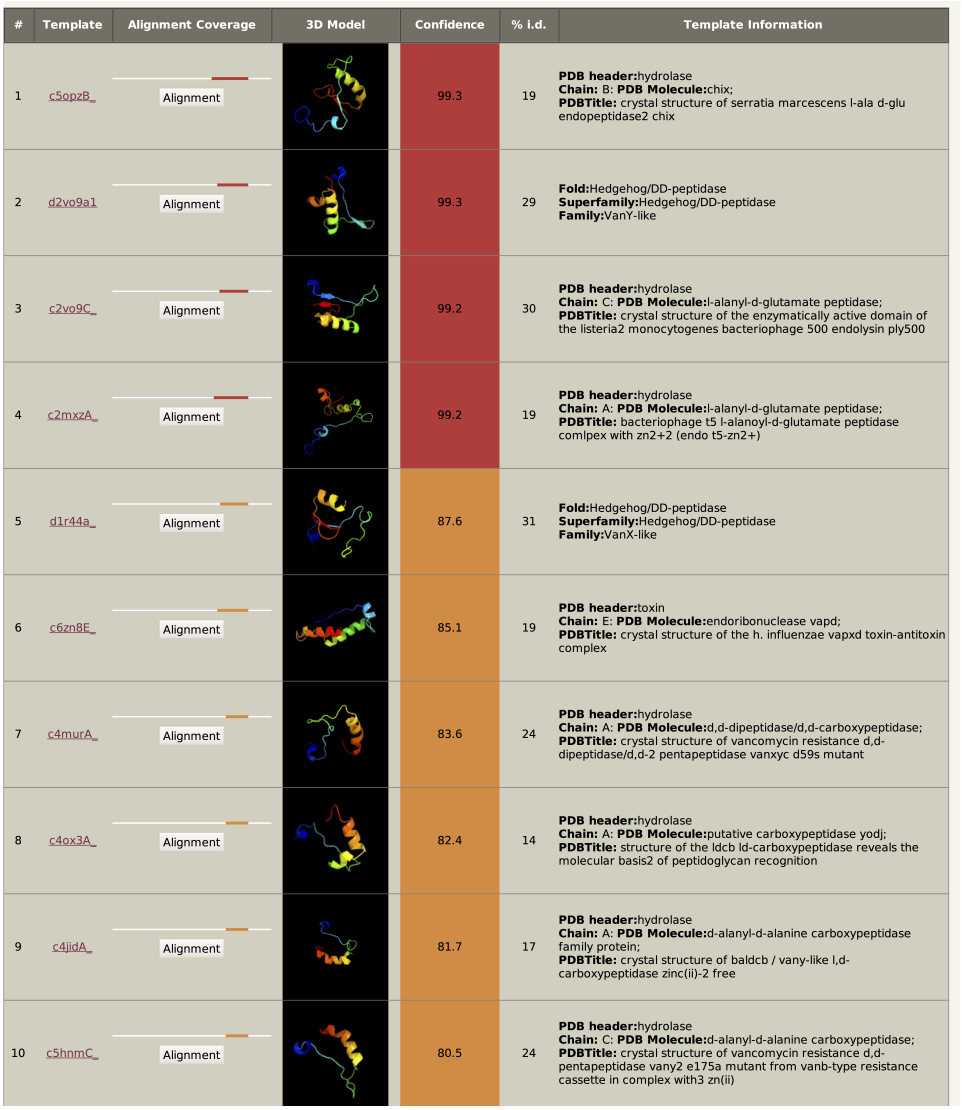
There are no identifiable effector-immunity protein pairs in the *R. sphaeroides* WS8N genome, which means that there are not obvious gene candidates encoding antibacterial toxins. However, one of the genes of the cluster encodes

a hypothetical protein with no homology to any of the core structural components of the T6SS, any T6SS-associated genes or any known T6SS effectors or immunity proteins. This gene, RSWS8N_RS18790, was investigated further *in silico*.

RSWS8N_RS18790 encodes a protein predicted by the NCBI conserved domain search to belong to the M15 family of metallopeptidases. Based on its amino acid sequence similarity to this family of peptidases, this could be an effector protein with a predicted D-alanyl-D-alanine carboxypeptidase activity. Peptidase activity prediction was corroborated by further assessment of this protein using Phyre2. According to Phyre2 analysis, this putative effector is predicted with high confidence (>99%) to be a homolog of several different proteins with peptidase activity (figure 3.16). There are many examples of experimentally characterised T6SS effector proteins that function as peptidases and have a role in interbacterial competition[107, 120, 121], making this gene the only antibacterial effector candidate from the *R. sphaeroides* WS8N cluster.

3.10 No putative function can be determined for the proteins encoded by RSWS8N_RS18670, RSWS8N_RS18690 and RSWS8N_RS18695

The putative function of the proteins encoded by RSWS8N_RS18670, RSWS8N_RS18690 and RSWS8N_RS18695 remains elusive as they share no homology to any known proteins, T6SS associated or otherwise, and do not contain any conserved domains indicative of their function.



#	Template	Alignment Coverage	3D Model	Confidence	% i.d.	Template Information
1	c5opzB_	Alignment		99.3	19	**PDB header:**hydrolase **Chain:** B: **PDB Molecule:**chix; **PDBTitle:** crystal structure of serratia marcescens l-ala d-glu endopeptidase2 chix
2	d2vo9a1	Alignment		99.3	29	**Fold:**Hedgehog/DD-peptidase **Superfamily:**Hedgehog/DD-peptidase **Family:**VanY-like
3	c2vo9C_	Alignment		99.2	30	**PDB header:**hydrolase **Chain:** C: **PDB Molecule:**l-alanyl-d-glutamate peptidase; **PDBTitle:** crystal structure of the enzymatically active domain of the listeria2 monocytogenes bacteriophage 500 endolysin ply500
4	c2mxzA_	Alignment		99.2	19	**PDB header:**hydrolase **Chain:** A: **PDB Molecule:**l-alanyl-d-glutamate peptidase; **PDBTitle:** bacteriophage t5 l-alanoyl-d-glutamate peptidase comlpex with zn2+2 (endo t5-zn2+)
5	d1r44a_	Alignment		87.6	31	**Fold:**Hedgehog/DD-peptidase **Superfamily:**Hedgehog/DD-peptidase **Family:**VanX-like
6	c6zn8E_	Alignment		85.1	19	**PDB header:**toxin **Chain:** E: **PDB Molecule:**endoribonuclease vapd; **PDBTitle:** crystal structure of the h. influenzae vapxd toxin-antitoxin complex
7	c4murA_	Alignment		83.6	24	**PDB header:**hydrolase **Chain:** A: **PDB Molecule:**d,d-dipeptidase/d,d-carboxypeptidase; **PDBTitle:** crystal structure of vancomycin resistance d,d-dipeptidase/d,d-2 pentapeptidase vanxyc d59s mutant
8	c4ox3A_	Alignment		82.4	14	**PDB header:**hydrolase **Chain:** A: **PDB Molecule:**putative carboxypeptidase yodj; **PDBTitle:** structure of the ldcb ld-carboxypeptidase reveals the molecular basis2 of peptidoglycan recognition
9	c4jidA_	Alignment		81.7	17	**PDB header:**hydrolase **Chain:** A: **PDB Molecule:**d-alanyl-d-alanine carboxypeptidase family protein; **PDBTitle:** crystal structure of baldcb / vany-like l,d-carboxypeptidase zinc(ii)-2 free
10	c5hnmC_	Alignment		80.5	24	**PDB header:**hydrolase **Chain:** C: **PDB Molecule:**d-alanyl-d-alanine carboxypeptidase; **PDBTitle:** crystal structure of vancomycin resistance d,d-pentapeptidase vany2 e175a mutant from vanb-type resistance cassette in complex with3 zn(ii)

Figure 3.16: **Phyre2 hit report for homologs of the putative *R. sphaeroides* WS8N T6SS effector protein encoded by RSWS8N_RS18790.** Only hits with >80% confidence are displayed.

3.11 Discussion

The *in silico* analysis of the structural components of the *R. sphaeroides* WS8N T6SS cluster conducted in this chapter places it firmly in the i3 phylogenetic group. This is in agreement with the classification predicted using the T6SS prediction function of the SecReT6 database. Unsurprisingly, when compared with diverse T6SS clusters from the i3 group, the *R. sphaeroides* WS8N T6SS cluster is most similar to i3 T6SS clusters of other alphaproteobacteria, while there is no indication that it has any similarities to T6SS clusters known to be involved in metal ion acquisition.

Bioinformatics analysis of the putative VgrG component of the *R. sphaeroides* WS8N T6SS cluster revealed it to be a canonical VgrG. This is based on the fact that it lacks any identifiable enzymatic domains indicative of effector protein function and its amino acid sequence is similar in length to other experimentally characterised canonical VgrG proteins, all of which are roughly 200 amino acids shorter than experimentally characterised evolved VgrG proteins. *In silico* analysis using the NCBI conserved domain search revealed a serine rich motif at the C-terminus of the VgrG protein, with homology to the ser_rich_anae_1 family of proteins that are found primarily in anaerobic bacteria, however, the presence of this motif cannot be corroborated using other protein domain prediction tools like Phyre2 and InterProScan. Interestingly, analysis of the canonical VgrG4a from *B. thailandensis* T6SS-4 using the NCBI conserved domain search, also revealed a similar serine rich motif at the C-terminus. The serine rich motif identified at the N-terminus of the *R. sphaeroides* WS8N VgrG protein shares an amino acid identity of 25.57 %

with that of the *B. thailandensis* VgrG4a protein. It is important to note here that this VgrG protein part of T6SS-4 of *B. thailandensis*, which is involved in metal ion acquisition[44, 46]. Looking more into the VgrG proteins belonging to T6SS clusters known to be involved in metal ion acquisition, most of them are canonical, except VgrG2b of *P. aeruginosa* that is classified as an evolved VgrG; VgrG2b is secreted by H2-T6SS of *P. aeruginosa*, a system that also delivers the experimentally characterised effectors, Azu and ModA that bind Cu^{2+} and MoO_4^{2-}, respectively[47, 61]. In fact, T6SS clusters demonstrated to function in the sequestration of metal ions do not seem to have commonalities in the type of VgrG proteins they use. They mostly share a common mode of operation, which is the secretion of a metal-binding effector protein.

It is worth noting that bioinformatic analysis of the VgrG protein of *R. sphaeroides* WS8N has yielded different results over the course of this D.Phil. theses. Although at present the C-terminus of VgrG is predicted to encode a serine-rich domain, previously *in silico* analyses had predicted the C-terminal domain to be involved in heme-utilisation, which, in the absence of any convincing metal-binding effector proteins, begged the following question: is the C-terminus of the *R. sphaeroides* WS8N VgrG protein capable of binding iron? This is explored further in chapter 6. That said, in the case of *B. thailandensis* T6SS-4 which has been shown to function in the acquisition of Mn^{2+} and Zn^{2+} ions, bioinformatic analysis of the metal-binding effector proteins with all the tools used in this chapter does not predict any conserved domains, and certainly does not point towards metal ion acquisition.

At the beginning of this research, analysis of the six-gene operon at the start of the T6SS cluster did not provide any evidence that these six genes are part of the T6SS cluster, and of course all subsequent predictions made here lack experimental validation. Nonetheless, the differences in genetic organisation between *R. sphaeroides* WS8N and *P. denitrificans* strain ATCC 19367 provided further support that this six-gene operon is part indeed part of the T6SS cluster. In *R. sphaeroides* strains *tssH* (*clpV*) is encoded in an operon with *RSWS8N_RS18700* which encodes a PRK07768 homolog. In *P. denitrificans* strain ATCC 19367, however, *tssH* appears to be in the same transcriptional operon as the genes encoding the DUF4150 domain-containing protein, the DUF2169 domain-containing protein and the 3-oxoacyl-ACP synthase protein as well as a a gene encoding another hypothetical protein. Analysis of the *P. denitrificans* strain ATCC 19367 T6SS cluster using the SecReT6 database identified the DUF4150 domain-containing protein encoded by EO213_RS05865 as a PAAR protein, suggesting that the six gene operon directly upstream of the T6SS cluster in *R. sphaeroides* WS8N is, in fact, part of the T6SS cluster. The PRK07768 homolog is also present in *P. denitrificans* strain ATCC 19367, directly upstream in the opposite transcriptional direction. In that organisms, it appears to be part of a two-gene operon, the second gene encoding a homolog of TIGR02270, which has been proposed to be a common domain found in adaptor proteins[119] and has been identified in other T6SS clusters from the i3 phylogenetic group (such as *P. aeruginosa* strain RIVM-EMC2982, *Pseudomonas chlororaphis* strain PCM120), but has not been verified experimentally. Finally, the inclusion of this six-gene operon in the T6SS cluster is supported by the recent addition of *R. sphaeroides* WS8N

to the SecReT6 database and the predicted annotations through that server.

In this chapter, three putative adaptor genes were also highlighted, RSWS8N_RS18675, RSWS8N_RS18680 and RSWS8N_RS18700, but while there is some evidence in the literature that would support this claim, it would need to be experimentally validated. Similarly RSWS8N_RS18790 was considered to encode a putative effector protein with peptidase activity. Unfortunately, this was not possible to explore further because of the fact that there is no suitable prey strain to be used in interbacterial competition assays. Preliminary bacterial warfare studies were conducted using *E. coli* as a prey strain, but with the growth rate of *R. sphaeroides* being dramatically slower, *E. coli* can easily outgrow it, confounding any killing effects. One way around this would be to use a susceptible slow growing bacteria, preferably one which inhabits the same niche and would thus be a natural competitor. Another obvious way around this, based on common practice in the T6SS field, would be to engineer a T6SS-susceptible *R. sphaeroides* mutant strain, that could then be used as a prey in competition experiments. This was not an option as there are no putative immunity protein genes within or adjacent to the T6SS cluster of *R. sphaeroides* WS8N. Thus, objectively the putative peptidase effector encoded by RSWS8N_RS18675 remains just a prediction. That said, peptidases are common T6SS effectors, so this prediction is an educated one. For example, the putative metallopeptidase Tpe1 is an effector of the T6SS of *Acinetobacter* ADP1 which causes cell lysis in *E. coli* [120].

Chapter 4

Optimisation of the growth conditions used to assess the phenotypic consequences of deleting the T6SS cluster in *R. sphaeroides* WS8N

4.1 Introduction

One challenge in the postgenomic era is the functional characterisation of genes identified by genome sequencing. Of the protein-coding genes that have been assigned a function so far, most are predictions based on homology with experimentally verified proteins. However, one-third of sequenced bacterial protein-coding genes cannot be annotated by this approach, as they bear no homology to proteins of known function[122]. As such, a vast proportion of bacterial genes lack experimental characterisation of the role of their protein products.

Mutant phenotypes can elucidate gene function, however, the number of genes which exhibit a phenotype under laboratory conditions are limited. Estimates range from 50% in *E. coli* [123] to 70% in *Shewanella oneidensis*[124]. *R. sphaeroides* is no exception to that. This bacterium has two flagellar systems, Fla1 and Fla2. Fla1 was identified experimentally in 1987[125] and produces a non-polar single flagellum that is always expressed under laboratory conditions[126]. The presence of a second flagellum, Fla2, which is normally quiescent, but encodes polar flagella under certain conditions, was unknown until the full *R. sphaeroides* genome was sequenced and was only shown to be expressed and functional years later[127, 128] when the appropriate growth conditions were established. Even under these conditions, expression of the Fla2 system was limited to 10% of the population, suggesting conditions required for expression of the Fla2 system could be further optimised.

The presence of T6SS genes in *R. sphaeroides* 2.4.1 was first acknowledged in a 2009 paper by Boyer *et al.*, who used available genomic resources to

perform an *in silico* analysis of bacterial T6SSs[12], and again in 2014 when *R. sphaeroides* 2.4.1 was one of the strains used by Forster *et al.* in the phylogenetic distinction of the T6SS classes[129]. The presence of T6SS genes in *R. sphaeroides* WS8N was highlighted following the publication of its whole-genome sequence in 2011[99]. As was the case for *R. sphaeroides* 2.4.1, these genes were assigned their type VI functionality by automated computational analysis using the protein homology method of gene prediction, which of course elucidates little about the conditions under which *R. sphaeroides* uses its single T6SS. The first step to characterisation of the *R. sphaeroides* T6SS is to identify growth conditions under which T6SS genes are expressed.

This chapter describes the construction of a T6SS knock-out mutant and optimisation of growth conditions in order to assess the phenotypic consequences of the absence of the T6SS apparatus under metal limiting conditions for *R. sphaeroides*.

4.2 Construction of *R. sphaeroides* ΔT6SS mutant strain

To study the importance of the T6SS for *R. sphaeroides* biology it was first necessary to generate a ΔT6SS mutant. Since there has been no previous experimental work on the *R. sphaeroides* T6SS, it was decided to first delete all 14 genes of the second operon in the T6SS cluster, which harbours most structural components of the apparatus. pK18mobsacB[98], a kanamycin-resistant, sucrose counter-selection allelic exchange vector was used to introduce mutations into the *R. sphaeroides* chromosomal sequence. pK18mobsacB mobilisation,

integration and excision is further explained in section 2.3.11.

To make pK18mobsacB-ΔT6SS, the 500 bp regions upstream and downstream of the main T6SS structural operon were amplified from the *R. sphaeroides* WS8N genome using primers ΔT6SS_P1 and ΔT6SS_P2 for the upstream region, and ΔT6SS_P3 and ΔT6SS_P4 for the downstream region (table 4.1). The location and sequence of these 500 bp flanking regions can be seen in figure 4.1. ΔT6SS_P2 contains a region overlapping with the downstream flanking region and ΔT6SS_P3 contains a region overlapping with the upstream flanking region, allowing the joining of the two fragments by overlap extension PCR to create a 1000 bp fragment. The overlap extension PCR workflow employed here is depicted in figure 4.3. Figure 4.2 shows the 1000 bp insert used for the generation of pK18mobsacB-ΔT6SS.

ΔT6SS_P1 and ΔT6SS_P4 contain EcoRI and HindIII restriction sites, respectively, allowing the 1000 bp fragment to be inserted at the EcoRI and HindIII sites of pK18mobsacB by restriction digestion cloning. The 1000 bp PCR product of overlap extension PCR was purified and its size confirmed by gel electrophoresis, before digestion with EcoRI and HindIII restriction enzymes, and ligation into EcoRI/HindIII-digested pK18mobsacB. The resulting plasmid was transformed into *E. coli* DH5αand DNA sequenced using the primers shown in table 2.15.

pK18mobsacB-ΔT6SS was transformed into *E. coli* S17-λpir (2.3.9) and from there introduced into *R. sphaeroides* by conjugation as described in sec-

Name	Sequence	Feature
ΔT6SS_P1	CACAGAATTCCACCCGCAGCGCGCC	*ecoRI* site
ΔT6SS_P2	CGGGTCCCGAGGAGCCTCTCCTGTTCCCCGATCATGCCCG	overlap with downstream region
ΔT6SS_P3	CGGGCATGATCGGGGAACAGGAGAGGCTCCTCGGGACCCG	overlap with upstream region
ΔT6SS_P4	CACAAAGCTTCGGCCAGCCGGTCG	*hindIII* site
ΔT6SS_CPF	CGTCAGATCGGTCGCATAGCGGGCGAG	
ΔT6SS_CPR	CGACAAGGACACGAGCGTGGGCCGGAAC	

Table 4.1: Primers used in the construction of *R. sphaeroides* ΔT6SS

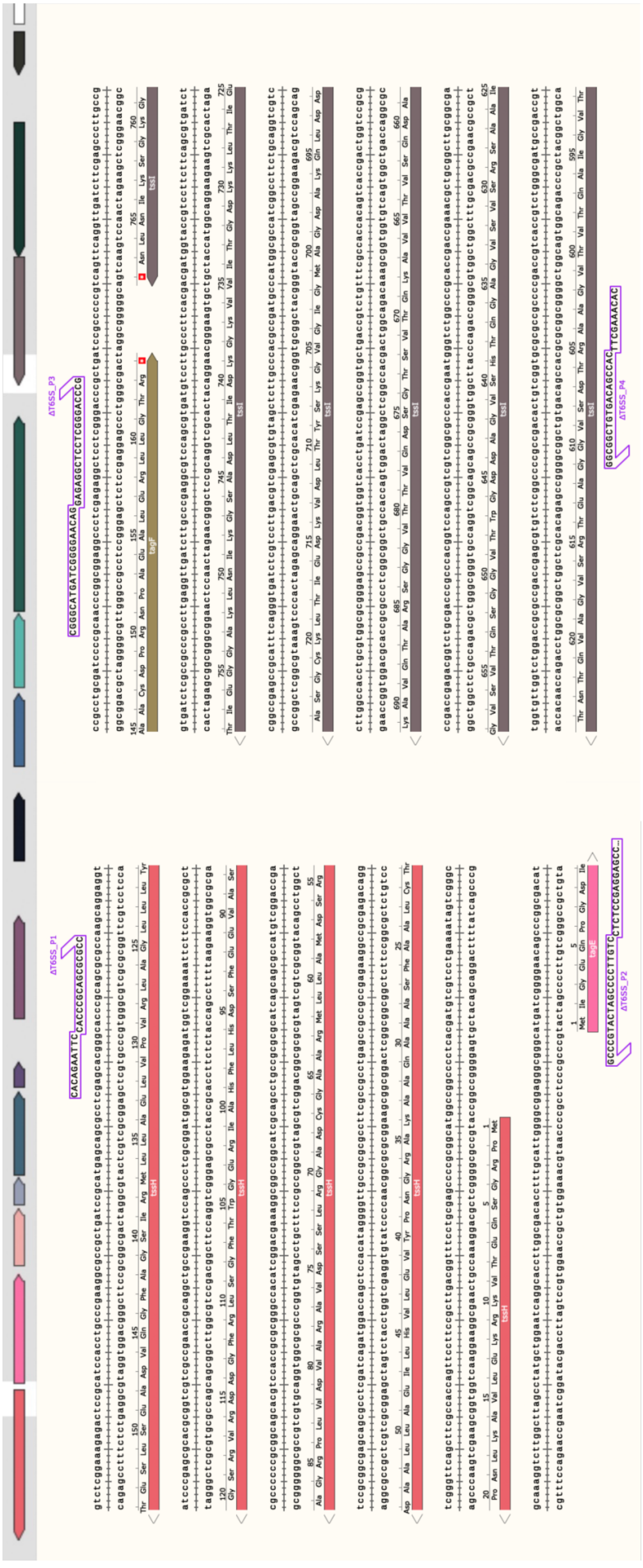


Figure 4.1: **DNA sequence of the 500 bp up and downstream flaking regions of the main structural T6SS operon of *R. sphaeroides* WS8N.** Primer binding sites are annotated.



Figure 4.2: 1000 bp insert used for the generation of pK18mobsacB-ΔT6SS

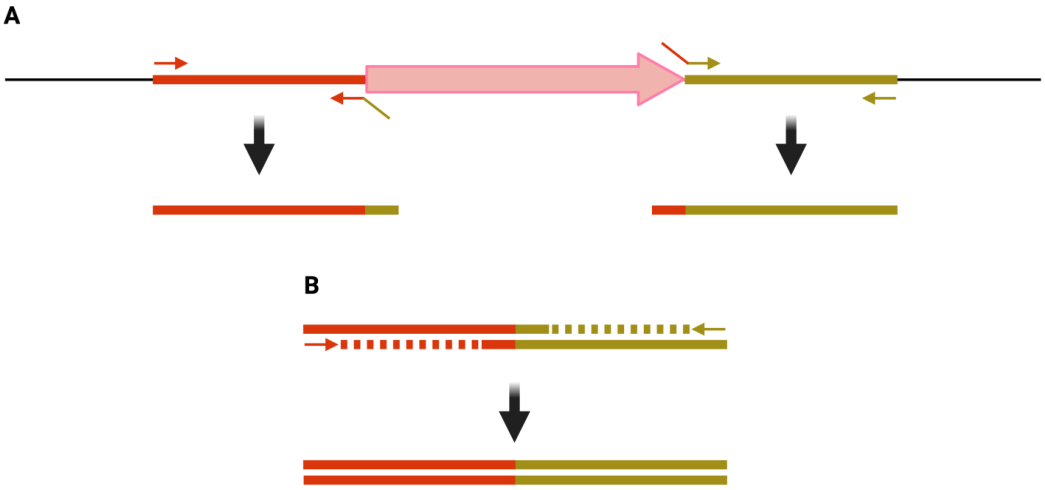


Figure 4.3: **Schematic outlining the overlap extension PCR workflow employed to generate a deletion construct. A** depicts the first round of PCR using primers to amplify the flanking 500 bp upstream (red) and downstream (yellow) of the region to be deleted (pink arrow). The red reverse primer and the yellow forward primers extend the products of the first round of PCR with a complimentary sequence. **B** depicts the second round of PCR whereby the products from the first round of PCR are used as the template. The complimentary regions anneal, permitting the extension of a single product using the red forward primer and the yellow reverse primer.

tion 2.3.10, before undergoing homologous recombination for genomic replacement (see section 2.3.11) of the T6SS main structural operon with the insert shown in figure 4.2. Successful ΔT6SS mutants were confirmed by sequencing using primers ΔT6SS_CP1 and ΔT6SS_CP1 which anneal outside of the mutation site. The resulting ΔT6SS gene cluster is shown in figure 4.4, alongside the wild-type T6SS gene cluster.

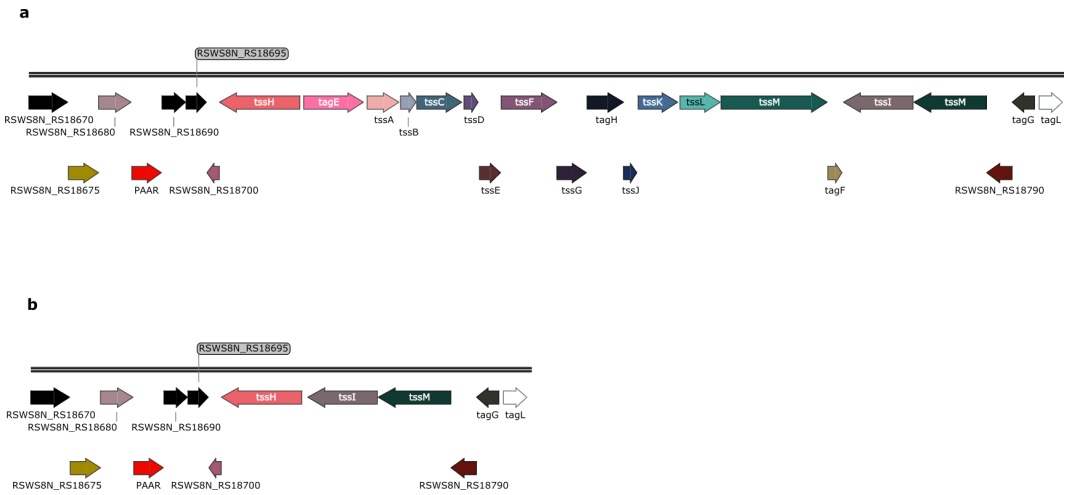


Figure 4.4: Genetic organisation of (**a**) *R. sphaeroides* WS8N T6SS and (**b**) *R. sphaeroides* ΔT6SS mutant

4.3 Optimisation of *R. sphaeroides* growth conditions to assess the phenotypic consequences of deleting the T6SS cluster

Preliminary growth assays under crude iron-limited conditions suggested a difference in growth between the ΔT6SS mutant and the wild-type strain (data not shown). For these experiments, succinate media[**SISTROM1960ASpheroides.**] was prepared as in 8.1.2, but without the addition of $FeSO_4.7H_2O$ to the concentrated base (8.1.4) or metals 44 solution (8.1.5), with no further precautions taken to exclude iron. Keeping in mind that *R. sphaeroides* is a slow growing

organism and considering that the initial growth assays were not performed under strict iron-limiting conditions, it was important to develop a more robust growth assay in order to further explore the potential role of the T6SS in metal acquisition. This required the optimisation of both the iron-depleted succinate media and the culturing method. It is well established that to make transition metal-free media the exclusion of added metals is insufficient. Metal-free media requires the active removal of transition metal ions via chelation, as well as considerations such as the use of plastic instead of borosilicate glass which is a source of metal contamination in (personal communication, Olivier Cunrath). The rest of this chapter describes the optimisation process for the iron-depleted succinate medium and the fine tuning process of the growth assay as to ensure the collection of reliable and reproducible data on the fitness of *R. sphaeroides* WS8N and its ΔT6SS mutant during metal limitation.

Broadly, two different strategies for the preparation of iron-depleted succinate media were tested. In both cases, media was prepared as described in 8.1.2, with the following modifications:

- Iron-depleted succinate media *without* the addition of $FeSO_4.7H_2O$ to the concentrated base or metals 44 solution, *with* chelated casamino acids, growth factor, phosphate buffer and MilliQ water - see section 4.3.1.1.
- Iron-depleted succinate media *without* the addition of $FeSO_4.7H_2O$, *with* chelated casamino acids - see section 4.3.1.2.

4.3.1 Testing growth of wild type *R. sphaeroides* WS8N and the ΔT6SS mutant strain in iron-depleted media

The preparation of *R. sphaeroides* growth media is laborious and complex. Considering that the majority of our planned experiments involved growth assays under different conditions, it was important to devise an iron-depleted growth medium that, while stringent, could be achieved routinely and reproducibly. For this reason, we sought to determine whether, in addition to the exclusion of $FeSO_4.7H_2O$ from succinate media components that contain it, chelating all the other media components (see 8.1.2), which do not contain metals (casamino acids (CAA), growth factor (GF), phosphate buffer (PB) and MilliQ water) leads to a more pronounced phenotypic difference between the two strains, than media where only the CAA is chelated. Using the iron-depleted media as a base, $FeCl_3.6H_2O$ was then re-introduced at a final concentration of 0 µM (depleted), 0.1 µM (limited), 1 µM or 10 µM. Succinate media contains 12.6 µM ferrous sulfate.

4.3.1.1 Growth in iron-depleted succinate media with chelated casamino acids, phosphate buffer, growth factor and MilliQ water

Succinate media was prepared as described in 8.1.2, without the addition of $FeSO_4.7H_2O$ to the concentrated base (8.1.4) or metals 44 solution (8.1.5). To ensure maximum iron-depletion the succinate media components lacking any metals (CAA, GF (8.1.6, PB (8.1.3 and MilliQ water) were subject to chelation with Chelex 100 Resin (Bio-Rad) for 5 h as per the manufacturers' instructions (batch method).

Starter cultures of wild-type *R. sphaeroides* WS8N and of its ΔT6SS mutant were grown photoheterotrophically directly from frozen glycerol stocks in succinate media for 48 h. The optical density at 700 nm (OD_{700}) of the starter cultures was measured and normalised to 1.5. Starter cultures were then diluted 1:1000 in succinate media or iron-depleted succinate media (-$FeSO_4.7H_2O$, chelated CAA, GF, PB, MilliQ water) supplemented with 0 µM, 0.1 µM, 1 µM or 10 µM $FeCl_3.6H_2O$ and nalidixic acid (see table 2.3). Cultures were grown in 1.5 mL tubes with minimal airspace and incubated under constant illumination (light intensity of 10 W/m^2) at 30°C for 96 h. Every 24 h, (24, 48, 72 and 96 h) 150 µL of culture was collected and transferred to a 96-well microtitre plate and the culture OD_{700} was measured. Continuous OD_{700} recording using a plate reader, instead of a measurements at a few specific time points, was not possible because of the slow growth rate of this bacterium that results in substantial evaporation of the growth media, as well as the white light requirement for photoheterotrophic growth.

There is a significant difference between the growth of *R. sphaeroides* WS8N and that of the ΔT6SS mutant for iron-depleted succinate media (-$FeSO_4.7H_2O$, chelated CAA, GF, PB, MilliQ water) supplemented with 0 µM ($P<0.0001$), 0.1 µM ($P<0.0001$) and 1 µM ($P<0.0001$) $FeCl_3.6H_2O$ (figure 4.5). In particular, when iron was entirely absent, wild-type *R. sphaeroides* reached an OD_{700} of 0.6286 ± 0.2381, whereas the ΔT6SS mutant barely grew (OD_{700} of 0.1464 ± 0.009914). A similar trend was observed for the additions of 0.1 µM $FeCl_3.6H_2O$ or 1 µM $FeCl_3.6H_2O$, with the wild-type strain showing considerable growth, while the ΔT6SS mutant lagged significantly behind

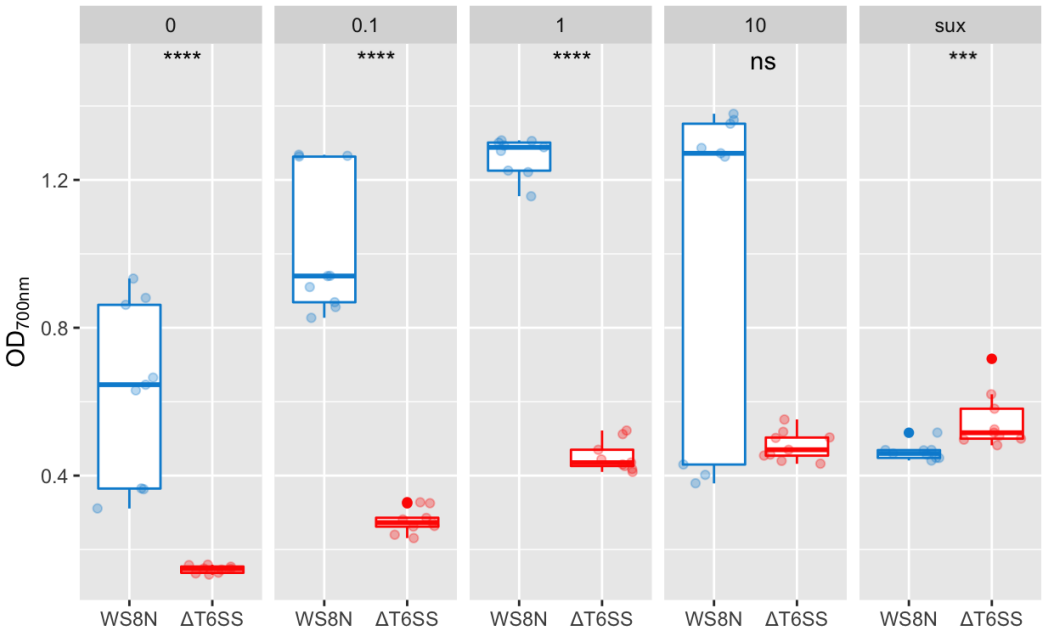


Figure 4.5: **Growth of wild-type *R. sphaeroides* WS8N and of its ΔT6SS mutant under increasing $FeCl_3.6H_2O$ concentrations in iron-depleted succinate media (-$FeSO_4.7H_2O$, chelated CAA, GF, PB, MilliQ water)**. Wild-type *R. sphaeroides* WS8N and its ΔT6SS mutant strain were grown in iron-depleted succinate media supplemented with the indicated concentrations of $FeCl_3.6H_2O$ under photoheterotrophic conditions. OD $_{700}$ after 48 h of growth is shown. A Mann-Whitney test was performed to detect significant differences between the OD_{700} of the wild type WS8N and the ΔT6SS mutant. This experiment was performed in biological triplicate, with each biological replicate performed in technical triplicate, all data points are displayed. **** P<0.0001, *** P<0.001, ns = not significant.

(only achieving an OD_{700} of 0.4519 ± 0.04071 even at 1 µM $FeCl_3.6H_2O$).

Although growth in iron-depleted succinate media (-$FeSO_4.7H_2O$, chelated CAA, GF, PB, MilliQ) leads to significant phenotypic differences between the wild-type and mutant strains under low iron conditions, the large statistical variation between biological replicates of the wild-type strains, evident in figure 4.5 where the box represents the interquartile range, points towards an unreliable growth assay. In addition, it was noticed that when grown in iron-depleted succinate media (-$FeSO_4.7H_2O$, chelated CAA, GF, PB, MilliQ water), the wild-type cells reach a peak in OD_{700} at 48 hours. After 72 h of growth a 61%, 57%, 45% and 38% reduction in OD_{700} is observed when media is supplemented with 0 µM, 0.1 µM, 1 µM and 10 µM, respectively (figure 4.6). This dramatic growth spike at 48 h is an anomalous trend, only observed when wild-type *R. sphaeroides* WS8N was grown in iron-depleted succinate media where the CAA, GF, PB and MilliQ water had been subject to chelation.

4.3.1.2 Growth in iron-free succinate media with chelated casamino acids

The chelation of CAA, phosphate buffer, growth factor and milliQ water is a time consuming and expensive process. Commercial CAA have a high iron content and are likely the biggest contributor of iron to the succinate media. Iron-depleted media prepared as in 8.1.2 without the addition of $FeSO_4.7H_2O$ to the concentrated base (8.1.4) or metals 44 solution (8.1.5) and with the application of a chelation step only to the CAA, was therefore tested. Using this growth medium, the same experimental process as described in section

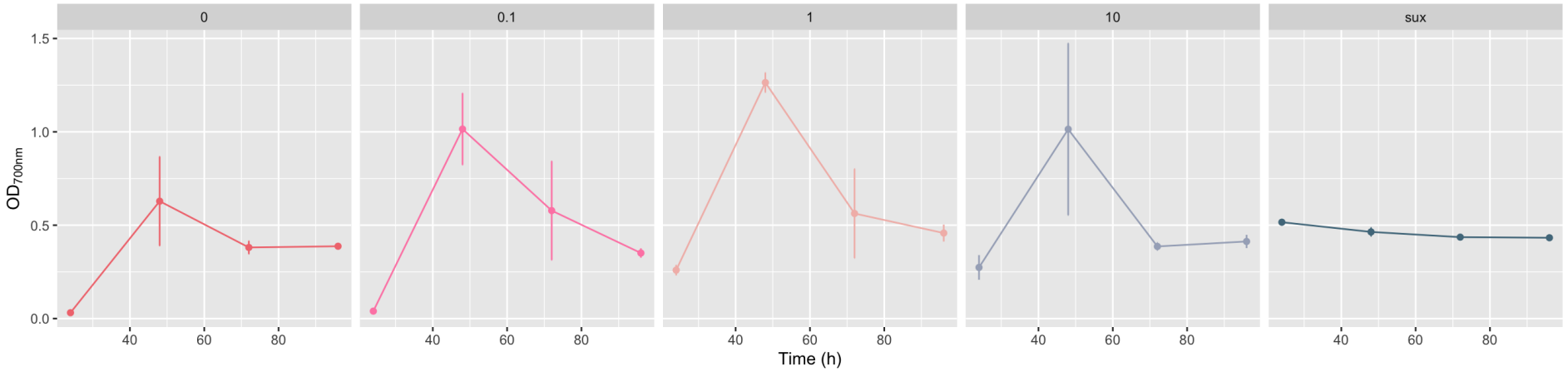


Figure 4.6: **Growth of wild-type *R. sphaeroides* WS8N under various $FeCl_3.6H_2O$ concentrations in iron-depleted succinate media (-$FeSO_4.7H_2O$, chelated CAA, GF, PB, MilliQ water)**. Wild-type *R. sphaeroides* WS8N was grown in iron-depleted succinate media (-$FeSO_4.7H_2O$, chelated CAA, GF, PB, MilliQ) supplemented with $FeCl_3.6H_2O$ to the indicated final concentration or regular succinate media under photoheterotrophic conditions. Cells were grown for 96 h. At every 24 h time interval (24, 48, 72 and 96 h) 150 µL of culture sample was collected and transferred to a 96 well microtitre plate and optical density at 700 nm (OD_{700}) was measured. Values are means from three repetitions and vertical bars represent ± standard deviation.

4.3.1.1 was carried out.

When iron-depleted succinate media (-$FeSO_4.7H_2O$, chelated CAA) was used, a significant difference in growth between wild type *R. sphaeroides* WS8N and the ΔT6SS mutant was observed after 48 h of growth only when the media was supplemented with 0.1 µM $FeCl_3.6H_2O$ (Mann-Whitney test, P<0.0001) (figure 4.7); wild-type *R. sphaeroides* WS8N reached an OD_{700} of 1.015±0.1911, while the ΔT6SS mutant strain reached an OD_{700} of 0.2767±0.03335. By contrast, there is no significant difference in growth between the wild-type and ΔT6SS strains when grown in succinate media or iron-depleted succinate media (-$FeSO_4.7H_2O$, chelated CAA) either lacking iron entirely or supplemented with 10 µM $FeCl_3.6H_2O$ (figure 4.7). Among the tested growth conditions with a defined iron content, the mean OD_{700} is highest when the wild-type strain is grown in iron-depleted succinate media (-$FeSO_4.7H_2O$, chelated CAA) supplemented with 10 µM $FeCl_3.6H_2O$ (1.483± 0.04763). Indeed at that non-limiting iron concentration the growth of *R. sphaeroides* WS8N is largely comparable to its growth in regular succinate media (see figure 4.5). Interestingly, the anomalous growth observed for the wild-type strain in section 4.3.1.1, whereby iron-depleted media were prepared with chelation of CAA, GF, PB and MilliQ water, did not occur when the bacteria were grown in media where only the CAA was chelated (figure 4.8). This is in agreement with the growth dynamics observed in the preliminary experiments where the wild-type strain was grown in crude iron-depleted succinate media prepared without a chelation step; in both cases wild-type *R. sphaeroides* WS8N reached peak OD_{700} at 48 h and then plateaued into stationary phase (data not shown).

This media was therefore carried forward for use in all subsequent experiments.

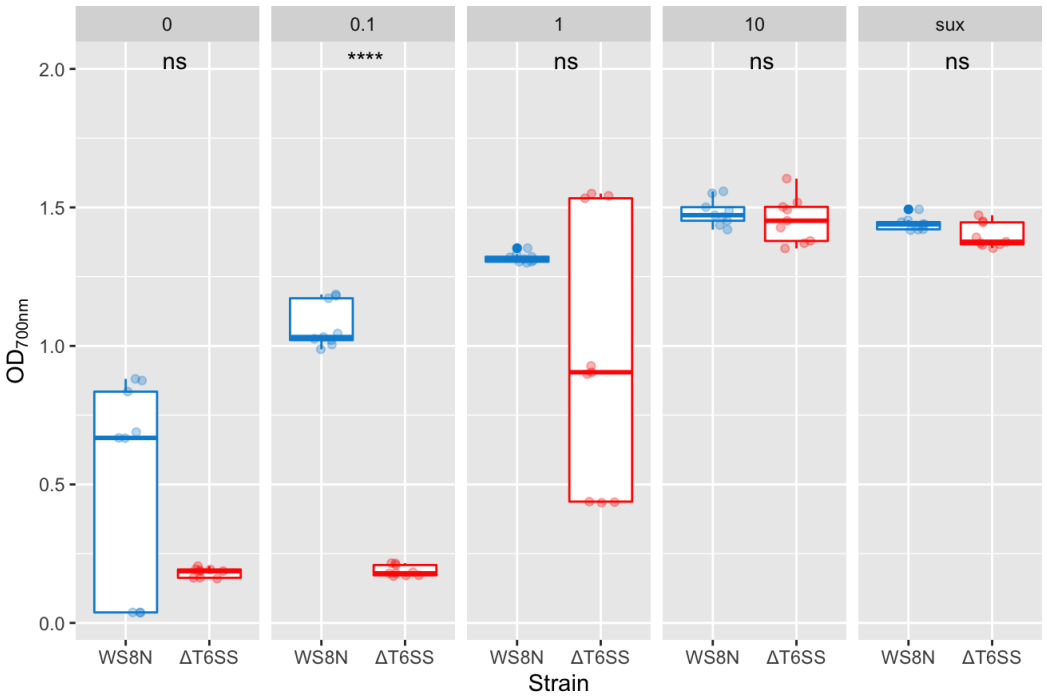


Figure 4.7: **Growth of wild-type *R. sphaeroides* WS8N and the ΔT6SS mutant under different $FeCl_3.6H_2O$ concentrations in iron-depleted succinate media (-$FeSO_4.7H_2O$, chelated CAA)**. Wild-type *R. sphaeroides* WS8N and the ΔT6SS mutant strain were grown in iron-depleted succinate media supplemented with the indicated concentration of $FeCl_3.6H_2O$ under photoheterotrophic conditions. OD_{700} after 48 h of growth is shown. A Mann-Whitney test was performed to detect significant differences between the OD_{700} of the wild type WS8N and the ΔT6SS mutant. This experiment was performed in biological triplicate, with each biological replicate performed in technical triplicate, all data points are displayed. **** P<0.0001, ns = not significant.

Although there is no drastic reduction in the observed variation between biological replicates when the growth results of the two different media strategies are compared, chelation of just the CAA component of the succinate media was the preferred option as we moved forward. The rationales for this choice were the following: 1) it made logistical sense to choose the less time-consuming option when it came to an already lengthy growth assay; 2) chelated CAA

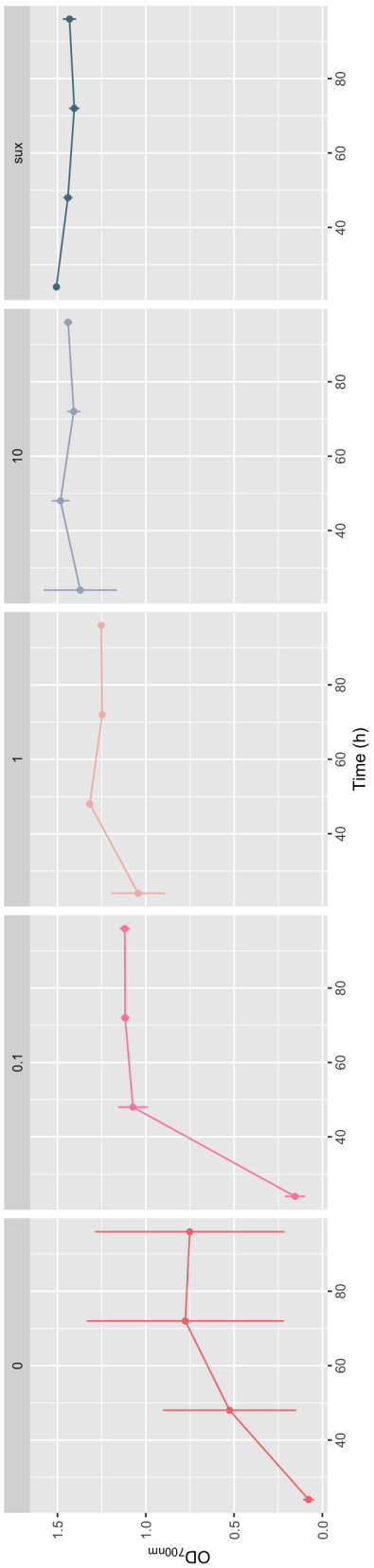


Figure 4.8: **Growth of wild-type *R. sphaeroides* WS8N under various $FeCl_3.6H_2O$ concentrations in iron-depleted succinate media (-$FeSO_4.7H_2O$, chelated CAA).** Wild-type *R. sphaeroides* WS8N was grown in iron-depleted succinate media (-$FeSO_4.7H_2O$, chelated CAA) supplemented with $FeCl_3.6H_2O$ to the indicated final concentration or regular succinate media. Cells were grown for 96 h. At every 24 h time interval (24, 48, 72 and 96 h) 150 µL of culture sample was collected and transferred to a 96 well microtitre plate and optical density at 700 nm (OD_{700}) was measured. Values represent the mean of three biological replicates each performed in technical triplicate, and vertical bars represent ± standard deviation.

only iron-depleted succinate media is significantly cheaper; 3) the use of iron-depleted succinate media (-$FeSO_4.7H_2O$, chelated CAA) restored the expected growth dynamics of the wild-type strain (figure 4.8) when 10 µM $FeCl_3.6H_2O$ was used; 4) a significant difference in OD_{700} was observed between wild-type *R. sphaeroides* WS8N and its ΔT6SS mutant strain when they were grown in iron-depleted succinate media (-$FeSO_4.7H_2O$, chelated CAA) supplemented with 0.1 µM $FeCl_3.6H_2O$ (Mann-Whitney, $P<0.0001$) with less variation between replicates for this condition especially. (figure 4.7).

Thus, iron-depleted succinate media made up as in 8.1.2 without the addition of $FeSO_4.7H_2O$ to the concentrated base (8.1.4) or metals 44 solution (8.1.5) and with application of metal chelation just to the CAA component is the medium that will be routinely used hereafter for any growth experiments under iron limiting conditions described in this thesis.

4.3.2 Optimisation of the culturing conditions of *R. sphaeroides* WS8N to reduce inter-replicate variability

Due to the slow growth rate of *R. sphaeroides* WS8N, it is common practice to sub-culture this bacterium directly from frozen glycerol stocks, thus decreasing the culture to experiment lead times by several days. Following this accepted practice, the experiments conducted in this chapter thus far have used starter cultures grown directly from frozen glycerol stocks into 1.5 mL tubes with minimal airspace and incubated under constant illumination (light intensity of 10 W/m^2) at 30°C for 48 h. Growing sub-cultures this way could undermine the development of a robust growth assay. Since there is no way to control the

number of cells scooped from a frozen glycerol stock during the inoculation step, one can end up with cultures at very different growth phases after 48 h; this is usually not an issue when working with fast-growing bacteria, but has to be considered for slow growers that do not reach saturation even at 48 h. Figure 4.9 contrasts the sub-culture protocols investigated in the following sections to the one used until now.

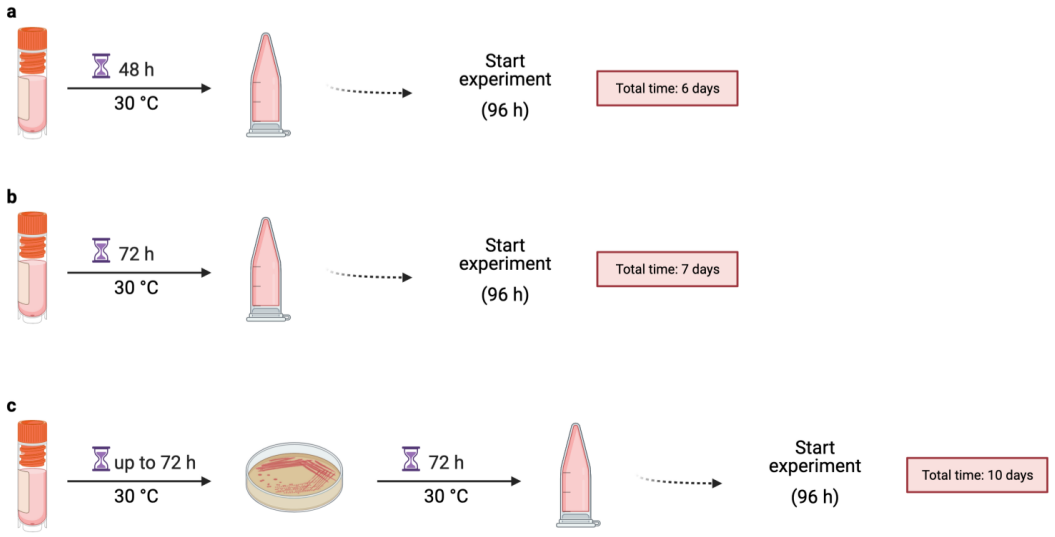


Figure 4.9: **Schematic of three different starter culture procedures used during growth assays performed in this thesis** (**a**) Starter cultures were grown directly from frozen glycerol stocks in 1.5 mL tubes containing succinate media with minimal airspace and incubated under constant illumination (light intensity of 10 W/m^2) at 30°C for 48 h. Cultures were then normalised to OD_{700} 1.5 and diluted 1:1000 into growth assay media. (**b**) Starter cultures were grown directly from frozen glycerol stocks in 1.5 mL tubes containing succinate media with minimal airspace and incubated under constant illumination (light intensity of 10 W/m^2) at 30°C for 72 h. Cultures were then normalised to OD_{700} 1.5 and diluted 1:1000 into growth assay media. (**c**) Starter cultures were inoculated using colonies from growth at 30 °C on solid media for up to 72 h (until colonies were visible). One or five colonies were inoculated into 1.5 mL tubes containing succinate media with minimal airspace and incubated under constant illumination (light intensity of 10 W/m^2) at 30°C for 72 h. Cultures were then normalised to OD_{700} 1.5 and diluted 1:1000 into growth assay media. The total experiment time required starting from using the frozen glycerol stock to inoculate a starter culture or streak an LB agar plate to the end of the growth assay is indicated for each option. Created with BioRender.com

In particular, we wanted to assess whether the following modifications to the starter culture procedure during growth assays help decrease the inter-replicate variability:

- Use of 72 h starter cultures grown directly from frozen glycerol stocks (section 4.3.2.1).
- Use of 72 h starter cultures inoculated with multiple colonies grown on LB agar (section 4.3.2.2).
- Use of 72 h starter cultures inoculated with a single colony grown on LB agar (section 4.3.2.3).

4.3.2.1 Use of 72 h starter cultures grown directly from frozen glycerol stocks improves the inter-replicate variation

Although the gold standard for microbiological practice is to inoculate starter cultures using a single colony grown on solid media, in the interest of decreasing the lead time of experiments, we first tested the use of starter cultures grown directly from frozen glycerol stocks for 72 h as, at this time point, it appears that *R. sphaeroides* cultures unambiguously reach saturation. To implement this, starter cultures of wild-type *R. sphaeroides* WS8N and of its ΔT6SS mutant were grown photoheterotrophically from frozen glycerol stock in 1.5 mL tubes containing succinate and appropriate antibiotics with minimal airspace and incubated under constant illumination (light intensity of 10 W/m^2) at 30°C for 72 h.

Starter cultures were then normalised to OD_{700} 1.5 and diluted 1:1000 in succinate media or iron-depleted succinate media (-$FeSO_4.7H_2O$, chelated

CAA), supplemented with 0 µM, 0.1 µM, 1 µM or 10 µM $FeCl_3.6H_2O$ and appropriate antibiotics and grown as described above for the starter cultures. At every 24 h time interval (24, 48, 72 and 96 h) 150 µL of culture sample was collected and transferred to a 96 well microtitre plate and OD_{700} was measured.

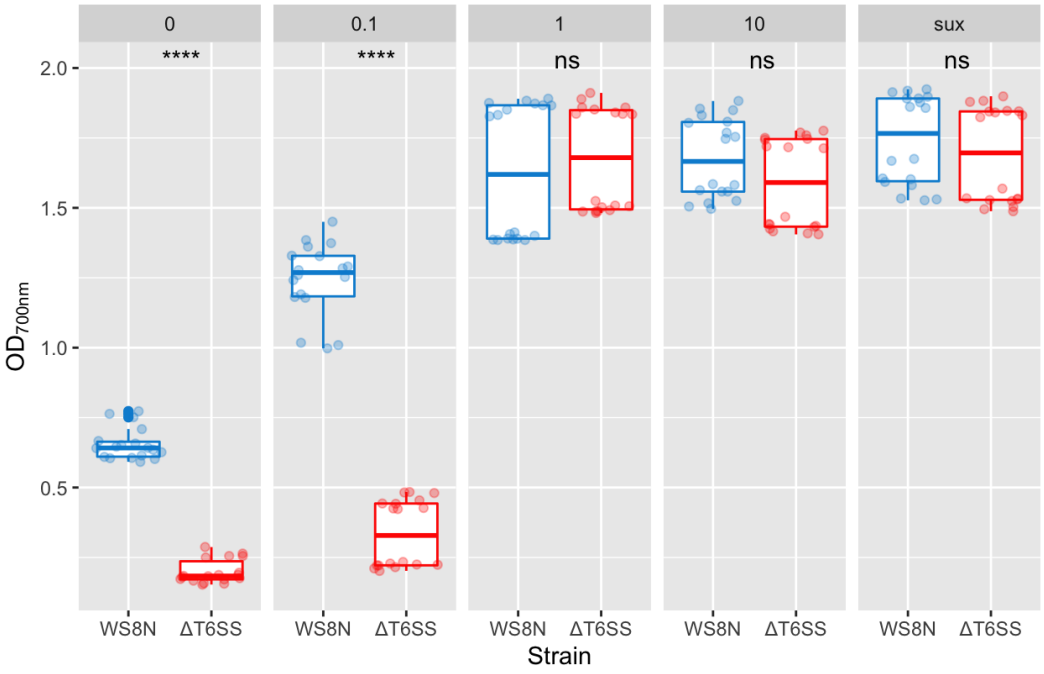


Figure 4.10: **Growth of wild-type *R. sphaeroides* WS8N and its ΔT6SS mutant after 48 h under different $FeCl_3.6H_2O$ concentrations in iron-depleted succinate media (-$FeSO_4.7H_2O$, chelated CAA) from 72 h starter cultures inoculated directly from frozen glycerol stock**. Starter cultures of both strains were inoculated directly from frozen glycerol stock and grown for 72 h. Starter cultures were then normalised to OD_{700} 1.5 and diluted 1:1000 in iron-depleted succinate media supplemented with the indicated concentration of $FeCl_3.6H_2O$ and grown under photoheterotrophic conditions. OD_{700} was measured after 48 h of growth. A Mann-Whitney test was performed to detect significant differences between the OD_{700} of the wild type WS8N and the ΔT6SS mutant. This experiment was repeated on two different occasions. On both occasions this experiment was performed in biological triplicate, with each biological replicate performed in technical triplicate, all data points are displayed. **** $P<0.0001$, ns = not significant.

As illustrated in figure 4.10, when grown in media containing at least 1 µM $FeCl_3.6H_2O$, after 48 h of growth there was no significant difference in

OD^{700} between wild-type *R. sphaeroides* WS8N and the ΔT6SS mutant. These strains do, however, display a significant difference in OD_{700} when grown under limited iron conditions; P<0.0001 for both 0 µM and 0.1 µM $FeCl_3.6H_2O$. In addition, the inter-replicate variability for both strains when using this growth regime is improved compared to previous experiments (figures 4.5 and 4.7).

4.3.2.2 Use of 72 h starter cultures inoculated with multiple colonies grown on LB agar is best practice for the reduction of inter-replicate variation

In order to test whether the use of colonies rather than glycerol stocks for the inoculation of the starter cultures offers any benefits, we started by growing wild-type*R. sphaeroides* WS8N and its ΔT6SS mutant onto LB agar plates containing the appropriate antibiotics. Plates were incubated at 30 °C for up to 72 h, until colonies were visible. Five colonies were inoculated in to 1.5 mL tubes containing succinate and appropriate antibiotics with minimal airspace and incubated under constant illumination (light intensity of 10 W/m^2) at 30°C for 72 h. Subsequently, inoculation and growth experiments were performed following the same method as described in section 4.3.2.1.

As shown in figure 4.11, growth under all tested conditions results in a significant difference in OD_{700} between wild-type *R. sphaeroides* WS8N and the ΔT6SS mutant, although when grown in succinate media, or iron-depleted succinate media (-$FeSO_4.7H_2O$, chelated CAA) supplemented with 10 µM $FeCl_3.6H_2O$, the difference in growth is very small (Mann-Whitney test, P=0.0063 for 10 µM $FeCl_3.6H_2O$, P=0.0138 for succinate)compared to that observed in conditions where the iron concentration is limited (P<0.0001

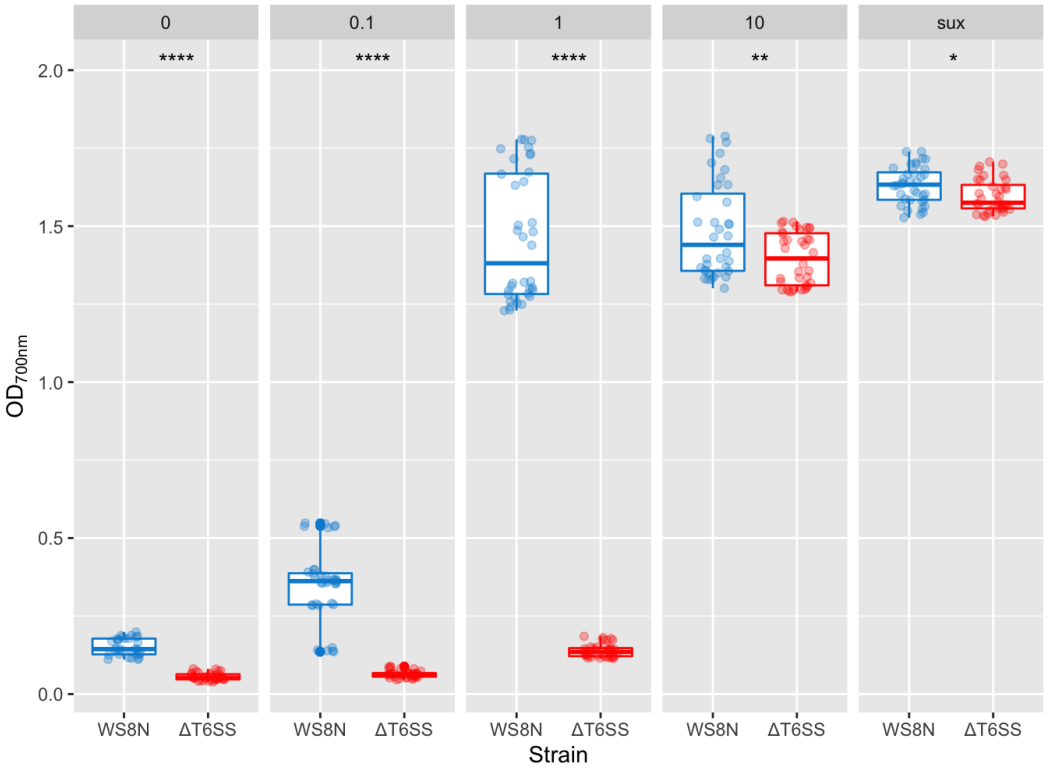


Figure 4.11: **Growth of wild-type *R. sphaeroides* WS8N and its ΔT6SS mutant under different $FeCl_3.6H_2O$ concentrations in iron-depleted succinate media (-$FeSO_4.7H_2O$, chelated CAA) from 72 h starter cultures grown from colonies**. Starter cultures of of both strains were obtained by growing them on LB agar plates, which were incubated at 30 °C for up to 72 h, until colonies were visible. Five colonies were inoculated into 1.5 mL tubes containing succinate media with minimal airspace and incubated under constant illumination (light intensity of 10 W/m^2) at 30°C for 72 h. Starter cultures were then normalised to OD_{700} 1.5 and diluted 1:1000 in iron-depleted succinate media supplemented with the indicated concentration of $FeCl_3.6H_2O$ and grown under photoheterotrophic conditions. OD_{700} was measured after 48 h of growth. A Mann-Whitney test was performed to detect significant differences between the OD_{700} of the wild type WS8N and the ΔT6SS mutant. This experiment was repeated on two different occasions. On both occasions this experiment was performed in biological triplicate, with each biological replicate performed in technical triplicate, all data points are displayed. **** $P<0.0001$, ** $P<0.01$, * $P<0.05$.

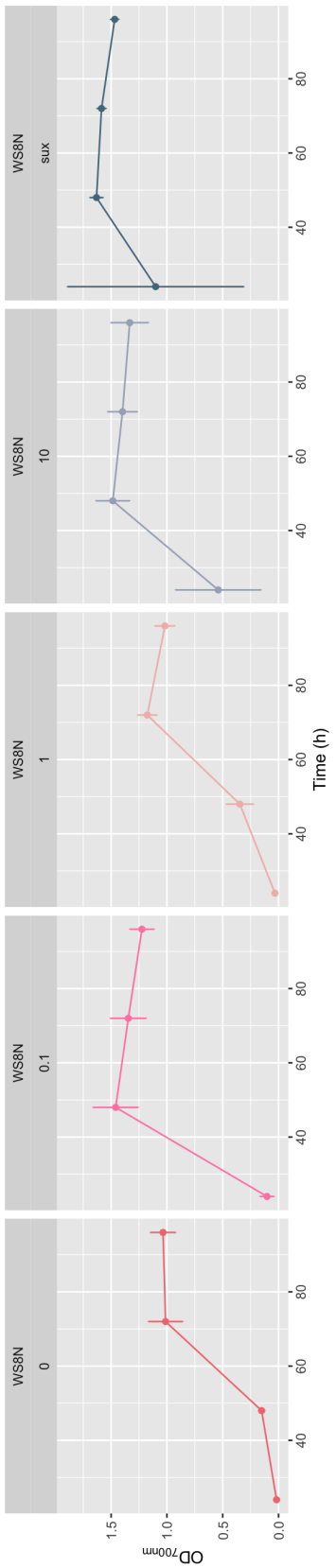


Figure 4.12: **Growth of wild-type *R. sphaeroides* WS8N in iron-depleted succinate media**. Wild-type *R. sphaeroides* WS8N was grown in iron-depleted succinate media (-$FeSO_4.7H_2O$ chelated CAA) supplemented with $FeCl_3.6H_2O$ to the indicated final concentration or succinate media. Values are means from three biological replicates conducted on two separate occasions and vertical bars represent ± standard deviation. Cells were grown for 96 h. At every 24 h time interval (24, 48, 72 and 96 h) 150 µL of culture sample was collected and transferred to a 96 well microtitre plate and optical density at 700 nm (OD_{700}) was measured.

for 0 µM, 0.1 µM and 1 µM $FeCl_3.6H_2O$). This experiment was carried out in triplicate on two separate occasions. Moreover, the growth dynamics of wild-type *R. sphaeroides* were checked (figure4.12) to ensure that no abnormalities are observed. Wild-type *R. sphaeroides* WS8N cells reach their maximum OD_{700} after 48 h of growth and then their growth plateaus steadily.

Interestingly, the phenotypic difference between the wild-type strain and its ΔT6SS mutant is at its most stark when grown in iron-depleted succinate media supplemented with 1 uM $FeCl_3.6H_2O$ when inoculation of starter cultures from single colonies is carried out. More specifically, wild-type *R. sphaeroides* WS8N reaches an OD_{700} of 1.459±0.2030, whereas the ΔT6SS mutant only reaches an OD_{700} of 0.1380±0.02105 (figure 4.11). This differs from what has been observed in previous experiments presented in this chapter, where the greatest difference in OD_{700} between the two strains was observed when iron-depleted succinate media was supplemented with 0.1 uM $FeCl_3.6H_2O$ (figures 4.7 and 4.10).

Taken together, the data from this section demonstrate that growth in iron-depleted succinate media ((-$FeSO_4.7H_2O$, chelated CAA) using starter cultures grown for 72 h inoculated with colonies (rather than glycerol stocks) (panel **c**, figure 4.9) is advantageous as it allows for more robust phenotypic differences and less variable results between biological replicates when compared to previous optimisation experiments (figures 4.5, 4.7 and 4.10).

4.3.2.3 Use of 72 h starter cultures inoculated with a single colony grown on LB agar does not improve the inter-replicate variability as compared to using multiple colonies for inoculation

The starter culture procedure outlined in section 4.3.2.2 involved growing the strains of interest on solid media and then using five colonies to inoculate the starter cultures. The ΔT6SS mutant was used to compare the use of single and multiple colonies for the starter culture inoculation. This exercise demonstrated that the use of a single colony did not help with decreasing the variation among biological replicates as compared to experiments where five colonies were used (figure 4.13). Standard deviation of the ΔT6SS mutant OD_{700} values after 48 h of growth in iron-depleted media using single-colony-derived starter cultures supplemented with different amounts of $FeCl_3.6H_2O$ ranged between 0.005 and 0.027. A very similar standard deviation range of 0.003 to 0.007 was recorded for ΔT6SS mutant OD_{700} values when multiple colonies were inoculated. Since the use of single- versus multiple-colony-derived starter cultures makes no detectable difference to inter-replicate variability in the growth assay (figure 4.13), all subsequent experiments were carried out using starter cultures with five single colonies for two reasons 1) the saturation of starter cultures after 72 h of growth is guaranteed when multiple colonies are used for inoculation; 2) it is not rare that a *R. sphaeroides* culture inoculated with a single colony might grow at all, something that would then waste 6 days that are required to grow the strains on solid media again and inoculate a new starter culture.

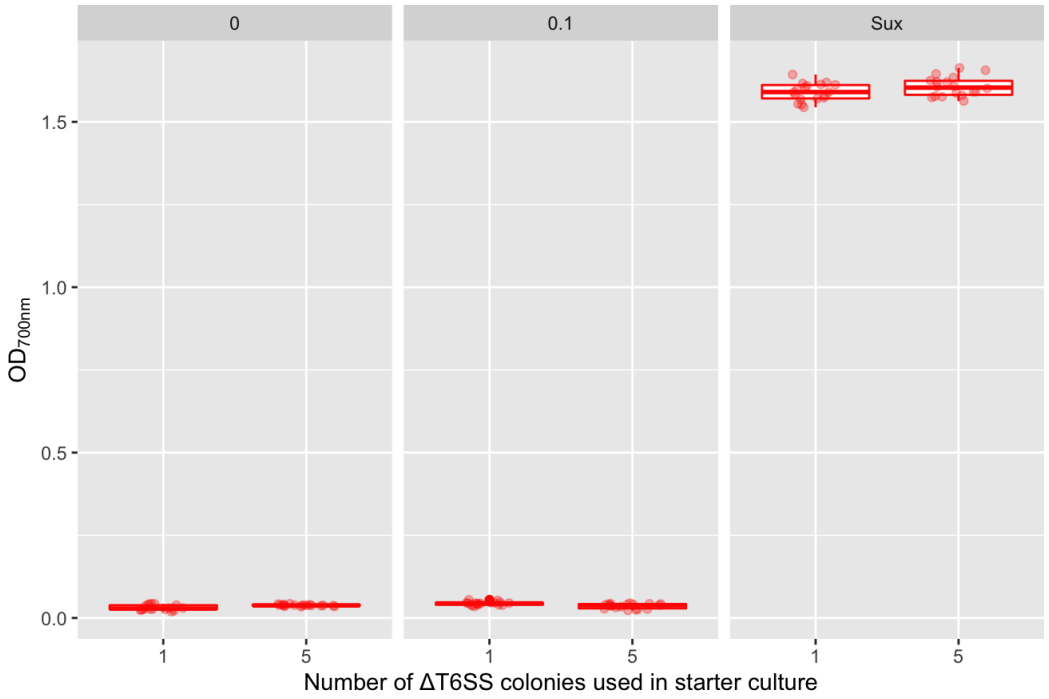


Figure 4.13: **Growth of the ΔT6SS mutant under different $FeCl_3.6H_2O$ concentrations in iron-depleted succinate media (-$FeSO_4.7H_2O$, chelated CAA) from 72 h starter cultures grown from single or multiple colonies**. Starter cultures of the ΔT6SS mutant strain were obtained by growing the strain onto LB agar plates that were incubated at 30 °C for up to 72 h, until colonies were visible. One or five single colonies were inoculated in 1.5 mL tubes containing succinate media with minimal airspace and incubated under constant illumination (light intensity of 10 W/m^2) at 30°C for 72 h. Starter cultures were then normalised to OD_{700} 1.5 and diluted 1:1000 in iron-depleted succinate media supplemented with the indicated concentration of $FeCl_3.6H_2O$ and grown under photoheterotrophic conditions. OD $_{700}$ was measured after 48 h of growth. This experiment was performed in biological triplicate, with each biological replicate performed in technical triplicate, all data points are displayed.

4.3.3 Overview of the inter-replicate variability after the different optimisation steps taken in this chapter

The standard deviation of OD_{700} measurements were calculated for each strain and $FeCl_3.6H_2O$ concentration for each different growth optimisation protocol detailed in this chapter. To recap, the following growth protocols were tested: 1) growth in iron-depleted succinate media prepared without the addition of -$FeSO_4.7H_2O$ with chelated CAA, GF, PB and MilliQ water; 2) growth in iron-depleted succinate media prepared without the addition of -$FeSO_4.7H_2O$ with chelated CAA only; 3) growth in iron-depleted succinate media (-$FeSO_4.7H_2O$, chelated CAA) using starter cultures inoculated directly from frozen glycerol stocks and grown for 72 h; 4) growth in iron-depleted succinate media (-$FeSO_4.7H_2O$, chelated CAA) using colony-derived starter cultures grown for 72 h. As depicted in figure 4.14, the optimisation protocol 1 and 2, which both used starter cultures inoculated directly from frozen glycerol stock and grown only for 48h, resulted in a high degree of variability, with data points falling in the upper right quadrants. By contrast, when using saturated starter cultures the variability of the collected growth data is minimised for both strains, while growth experiments performed using starter cultures inoculated from multiple colonies (rather than glycerol stocks) allowed for observation of even small changes in the growth patterns of the two strains in question (see figure 4.11). For this reason, for the rest of this thesis, and unless otherwise stated, all growth assays have been carried out using starter cultures that were inoculated with five colonies and were grown to saturation (72 h), and iron-depleted succinate media prepared as described in 8.1.2 without the addition of $FeSO_4.7H_2O$ to the concentrated base 8.1.4 or metals 44 solution 8.1.5

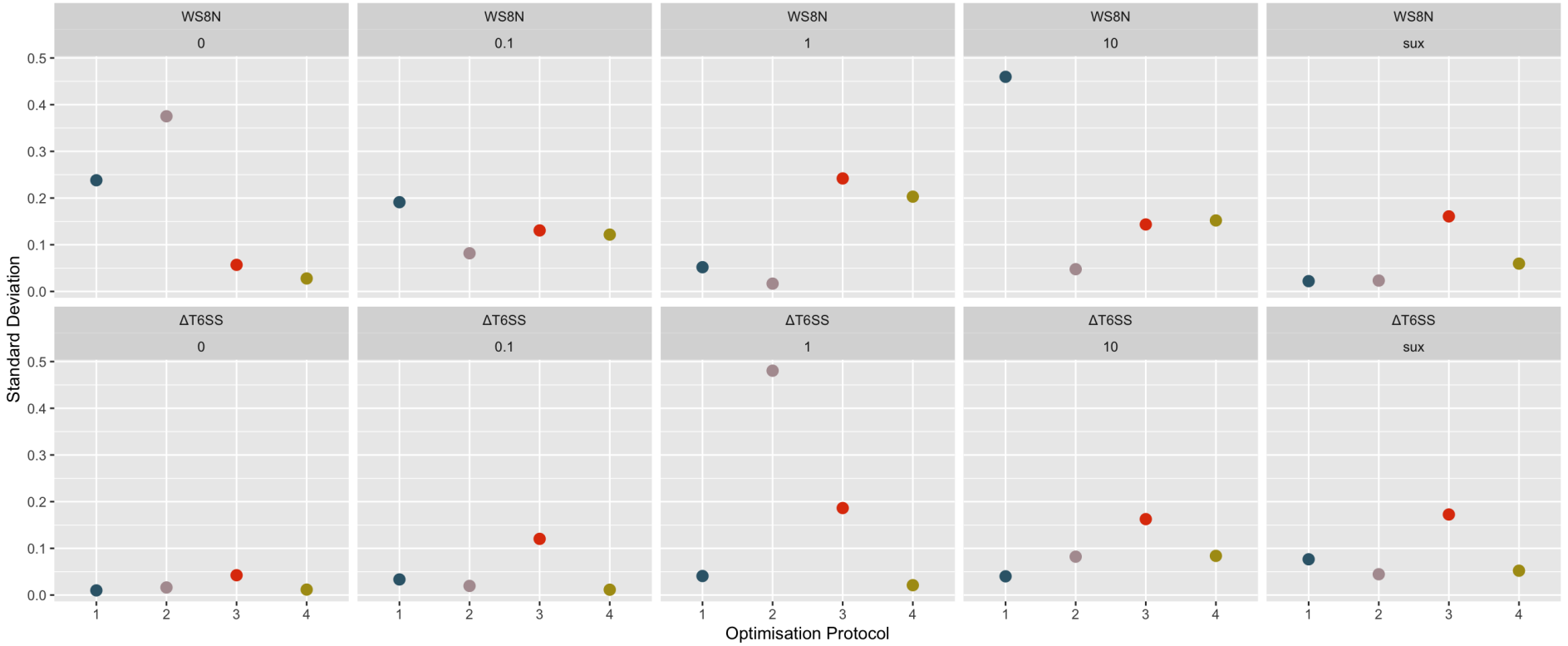


Figure 4.14: **Standard deviation of OD_{700} measurements of wild-type *R. sphaeroides* WS8N and its ΔT6SS mutant after 48 h of growth in regular succinate media or iron-depleted media supplemented with the indicated $FeCl_3.6H_2O$ concentration for each optimisation protocol**. Optimisation protocol number corresponds to (**1**) growth in iron-depleted succinate media (-$FeSO_4.7H_2O$, chelated CAA, GF, PB and MilliQ water), (**2**) growth in iron-depleted succinate media (-$FeSO_4.7H_2O$, chelated CAA), (**3**) growth in iron-depleted succinate media (-$FeSO_4.7H_2O$, chelated CAA) using starter cultures inoculated directly from frozen glycerol stocks and grown for 72 h, (**4**) growth in iron-depleted succinate media (-$FeSO_4.7H_2O$, chelated CAA) using starter cultures inoculated from colonies and grown for 72 h.

and with chelated CAA only. Metal-depleted media lacking other metals than iron were also prepared following the same protocol, i.e., by omitting the metal of choice from all relevant stock solutions and performing a chelation step on the CAA component.

4.3.4 Discussion

The results presented in this chapter demonstrate that the rigorous optimisation of both the iron-depleted growth media and the cultivation procedure for the starter cultures was necessary to ensure that the growth assays performed and presented in the next chapter are sensitive and reproducible. This is particularly important for slow growing organisms, like *R. sphaeroides*, and even more so when stringent growth conditions are be applied, such as growth in media where the availability of essential components is limited.

The first iron-depleted succinate media tested in this chapter was prepared as described in 8.1.2 without the addition of $FeSO_4.7H_2O$ to the concentrated base (8.1.4) or metals 44 solution (8.1.5) and with the application of a chelation step to the casamino acids, growth factor (8.1.6), phosphate buffer (8.1.3) and MilliQ water components. Use of these media led to variable results among biological replicates, which were particularly pronounced for wild-type *R. sphaeroides* WS8N grown in 0 µM, 0.1 µM and 10 µ$FeCl_3.6H_2O$. Moreover, anomalous growth dynamics of the wild-type strain were observed when grown in these media. In particular there was a spike in growth at 48 h followed by approximately 50 % reduction in OD_{700} at 72 h. This peculiar behaviour has not been observed in either succinate media, crude iron-depleted media or

iron-depleted media where only the casamino acids had been chelated (figures 4.8 and 4.12), where cells reach stationary phase as they approach 48 h of photoheterotrophic growth. The anomalous spike in growth observed at 24 h was the main reason for choosing not to use fully chelated media for subsequent experiments, since the use of media containing just chelated CAA did not really improve the standard deviation between replicates. Furthermore, chelation of all media components is not only time consuming but also very expensive, both being very legitimate additional reasons to avoid full chelation.

With OD_{700} readings being still variable between biological replicates when *R. sphaeroides* was grown in iron-depleted succinate media (-$FeSO_4.7H_2O$, chelated CAA), it was important to investigate additional ways to improve the implementation of the growth assay, before embarking into lengthy and technically demanding comparisons of the fitness of wild-type *R. sphaeroides* WS8N and its ΔT6SS mutant during metal ion starvation. The growth phase of the starter cultures that were used as inocula for the growth assays was identified as a parameter that might contribute to the variability between biological replicates. The use of starter cultures inoculated directly from frozen glycerol stock and grown for 72 h rather than 48 h did not seem to lead to a statistically significant difference in standard deviation overall. However, it was noticed that when starter cultures were grown for 48 h only, the standard deviation of the recorded values was very high for specific conditions, something that was not the case for any condition when 72 h starter cultures were used. This is likely because at 72 h every starter culture of *R. sphaeroides* will have reached saturation, whereas at 48 h the growth phase of each starter

culture will be highly variable. For this reason a 78 h incubation was adopted for starter cultures. A further decrease in the variability between biological replicates was achieved when starter cultures were inoculated with five colonies first grown on solid media for 72 h, rather than directly from a frozen glycerol stock. Once more, the improvement is related to the generation of a much more tractable and comparable inoculum between the tested conditions. Taking these modification together we concluded to use iron-depleted succinate media (-$FeSO_4.7H_2O$, chelated CAA) and starter cultures inoculated with colonies grown first on solid media for all growth assays described in the next chapter.

Chapter 5

The T6SS of *R. sphaeroides* WS8N has a role in ferrous and ferric iron acquisition under iron limiting conditions

5.1 Introduction

Dealing with nutrient-limiting conditions is business as usual in the bacterial world, necessitating the employment of starvation survival strategies to ensure persistence in the environment until conditions are more favourable and bacterial growth can resume. The T6SS is a molecular machine that is often expressed under hardship conditions, such as interbacterial competition, low resources, scarce nutrients, or interaction with a host. Since 2015, six T6SS have been identified to play a role in scavenging metal ions from the environment to meet the nutritional needs of their producers [43–47, 61]. In *Y. pseudotuberculosis*, zinc acquisition is mediated by T6SS-4 that delivers a Zn^{2+} binding protein into the extracellular milieu. *B. thailandensis* T6SS-4 has been shown to be involved in the sequestration of both Mn^{2+} and Zn^{2+} and *P. aeruginosa* uses its H2-T6SS and H3-T6SS to acquire Cu^{2+} and Fe^{3+}, respectively. The common mechanism behind T6SS-mediated ion acquisition for most of these systems is the secretion of an ion-binding protein by the T6SS. The notable exception to this is *P. aeruginosa* H3-T6SS, where no interactions between the secreted protein and iron ions were detected. In this case, the protein secreted by H3-T6SS interacts with an iron-binding intermediate. For all the cases mentioned above, the mechanisms by which bound metal ions are then taken up by the T6SS producer remain poorly understood.

With no anti-eukaryotic or antibacterial behaviours of *R. sphaeroides* described in the literature to date, we looked for other T6SS functions, namely metal acquisition and in particular iron sequestration. Chapter 4 described the construction of the ΔT6SS mutant and the development and optimisation

of a robust growth assay protocol. The latter aimed to identify an optimal iron-depleted medium for the growth of *R. sphaeroides* WS8N strains and to decide on a starter culture preparation procedure that would allow the recording of reproducible growth assay results for the assessment of the role of the T6SS.

Building on preliminary data collected during this D.Phil (not shown) that identified a phenotypic difference between wild-type *R. sphaeroides* WS8N and its ΔT6SS knock-out mutant when grown under iron-limited conditions, this chapter will employ the growth assay developed in chapter 4 to further interrogate the role of the *R. sphaeroides* T6SS, with a particular focus on iron acquisition. To this aim, the following questions will be answered: **1)** Does the absence of the T6SS genes cause a fitness defect to *R. sphaeroides* WS8N under normal laboratory conditions, both aerobic and photoheterotrophic? **2)** Does the *R. sphaeroides* T6SS have a role in the sequestration of divalent transition metals used in succinate media (Fe, Zn, Mn, Cu and Co) under photoheterotrophic growth? **3)** What form of iron does the *R. sphaeroides* T6SS sequester, ferrous, ferric or heme-bound? **4)** Does the *R. sphaeroides* T6SS play a role for iron sequestration during aerobic growth?

5.2 Growth of wild-type *R. sphaeroides* WS8N and of its ΔT6SS mutant strain under normal laboratory conditions

5.2.1 There is no difference between the growth profiles of wild-type *R. sphaeroides* WS8N and its ΔT6SS mutant under standard laboratory conditions after 48 h of photoheterotrophic growth in regular succinate media

Growth assays were performed to determine whether the deletion of the T6SS structural genes leads to decrease of the general fitness of this strain in comparison to its parent, *R. sphaeroides* WS8N. Starter cultures of wild-type *R. sphaeroides* WS8N and its ΔT6SS mutant were inoculated with five single colonies as described in sections 2.2.3 and 4.3.2.2 for 72 h. Starter cultures were then normalised to OD_{700} 1.5 and diluted 1:1000 into regular succinate media, supplemented with the appropriate antibiotics in 1.5 mL tubes with minimal airspace and incubated under constant illumination (light intensity of 10 W/m^2) at 30 °C for 96 h[130]. At every 24 h time interval (24, 48, 72 and 96 h) 150 µL of culture sample was transferred to a 96 well microtitre plate and the OD_{700} was measured. Owing to constraints regarding space in the light cabinet and the lengthy nature of the growth assay, it was necessary to take samples as infrequently as possible. 24 h permits the sampling of *R. sphaeroides* WS8N in exponential phase and 48 h allows us to sample *R. sphaeroides* WS8N in stationary phase[131]. Slow growing *R. sphaeroides* mutant strains which are still in exponential phase after 60 h of growth have been described in the literature, so we also opted to sample at 72 and 96 h[130].

While the ΔT6SS mutant showed decreased growth at the 24 h time point

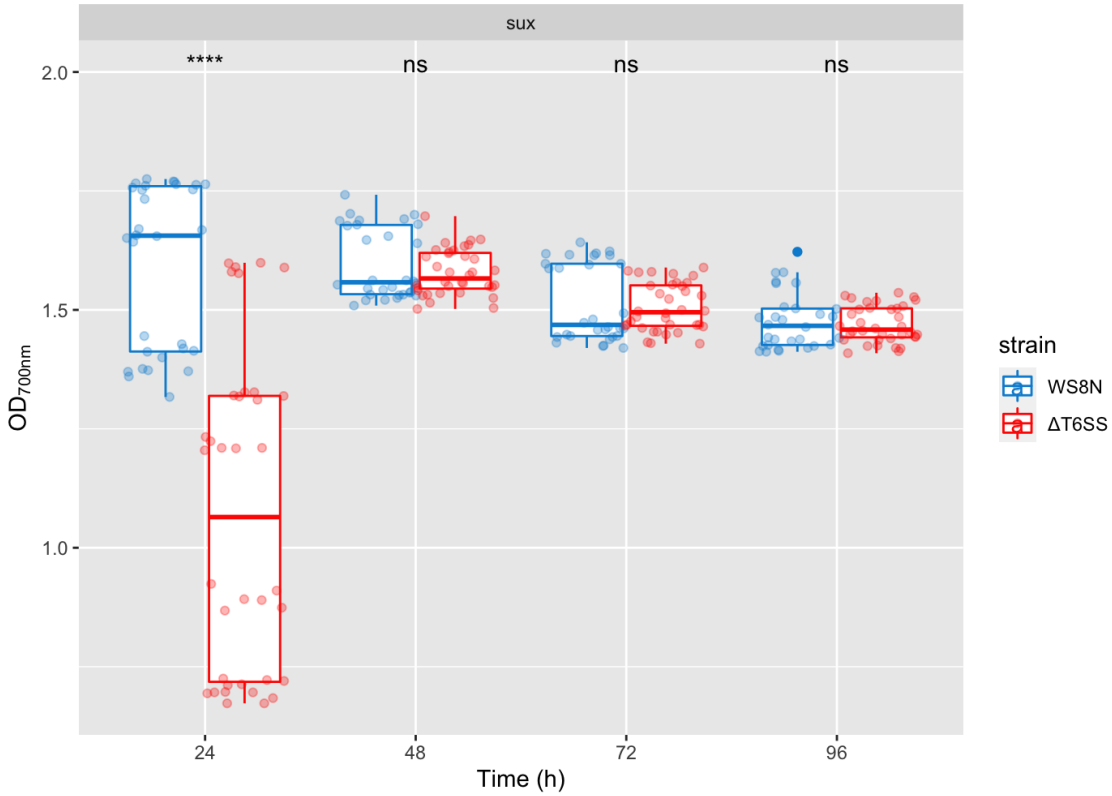


Figure 5.1: **Photoheterotrophic growth of wild-type *R. sphaeroides* and its ΔT6SS mutant in regular succinate media.** Wild-type *R. sphaeroides* and the ΔT6SS mutant were grown photoheterotrophically in succinate media incubated under constant illumination (light intensity of ~10 W/m^2) at 30 °C. Cultures were grown for 96 h and OD_{700} values were taken at every 24 h interval.A Mann-Whitney test was performed to detect significant differences between the OD_{700} of the wild type WS8N and the ΔT6SS mutant. This experiment was repeated on two different occasions. On both occasions this experiment was performed in biological triplicate, with each biological replicate performed in technical triplicate, all data points are displayed. **** $P<0.0001$, ns = not significant.

(Mann-Whitney test, P<0.0001), this growth lag was undetectable in all other tested time points; after 48 h of growth both the wild-type strain and the mutant reached an OD_{700} of approximately 1.5 (figure 5.1). It is worth noting that even though the optimisation of the growth assay detailed in chapter 4, sought to decrease inter-replicate variability at the 48 h time point of the growth assay, as illustrated in figures 4.6, 4.8 and 4.12, at 24 h the spread of OD_{700} values between replicates remains large for both wild-type *R. sphaeroides* WS8N and its ΔT6SS mutant strain grown in succinate. The data shown in figure 5.1 for the 24 h time point are also very variable. Therefore, based on the fact that no growth defect is observed on any of the subsequent time points, the results obtained at 24 h can likely be ignored.

5.2.2 There is no difference between the growth profiles of wild-type *R. sphaeroides* WS8N and its ΔT6SS mutant when grown aerobically in regular succinate media

Cultures of wild-type *R. sphaeroides* WS8N and its ΔT6SS mutant were grown aerobically after being inoculated with normalised photoheterotrophic starter cultures which were grown as described above (see section 5.2.1. Briefly,starter cultures were diluted 1:100 into 1.5 mL succinate media containing the appropriate antibiotics and transferred into 24-well plates (VWR) covered with a transparent Breathe-Easy sealing membrane (Sigma). Plates were incubated at 30 °C with shaking (200 rpm) using a CLARIOstar plate reader; automated measurements of OD_{700} were taken at 20 min intervals for 24 h.

When grown aerobically in regular succinate media, the ΔT6SS mutant

strain lagged behind the wild-type strain during the exponential phase of growth, however, by 24 h of growth both strains had reached the same OD_{700} (figure 5.2). This growth lag observed for the ΔT6SS mutant during the exponential phase is similar to what was observed at 24 h when these strains were grown under photoheterotrophic conditions (figure 5.1). That said, when the acquired growth curve data from six independent experiments each carried out in biological triplicate were analysed, there was no significant difference between the growth rates of the two strains (Wilcoxon test, P=0.5798, figure 5.3). It is possible that once more, any data collected in the first 24 h are too variable to lead to any reliable conclusions. Together, the data shown in sections 5.2.1 and 5.2.2 suggest that *R. sphaeroides* is not dependent on its T6SS for aerobic or photoheterotrophic growth under standard laboratory media and conditions.

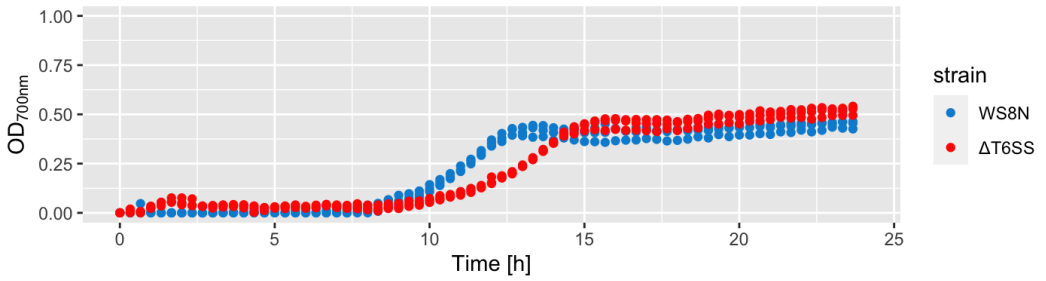


Figure 5.2: **Growth curves of wild-type *R. sphaeroides* WS8N and its ΔT6SS mutant grown aerobically in regular succinate media.** Wild-type *R. sphaeroides* WS8N and its ΔT6SS mutant were grown aerobically at 30°C with shaking at 200 rpm. Automated measurements of OD_{700} were taken at 20 min intervals for 24 h. This experiment was conducted in triplicate.

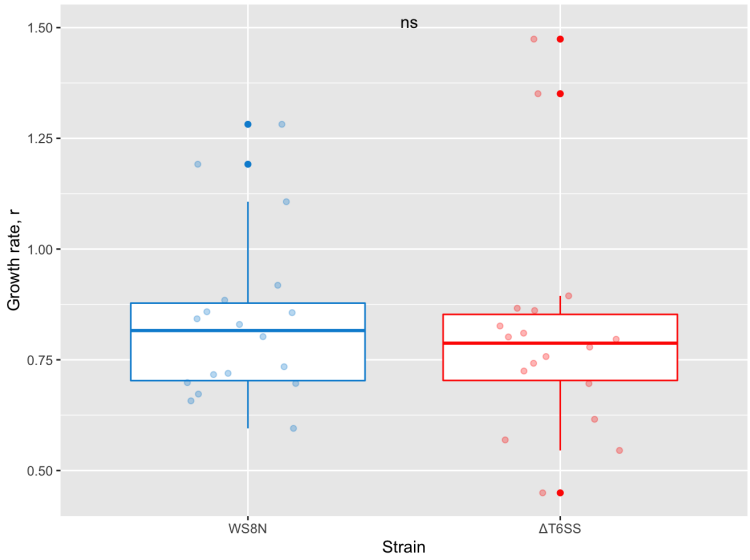


Figure 5.3: **Growth rates of wild-type *R. sphaeroides* WS8N its ΔT6SS mutant when grown aerobically in regular succinate media.** Growth rates were calculated for each growth curve shown in figure 5.2 using the growthcurver R package. This experiment was conducted in biological triplicate on six separate occasions. n=18 for each strain, ns = not significant.

5.3 Testing the growth dependence of wild-type *R. sphaeroides* WS8N on divalent transition metal ions

The growth dependence of wild-type *R. sphaeroides* WS8N on divalent transition metal ions was investigated before comparing the growth profiles of the wild-type and ΔT6SS strains under metal-limited growth conditions. Regular succinate is a metal-rich medium containing $ZnSO_4.7H_2O$ at 19 µM, $FeSO_4.7H_2O$ at 12.6 µM, $MnSO_4.4H_2O$ at 4.48 µM, $CuSO_4.5H_2O$ at 0.78 µM, and $CoCl_2.6H_2O$ at 0.42 µM (see 8.1.2). Photoheterotrophic growth assays for wild-type *R. sphaeroides* WS8N were performed in metal-depleted succinate media, in each case lacking one the metal ions listed above, prepared as described in section 2.2.6. Metals were supplemented aiming to achieve 0 %, 0.8 % , 8 % or 80 % of the concentration used in regular succinate media.

There was no significant difference in the OD_{700} achieved by wild-type *R. sphaeroides* WS8N when it was grown in succinate or Mn-depleted succinate media supplemented with 0, 0.04, 0.4 or 4 µM $MnSO_4.4H_2O$ (figure 5.4, panel **c**). This suggests that there is no growth dependence of wild-type *R. sphaeroides* WS8N on Mn^{2+} when grown photoheterotrophically (Kruskal-Wallis test, P=0.2270). Similarly no effects were observed in the case of $CuSO_4.5H_2O$, with all *R. sphaeroides* WS8N cultures reaching at least OD_{700} 1.5 (figure 5.4, panel **d**). For $CoCl_2.6H_2O$, higher concentrations of the metal ion lead to a small increase in OD_{700}, but ultimately there was no detrimental effect on growth under any of the tested concentrations (figure 5.4, panel **e**). When grown in the absence of $ZnSO_4.7H_2O$, cells reach an OD_{700} of approximately 2.200, which is significantly higher than that reached when grown in Zn-depleted media supplemented with any amount of zinc (figure 5.4, panel **a**). Whilst this growth advantage was observed, growth is not concentration dependent when Zn^{2+} is present and under all tested concentrations cells reach at least an OD_{700} 1.5. Finally, there is a clear growth dependence of wild-type *R. sphaeroides* WS8N on $FeSO_4.7H_2O$ concentration, with growth favouring higher Fe^{2+} concentrations (figure 5.4, panel **b**). A ten-fold increase in $FeSO_4.7H_2O$ concentration from 0.1 µM to 1 µM resulted in a 500 % increase in OD_{700}. This clearly indicates that cellular import of Fe^{2+} under photoheterotrophic conditions is actively occurring at concentrations at and above 1 µM.

The difference in growth between the lowest and the highest Co^{2+} concen-

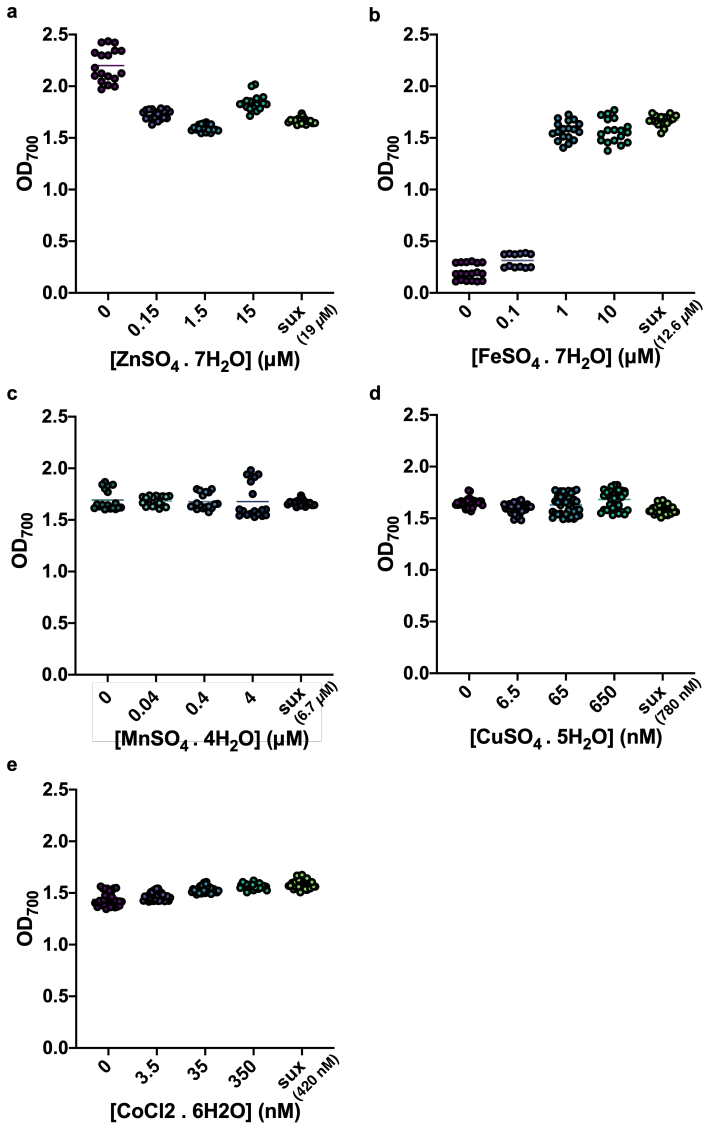


Figure 5.4: **The growth dependence of wild-type *R. sphaeroides* WS8N on divalent transition metals.** Wild-type *R. sphaeroides* WS8N was grown photoheterotrophically in (**a**) Zn-depleted succinate media supplemented with the indicated concentrations of $ZnSO_4.7H_2O$, (**b**) Fe-depleted succinate media supplemented with the indicated concentrations of $FeSO_4.7H_2O$, (**c**) Mn-depleted succinate media supplemented with the indicated concentrations of $MnSO_4.4H_2O$,(**d**) Cu-depleted succinate media supplemented with the indicated concentration of $CuSO_4.5H_2O$, (**e**) Co-depleted succinate media supplemented with the indicated concentration of $CoCl_2.6H_2O$. OD_{700} readings were taken at 48 h of growth. Each experiment was conducted in triplicate.

trations tested was significant (Mann-Whitney test, P<0.0001) with an effect size of 2.74 (Cohen's d). Growth in Zn-depleted succinate media supplemented with 0 µM or 0.15 µM $ZnSO_4.7H_2O$ yielded significantly different OD_{700} read-

ings (P<0.0001) with an effect size of 3.91 (Cohen's d) between the two groups. To put the effect of divalent transition metal concentration on the growth of wild-type *R. sphaeroides* WS8N into context, the effect size when grown in iron-depleted succinate media supplemented with 0.1 µM compared to supplementation with 1 µM $FeSO_4.7H_2O$ was 25.7 (Cohen's d). This demonstrates that iron acquisition is a crucial process for the photoheterotrophic growth of *R. sphaeroides*. These growth profiles of *R. sphaeroides* under metal limitation will form the basis to compare the growth of the wild-type strain with its ΔT6SS mutant under the same limiting conditions.

5.4 Determining the phenotypic consequence of T6SS absence in divalent-transition-metal-depleted growth conditions

Growth assays were performed in conditions where each of the divalent transition metals tested in section 5.3 were absent for both the wild-type *R. sphaeroides* WS8N and its ΔT6SS mutant. Experiments were performed as detailed in sections 5.3 and 2.2.6.

5.4.1 There is no difference in growth between wild-type *R. sphaeroides* and its ΔT6SS mutant when grown under zinc-, manganese-, copper- or cobalt-limited conditions

As for wild-type *R. sphaeroides* WS8N, the ΔT6SS mutant does not demonstrate a growth dependence on Zn^{2+} under photoheterotrophic conditions. Although there is a statistically significant difference in growth between the

wild-type strain and the ΔT6SS mutant in four out of the five $ZnSO_4.7H_2O$ concentrations tested, this difference is minimal, with no detrimental consequence to growth under any concentration for either strain. The fact that this difference is negligible is further supported by the fact that for some concentrations of $ZnSO_4.7H_2O$ tested the wild-type strains grows better on average, while for others the mutant does better. For example, when Zn-depleted media is supplemented with 15 µM $ZnSO_4.7H_2O$, *R. sphaeroides* WS8N reached an OD_{700} of 1.841±0.07557 and ΔT6SS reached an OD_{700} of 1.737±0.04193. By contrast, when Zn-depleted media was supplemented with 1.5 µM $ZnSO_4.7H_2O$, the trend was reversed with the wild-type strain reaching an OD_{700} of 1.593±0.03280 and the mutant growing to an OD_{700} of 1.636±0.05474 (figure 5.5).

There was no meaningful difference in OD_{700} between wild-type *R. sphaeroides* WS8N and its ΔT6SS mutant after 48 h of photoheterotrophic growth in any of the $MnSO_4.4H_2O$, $CuSO_4.5H_2O$, or $CoCl_2.6H_2O$ concentrations tested (figure 5.6, figure 5.7, and figure 5.8).

5.4.2 The ΔT6SS mutant exhibits a severe growth defect under iron-limited conditions

When grown in high Fe^{2+}, the growth of the ΔT6SS mutant was comparable to that of its parent, with both strains reaching to at least an OD_{700} of 1.5. More specifically, the difference in OD_{700} between wild-type *R. sphaeroides* WS8N and its ΔT6SS mutant was not significant (Unpaired t test, P=0.1109) or small (Unpaired t test, P=0.0357) when the two strains were grown in iron-depleted

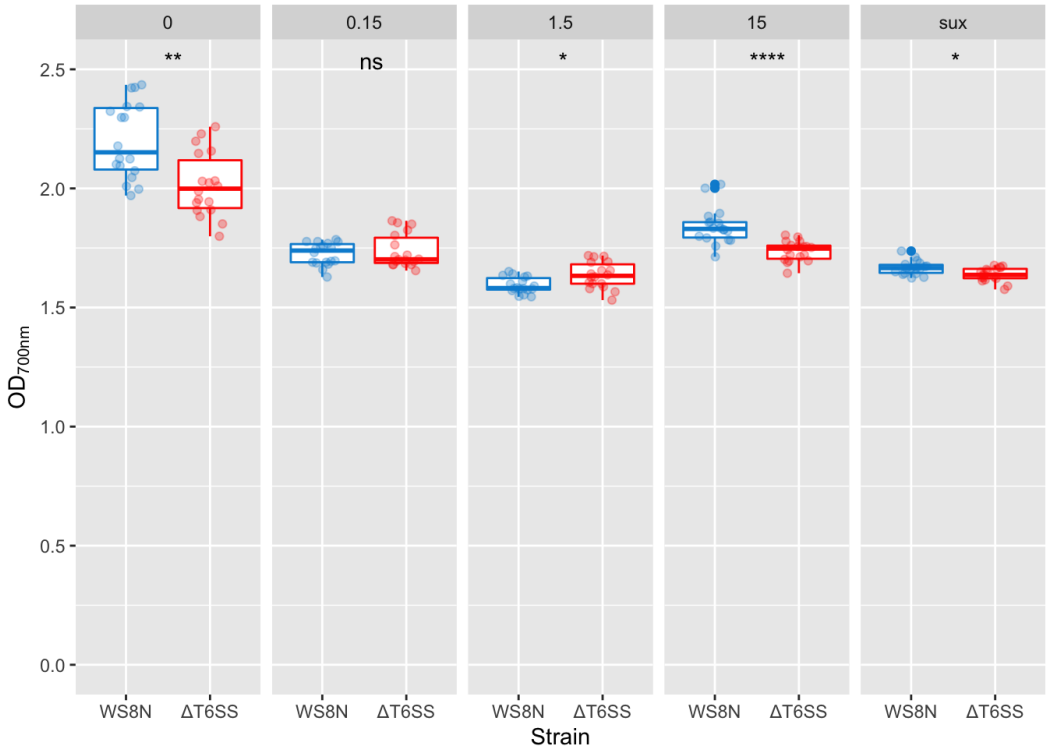


Figure 5.5: **Growth of wild-type *R. sphaeroides* WS8N and its ΔT6SS mutant under different $ZnSO_4.7H_2O$ concentrations in Zn-depleted succinate media.** Wild-type *R. sphaeroides* WS8N and its ΔT6SS mutant were grown photoheterotrophically from colony-derived 72 h starter cultures, either in regular succinate media or zinc-depleted succinate media supplemented with the indicated concentrations of $ZnSO_4.7H_2O$ (µM). OD_{700} was measured after 48 h of growth. A Mann-Whitney test was performed to detect significant differences between the OD_{700} of the wild-type WS8N and its ΔT6SS mutant. This experiment was repeated on two different occasions. On both occasions this experiment was performed in biological triplicate, with each biological replicate performed in technical triplicate, all data points are displayed. **** P<0.0001, ** P<0.01, * P<0.05, ns = not significant.

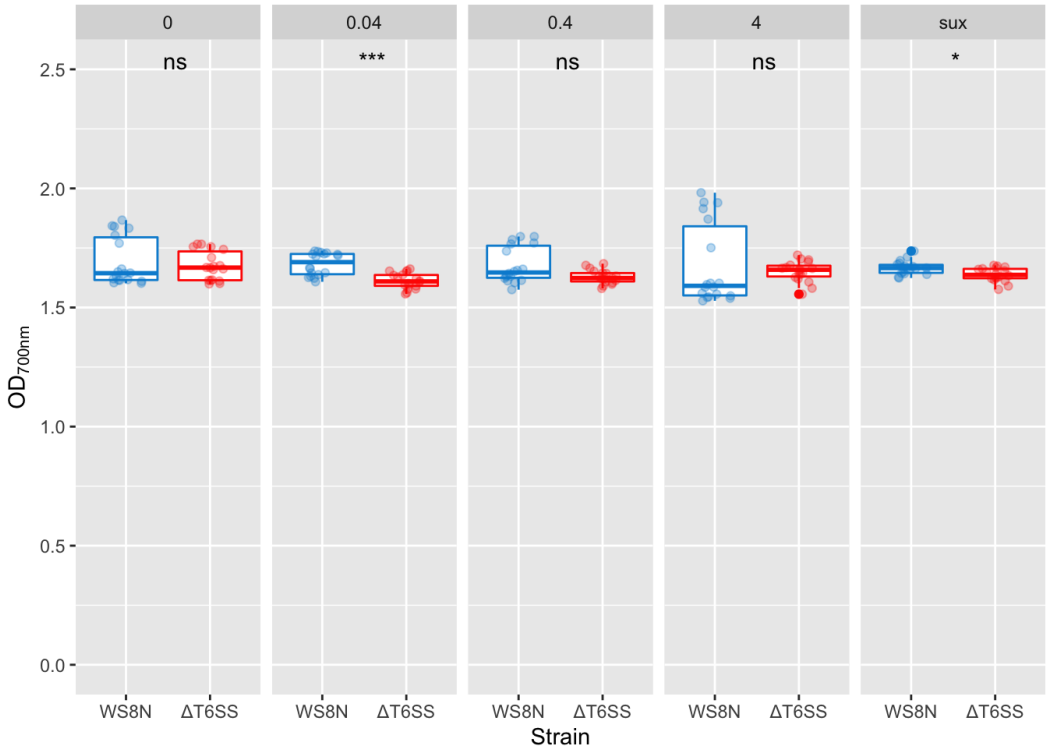


Figure 5.6: **Growth of wild-type *R. sphaeroides* WS8N and its ΔT6SS mutant under different $MnSO_4.4H_2O$ concentrations in manganese-depleted succinate media.** Wild-type *R. sphaeroides* WS8N and its ΔT6SS mutant were grown photoheterotrophically from colony-derived 72 h starter cultures, either in regular succinate media or manganese-depleted succinate media supplemented with the indicated concentrations of $MnSO_4.4H_2O$ (µM). OD $_{700}$ was measured after 48 h of growth. A Mann-Whitney test was performed to detect significant differences between the OD_{700} of the wild-type WS8N and its ΔT6SS mutant. This experiment was repeated on two different occasions. On both occasions this experiment was performed in biological triplicate, with each biological replicate performed in technical triplicate, all data points are displayed. *** $P<0.001$, * $P<0.05$, ns = not significant.

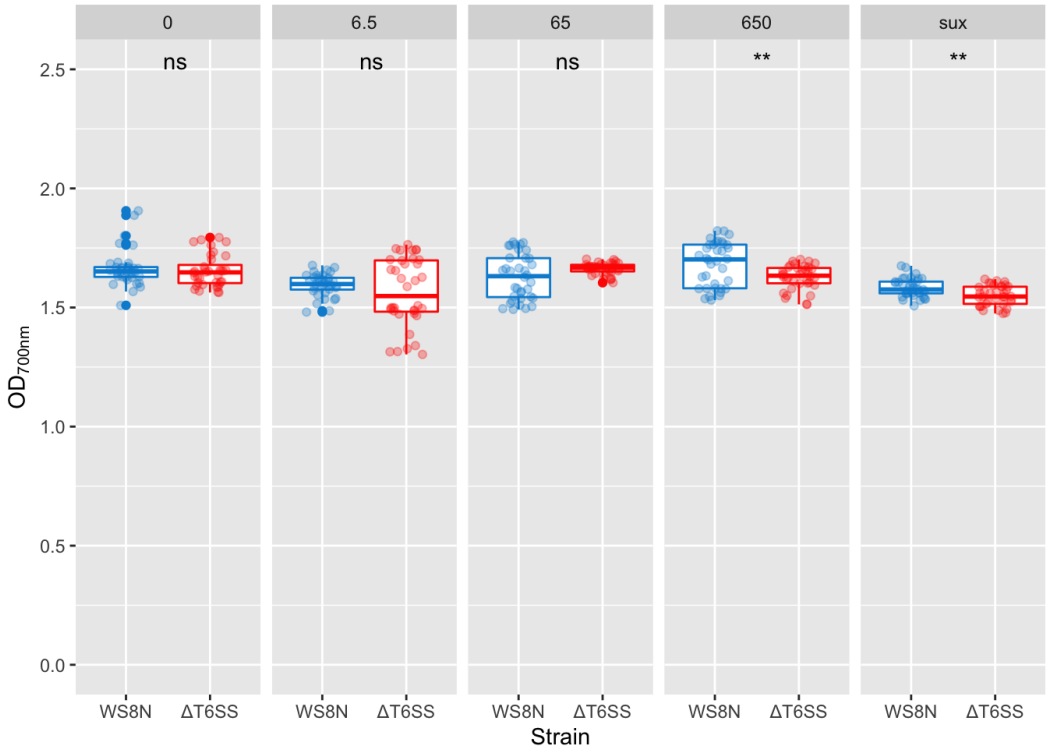


Figure 5.7: **Growth of wild-type *R. sphaeroides* WS8N and its ΔT6SS mutant under different $CuSO_4.5H_2O$ concentrations in copper-depleted succinate media.** Wild-type *R. sphaeroides* WS8N and its ΔT6SS mutant were grown photoheterotrophically from colony-derived 72 h starter cultures, in regular succinate media or copper-depleted succinate media supplemented with the indicated concentrations of $CuSO_4.5H_2O$ (nM). OD_{700} was measured after 48 h of growth. A Mann-Whitney test was performed to detect significant differences between the OD_{700} of the wild-type WS8N and its ΔT6SS mutant. This experiment was repeated on two different occasions. On both occasions this experiment was performed in biological triplicate, with each biological replicate performed in technical triplicate, all data points are displayed. ** $P<0.01$, ns = not significant.

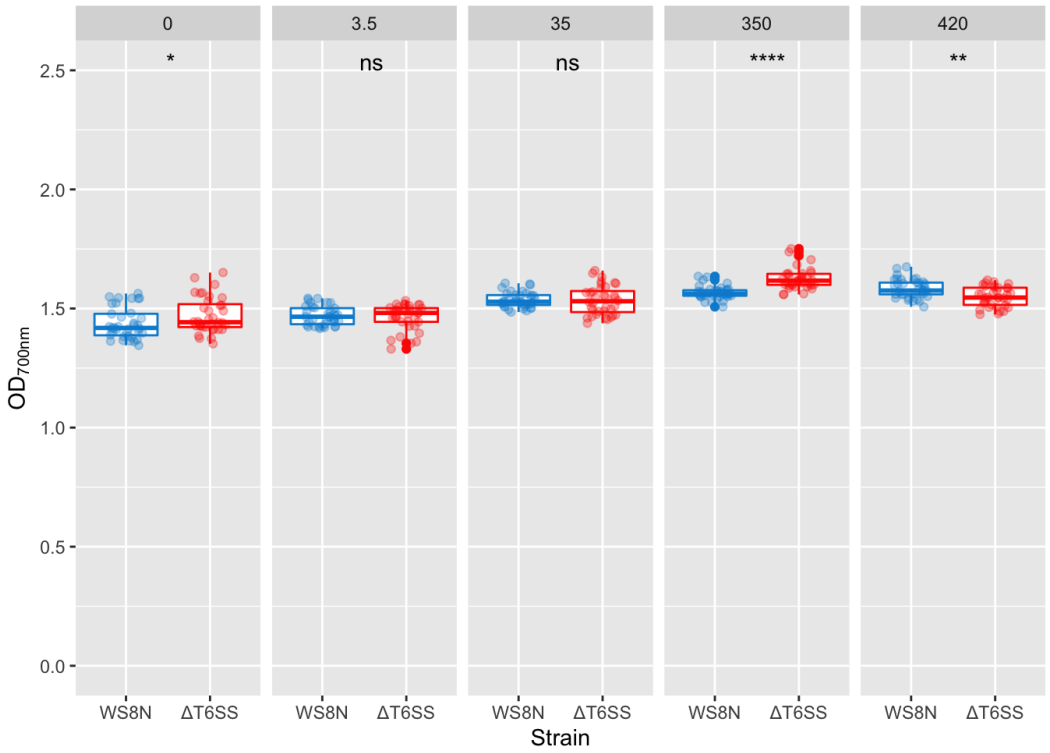


Figure 5.8: **Growth of wild-type *R. sphaeroides* WS8N and its ΔT6SS mutant under different $CoCl_2.6H_2O$ concentrations in cobalt-depleted succinate media.** Wild-type *R. sphaeroides* WS8N and its ΔT6SS mutant were grown photoheterotrophically from colony-derived 72 h starter cultures, either in regular succinate media or cobalt-depleted succinate media supplemented with the indicated concentrations of $CoCl_2.6H_2O$ (nM). OD $_{700}$ was measured after 48 h of growth. A Mann-Whitney test was performed to detect significant differences between the OD_{700} of the wild-type WS8N and its ΔT6SS mutant. This experiment was repeated on two different occasions. On both occasions this experiment was performed in biological triplicate, with each biological replicate performed in technical triplicate, all data points are displayed. **** P<0.0001, ** P<0.01, * P<0.05, ns = not significant.

media supplemented with 10 µM $FeSO_4.7H_2O$ or succinate media containing 12.6 µM $FeSO_4.7H_2O$, respectively (figure 5.9).

Although both strains demonstrate poor growth under low Fe^{2+} conditions, the ΔT6SS mutant exhibits a clear growth deficiency with respect to the wild-type strain; wild-type *R. sphaeroides* WS8N reached OD_{700} of 0.2±0.07665 and OD_{700} of 0.3137±0.06741 in 0 µM and 0.1 µM $FeSO_4.7H_2O$, respectively, while the mutant strain only grew to OD_{700} of 0.06422±0.009681 and OD_{700} of 0.08217±0.01441 in 0 µM and 0.1 µM $FeSO_4.7H_2O$, respectively. Essentially, the ΔT6SS mutant is unable to grow in low-iron succinate media, while the parent strain manages to hang on (figure 5.9).

Interestingly, when iron-depleted media supplemented with 1 µM $FeSO_4.7H_2O$ were tested, the phenotypic difference between the two strains was vast. Wild-type *R. sphaeroides* WS8N reaches an OD_{700} of 1.570±0.09083, whereas the ΔT6SS mutant only grows to an OD_{700} of 0.1450±0.01868 (figure 5.9). The effects of iron concentration change dramatically when another ten fold increase in Fe^{2+} concentration is applied; while the growth of the wild-type strain remains similar to what was observed at 1 µM $FeSO_4.7H_2O$, the growth of the mutant fully recovers. Since the mutant strain only lacks the T6SS apparatus, these results suggest that at 10 µM $FeSO_4.7H_2O$ both strains are capable of importing iron, through the many mechanisms *R. sphaeroides* possesses[77], but at 1 µM $FeSO_4.7H_2O$ the T6SS is essential for iron import.

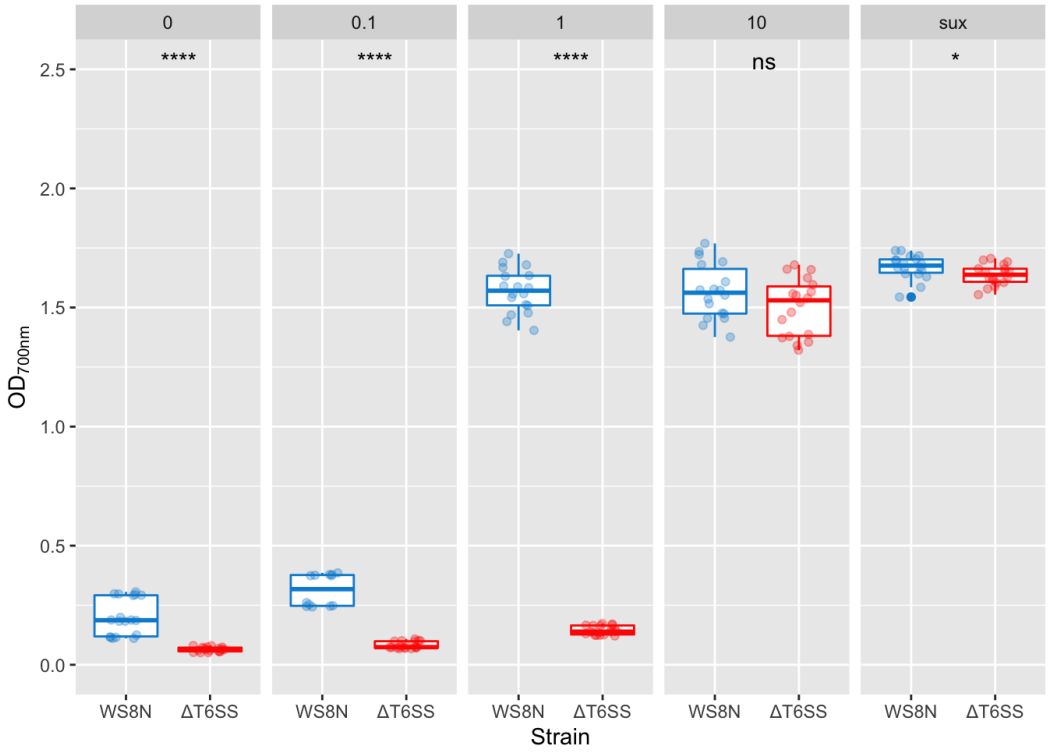


Figure 5.9: **Growth of wild-type *R. sphaeroides* WS8N and its ΔT6SS mutant under different $FeSO_4.7H_2O$ concentrations in iron-depleted succinate media.** Wild-type *R. sphaeroides* WS8N and itsΔT6SS mutant were grown photoheterotrophically from colony-derived 72 h starter cultures, either in regular succinate media or iron-depleted succinate media supplemented with the indicated concentrations of $FeSO_4.7H_2O$ (µM). OD_{700} was measured after 48 h of growth. A Mann-Whitney test was performed to detect significant differences between the OD_{700} of the wild-type WS8N and its ΔT6SS mutant. This experiment was repeated on two different occasions. On both occasions this experiment was performed in biological triplicate, with each biological replicate performed in technical triplicate, all data points are displayed. **** $P<0.0001$, * $P<0.05$, ns = not significant.

5.5 The T6SS is required for growth under limited iron conditions

The difference in the growth profiles of wild-type *R. sphaeroides* WS8N and its ΔT6SS mutant observed under low concentrations of Fe^{2+} (figure 5.9) prompted further investigation. With ferrous iron being scarce in the environment we wanted to test whether these effects were unique to that oxidation state of iron, or whether we would observe similar trends when the more widely

available ferric iron is used to supplement our iron-depleted succinate media. Although in no way definitive, bioinformatic analysis also predicted a heme utilisation domain at the C-terminus of the *R. sphaeroides* WS8N VgrG protein, which prompted the expansion of iron types tested to include iron bound in heme.

Succinate media contains 12.6 µM of ferrous sulfate, that provides 0.7 mg of Fe^{2+} per litre of culture. The appropriate molar concentrations of iron in its ferric form, $FeCl_3.6H_2O$, and bound form, $C_{34}H_{32}ClFeN_4O_4$ (hemin), were added to provide 0.56 mg Fe per litre of culture, which is equivalent to 80 % of the amount that regular succinate media contain. 8 % and 0.8 % of the concentration of Fe found in regular succinate media were also tested. This amounted to 10 µM, 1 µM and 0.1 µM for all forms of iron. Experiments were performed as detailed in sections 5.3 and 2.2.6.

Initially, growth dependence of wild-type *R. sphaeroides* WS8N on hemin was investigated. When grown in iron-depleted media supplemented with 0 µM, 0.1 µM, 1 µM or 10 µM of hemin, there was no significant difference in OD_{700} at 48 h (one-way ANOVA, P=0.2158). Negligible growth of *R. sphaeroides* WS8N at all concentrations of hemin compared to the growth achieved in regular succinate media, suggests that under photoheterotrophic conditions *R. sphaeroides* WS8N cannot import heme (figure 5.10). Statistical analysis showed a further decrease in the fitness of the ΔT6SS mutant compared to the parent strain, when grown in iron-depleted succinate media supplemented with the same amount of hemin as above. However, this ef-

fect size is small (Cohen's d = 3.00) and of little biological relevance as growth was not established for either strain at all concentrations of hemin (figure 5.11).

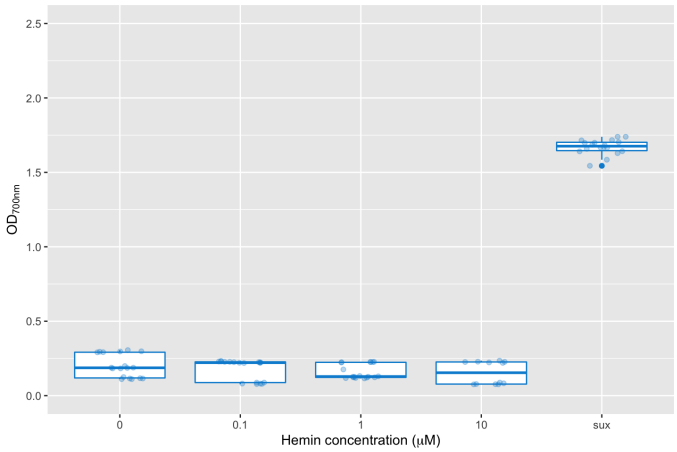


Figure 5.10: **The growth dependence of wild-type *R. sphaeroides* WS8N on hemin.** Wild-type *R. sphaeroides* WS8N was grown photoheterotrophically in iron-depleted succinate media supplemented with the indicated concentration of hemin (μM). OD_{700} readings were taken at 48 h. Each experiment was conducted in triplicate.

Similarly to Fe^{2+}, wild-type *R. sphaeroides* WS8N displayed a growth dependence on Fe^{3+}, with lower concentrations being detrimental to growth (figure 5.12). Assessing the performance of wild-type *R. sphaeroides* WS8N across the various concentrations of Fe^{2+} and Fe^{3+} there is a consistent pattern, with 1 μM Fe being the permissive concentration for growth after 48 h under photoheterotrophic conditions. When compared to growth in iron-depleted media supplemented with ferrous and ferric iron, it is clear that under these conditions bound iron in the form of heme is not imported (figures 5.12 and 5.10).

Although both strains demonstrate poor growth when in low Fe^{3+}, the ΔT6SS mutant exhibits a growth deficiency with respect to the wild-type strain; wild-type *R. sphaeroides* WS8N reached an OD_{700} of 0.1512±0.01944

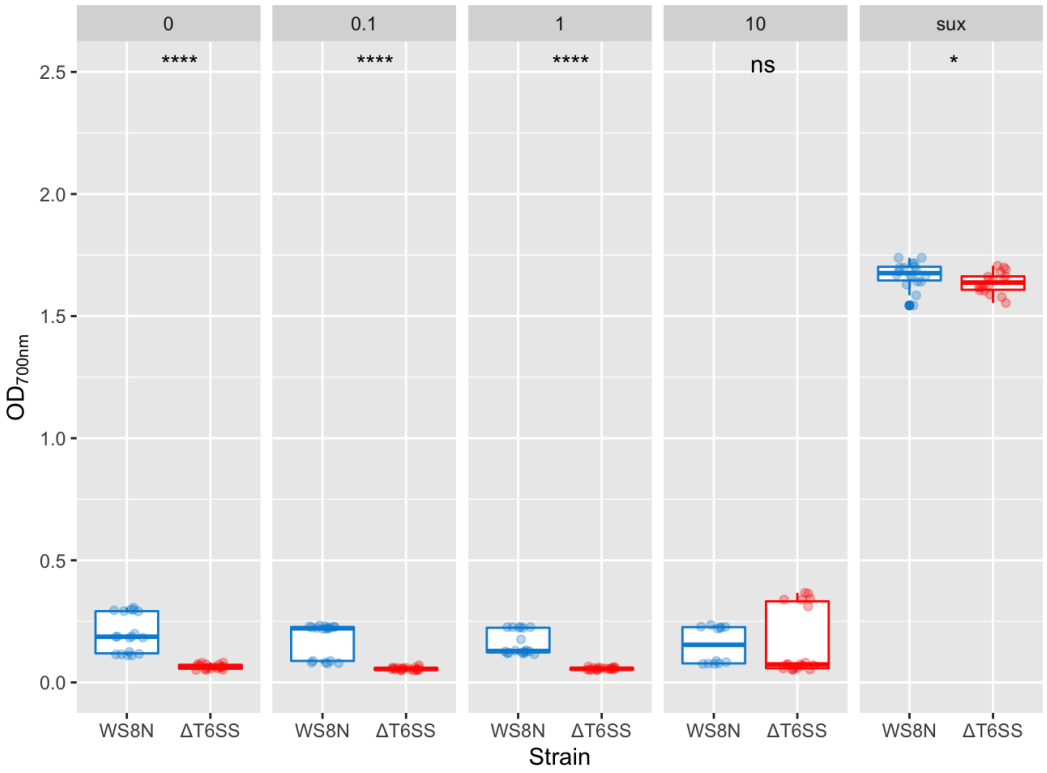


Figure 5.11: **Growth of wild type *R. sphaeroides* WS8N and its ΔT6SS mutant in iron-depleted succinate media supplemented with hemin**. Wild-type *R. sphaeroides* WS8N and its ΔT6SS mutant were grown photoheterotrophically from colony-derived 72 h starter cultures, either in regular succinate media or iron-depleted succinate media supplemented with the indicated concentration of hemin (µM). OD $_{700}$ was measured after 48 h of growth. A Mann-Whitney test was performed to detect significant differences between the OD_{700} of the wild type WS8N and its ΔT6SS mutant. This experiment was repeated on two different occasions. On both occasions this experiment was performed in biological triplicate, with each biological replicate performed in technical triplicate, all data points are displayed. **** P<0.0001, * P<0.05, ns = not significant.

and an $OD_{700}$of 0.3476±0.04547 in 0 µM and 0.1 µM $FeCl_3.6H_2O$, respectively, whereas the ΔT6SS mutant only grew to an OD_{700} of 0.04665±0.004061 and an OD_{700} of 0.05533±0.005336, respectively (figure 5.13). In a similar manner as observed with ferrous iron, the growth of the ΔT6SS mutant is prohibited in iron-depleted succinate media or media only supplemented with 0.1 µM $FeCl_3.6H_2O$.

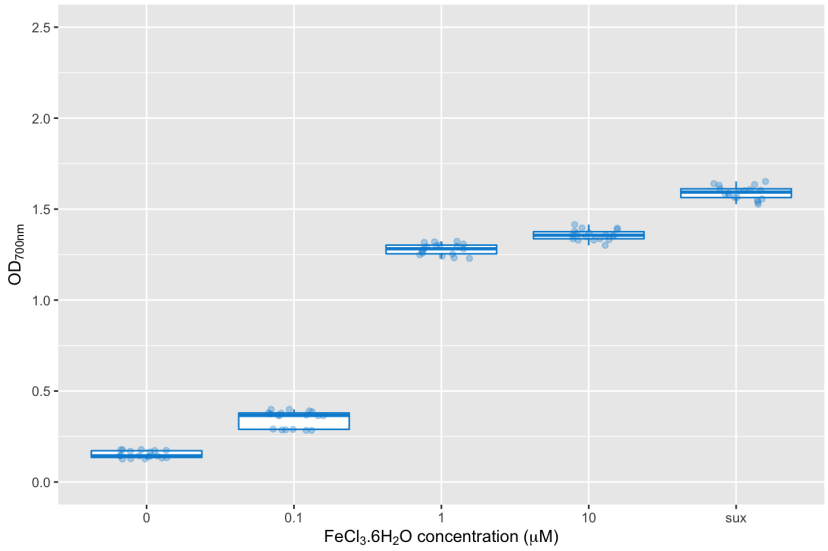


Figure 5.12: **The growth dependence of wild-type *R. sphaeroides* WS8N on Fe^{3+}.** Wild-type *R. sphaeroides* WS8N was grown photoheterotrophically in iron-depleted succinate media supplemented with the indicated concentration of $FeCl_3$.$6H_2O$ (µM). OD_{700} readings were taken at 48 h. Each experiment was conducted in triplicate.

Exactly as observed with ferrous iron, addition of 1 µM or 10 µM $FeCl_3.6H_2O$ allows growth of wild-type *R. sphaeroides* WS8N, but only the latter concentration allows the growth of the ΔT6SS mutant (figure 5.13). The size of the observed effects (as given by Cohen's d) was determined by calculating the mean difference between the growth of the two strains in certain conditions, and then dividing the result by the pooled standard deviation for the measurements obtained for these conditions. The effect size of iron concentration was compared for the growth of the wild-type and mutant strains in iron-depleted media supplemented with 1 µM iron (figure 5.14). A strong growth defect phenotype was observed when wild-type *R. sphaeroides* WS8N and its ΔT6SS mutant were grown in iron-depleted media supplemented with 1 µM $FeSO_4.7H_2O$ (d = 21.73) or 1 µM $FeCl_3.6H_2O$ (d = 39.98). This strong phenotype was not exhibited when strains were supplemented with 1 µM hemin (d = 3.00).

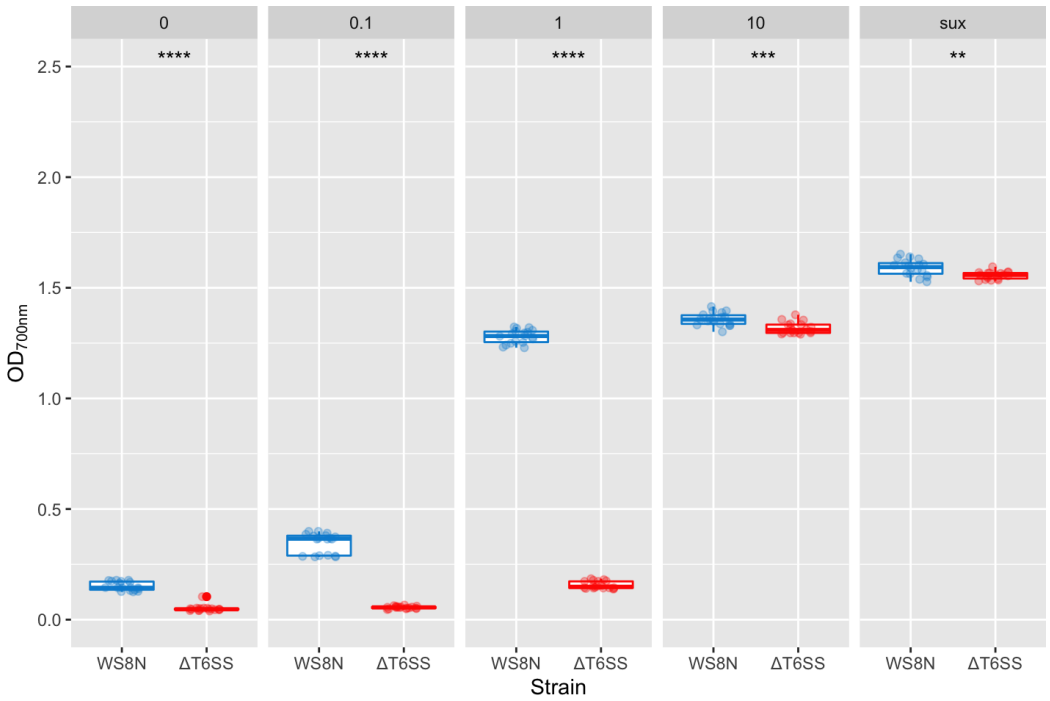


Figure 5.13: **Growth of wild-type *R. sphaeroides* WS8N and its ΔT6SS mutant under different $FeCl_3.6H_2O$ concentrations in iron-depleted succinate media.** Wild-type *R. sphaeroides* WS8N and its ΔT6SS mutant were grown photoheterotrophically from colony-derived 72 h starter cultures, either in regular succinate media or iron-depleted succinate media supplemented with the indicated concentration of $FeCl_3.6H_2O$ (µM). OD_{700} was measured after 48 h of growth. A Mann-Whitney test was performed to detect significant differences between the OD_{700} of the wild-type WS8N and its ΔT6SS mutant. This experiment was repeated on two different occasions. On both occasions this experiment was performed in biological triplicate, with each biological replicate performed in technical triplicate, all data points are displayed. **** $P<0.0001$, * $P<0.05$, ns = not significant.

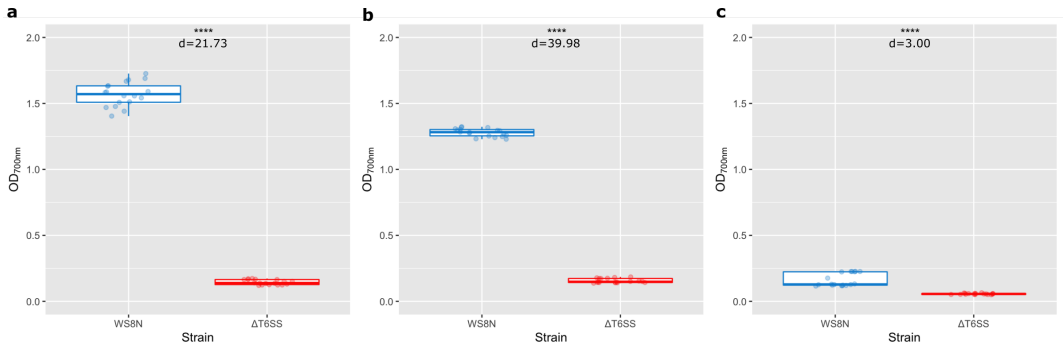


Figure 5.14: **There is a phenotypic difference between wild-type *R. sphaeroides* and its ΔT6SS mutant when grown in iron-depleted media supplemented with iron in its ferrous and ferric forms, but not in its bound form.** Wild-type *R. sphaeroides* WS8N and its ΔT6SS mutant were grown photoheterotrophically from colony-derived 72 h starter cultures in iron-depleted succinate media supplemented with 1 µM (**a**) $FeSO_4.7H_2O$, (**b**) $FeCl_3.6H_2O$, or (**c**) hemin. OD $_{700}$ was measured after 48 h of growth. A Mann-Whitney test and was performed to detect significant differences between the OD_{700} of the wild type WS8N and its ΔT6SS mutant. Cohen's d was calculated to determine the effect size, d values comparing both strains are annotated (n = 18). This experiment was performed in triplicate. **** P<0.0001.

5.6 There is no significant difference between the aerobic growth of wild-type *R. sphaeroides* WS8N and its ΔT6SS mutant under iron limitation

To investigate whether the growth defect of the ΔT6SS mutant growth phenotype, observed during iron limitation and photoheterotrophic conditions, also occurs during growth under aerobic conditions, a growth assay was performed aerobically in iron-depleted succinate media supplemented supplemented with defined of $FeCl_3.6H_2O$ at defined concentrations.

The same starter culture procedure that was optimised for photoheterotrophic growth in chapter 4 was used to prepare the inoculum for these growth assays. Subsequently, starter cultures of wild-type *R. sphaeroides* WS8N and its

ΔT6SS mutant strain were normalised to OD_{700} 1.5 and diluted 1:1000 in 1.5 mL of regular succinate media or iron-depleted succinate media (-$FeSO_4.7H_2O$, chelated CAA) supplemented with 0 µM, 0.1 µM or 1 µM $FeCl_3.6H_2O$ and the appropriate antibiotics. Bacterial suspensions were then placed in a 24-well plate covered with a Breathe-Easy transparent sealing membrane (Sigma), which was then incubated at 30 °C with shaking (200 rpm) using a CLARIOstar plate reader. Automated measurements of OD_{700} were taken at 20 min intervals for 24 h.

Two-way ANOVA with the Geisser-Greenhouse correction followed by Šídák's multiple comparison test was performed using GraphPad Prism version 9.0.2 to compare the growth of the two strains under iron-limited conditions supplemented with different amounts of $FeCl_3.6H_2O$. While the cells grew very poorly during iron starvation, there was no statistical evidence for difference in growth between the two strains under any of the iron-limiting conditions tested. This suggests that the T6SS is not used by *R. sphaeroides* WS8N to rescue growth under iron limiting conditions while the cells grow aerobically (figure 5.15).

5.7 The confinement of T6SS activity to photoheterotrophic conditions is supported by existing microarray data

Growth assays performed in sections 5.5 and 5.6 indicate that T6SS activity only rescues *R. sphaeroides* WS8N growth during iron starvation under photoheterotrophic and not aerobic conditions . This observation is sup-

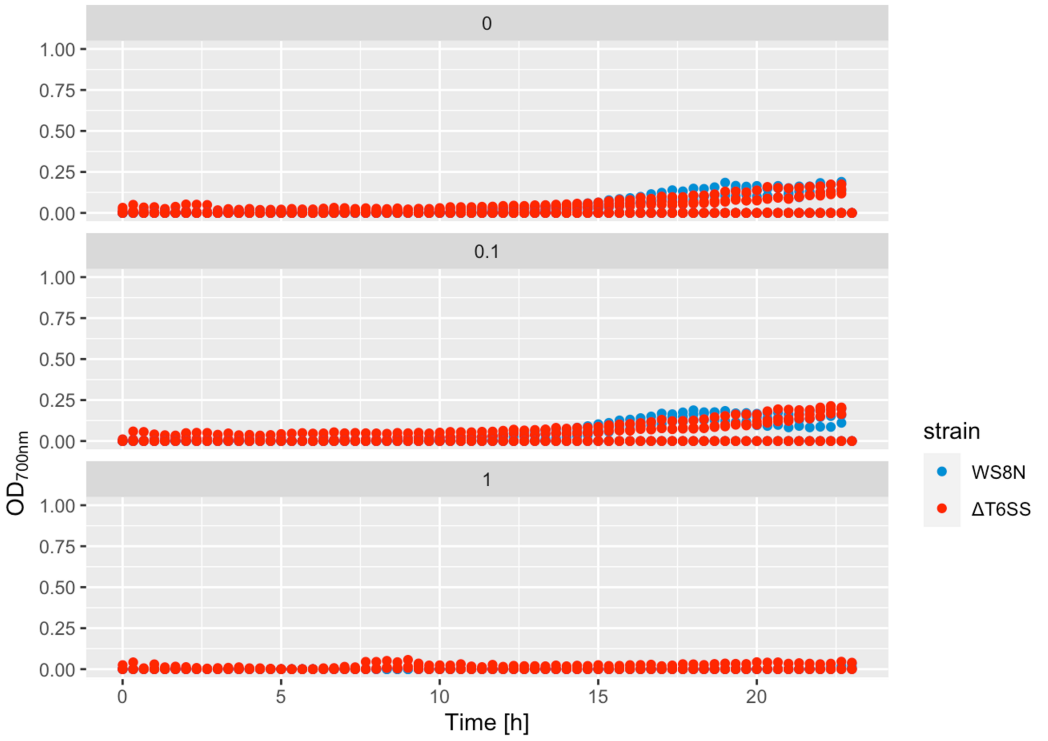


Figure 5.15: **Aerobic growth of wild-type *R. sphaeroides* WS8N and its ΔT6SS mutant in iron-depleted media supplemented with $FeCl_3.6H_2O$.** Wild-type *R. sphaeroides* WS8N and its ΔT6SS mutant were grown in iron-depleted succinate media supplemented with the indicated concentration of $FeCl_3.6H_2O$ (µM) under aerobic conditions at 30 °C with shaking at 200 rpm. Automated measurements of OD_{700} were taken at 20 min intervals for 24 h. This experiment was performed in triplicate and repeated on two different occasions.

ported by existing microarray data which show down regulation of T6SS genes during the transition from anaerobic photosynthesis to aerobic respiration in *R. sphaeroides* strain 2.4.1 (figure 5.16)[132]. The DNA sequence of the T6SS cluster of *R. sphaeroides* 2.4.1 is 97.51% identical to that of *R. sphaeroides* WS8N as determined by multiple sequence alignment (Clustal Omega). The DNA sequences of the T6SS clusters of *R. sphaeroides* WS8N and 2.4.1 can be found at https://www.ncbi.nlm.nih.gov/nuccore/NZ_CM001162.1?report=fasta&from=763103&to=791305 and https://www.ncbi.nlm.nih.gov/nuccore/CP000144.2?report=fasta&from=541054&to=569254, respectively.

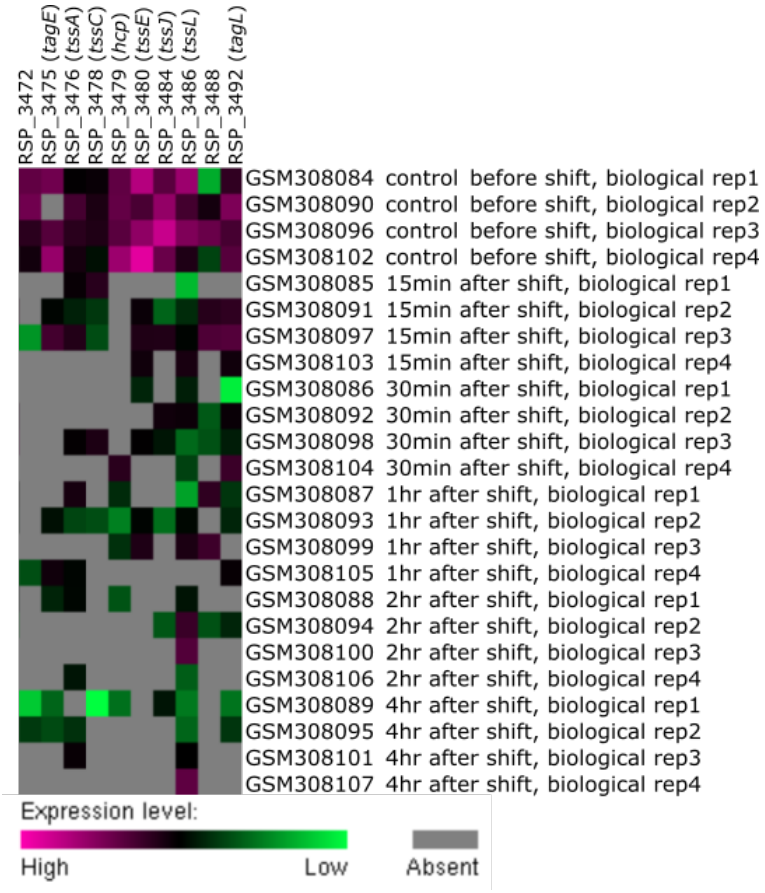


Figure 5.16: **T6SS gene expression during the transition from anaerobic photosynthesis to aerobic respiration in *R. sphaeroides* 2.4.1.** Visual representation of microarray analysis to investigate the transcriptome dynamics of *R. sphaeroides* 2.4.1 at various time points during the shift from anaerobic photosynthesis to aerobic respiration. Expression level at each time point is indicated as per the key. Data taken from Arai *et al.* and visualised using the GEO dataset (GDS) cluster analysis program[132].

5.8 Discussion

This chapter sought to identify a phenotype for a the *R. sphaeroides* WS8N T6SS structural cluster mutant. Initially, growth assays were performed to determine whether the introduced mutations had an effect on the general fitness of the ΔT6SS strain when it was grown under normal laboratory conditions. Although under both photoheterotrophic and aerobic conditions the ΔT6SS

mutant lags behind the wild-type strain during the exponential phase, absence of the T6SS did not abrogate growth. In fact T6SS$^+$ and T6SS$^-$ cells exhibit no significance difference in growth rate under aerobic conditions and arrive at the same OD_{700} reached after 15 h and 48 h of growth for cells grown aerobically or photoheterotrophically, respectively. Given the fact that established laboratory growth conditions are optimised not to stress *R. sphaeroides* and considering that usually the T6SS is deployed when bacteria are under duress, it is not too surprising that lack of T6SS activity did not result in big fitness differences between the wild-type and mutants strains in this case.

To date, there are six published examples of T6SSs used to scavenge metals from the environment [43–47, 61]. Here, the possibility that *R. sphaeroides* WS8N uses its T6SS for a similar function was considered. When the effects of removing, one at a time, all five divalent transition metals routinely added to succinate media, only lack of iron (figure 5.9) elicited a growth dependent phenotype under photoheterotrophic conditions, while absence of zinc (figure 5.5), manganese (figure 5.6), copper (figure 5.7) or cobalt (figure 5.8) did not affect the growth of the ΔT6SS mutant strain. This fits well with the high iron requirements of *R. sphaeroides* photoheterotrophic metabolism that is in part due to the high demand for iron-sulfur clusters that are essential for the biogenesis of photosynthetic complexes[133]. This study identified 1 µM $FeSO_4.7H_2O$ as the threshold concentration below which iron levels are insufficient to support normal photoheterotrophic growth of wild-type *R. sphaeroides* WS8N. When grown in iron-depleted succinate media supplemented with 1 µM $FeSO_4.7H_2O$, i.e., with iron in its ferrous state, the ΔT6SS strain was unable

to grow, while the wild-type strain grew as it would in regular succinate media (figure 5.9). A growth defect for the mutant strain was also observed at lower concentrations of ferrous iron, but it should be noted that such stringent iron-limiting conditions also affected the fitness of wild-type *R. sphaeroides*. These results were quite different to the ones obtained when we examined the role of the T6SS for fitness under aerobic conditions in limited iron. In that case, both strains could not grow. Wild-type *R. sphaeroides* struggled to grow even at 1 µM $FeCl_3.6H_2O$, a concentration that fully permits photoheterotrophic growth (figure 5.15). The latter observation suggests that during aerobic metabolism the T6SS is not involved in iron acquisition.

Since bioinformatic analysis highlighted a putative heme utilisation domain at the C-terminus of the *R. sphaeroides* VgrG protein, we were compelled to investigate whether supplementation of iron-depleted media with bound iron in the form of heme also led to a fitness advantage of the wild-type over the ΔT6SS strain. This seemed reasonable because during photoheterotrophic growth of *R. sphaeroides* along with the light harvesting complexes, which need the magnesium-containing cofactor bacteriochlorophyll, also a large number of heme-containing cytochrome proteins are essential[77]. That said, wild-type *R. sphaeroides* WS8N does not appear to be able to import heme under photoheterotrophic growth, and growth of both tested strains was essentially abrogated when heme was used to supplement iron-depleted succinate media.

To complete our investigation on iron acquisition by the *R. sphaeroides* T6SS, we tested whether iron in its more commonly available ferric form also

conferred the same fitness advantage to wild-type *R. sphaeroides* as ferrous iron did. We, indeed, found that there is a large difference in growth between wild-type *R. sphaeroides* WS8N and its ΔT6SS mutant after 48 h when grown in iron-depleted media supplemented with $FeCl_3.6H_2O$ (figure 5.13). Like for ferrous iron also when ferric iron was used, the biggest difference in growth was observed when media were supplemented with 1 µM $FeCl_3.6H_2O$, while the effect was smaller at lower iron amounts because the growth of the wild-type strain is negatively affected. Although, cells were grown in an anaerobic environment and thus oxidation of ferrous iron to ferric iron is unlikely, no additional precautions were taken to mitigate the oxidation of $FeSO_4.7H_2O$ in these experiments.

Although the effect size observed between wild-type *R. sphaeroides* WS8N and its ΔT6SS mutant is greatest when cells are grown in iron-depleted media supplemented with 1 µM iron in either its ferrous or ferric form, at this concentration the mutant eventually (past 48 h of growth) reaches 83 and 91 % of its maximum OD_{700}, respectively, suggesting that its growth is rescued by other mechanisms of iron import. This agrees with the fact that when cells were grown in iron-depleted media supplemented with 0.1 µM iron T6SS$^-$ cells do not recover, even after 96 h of growth. One can imagine that at 1 µM iron, sequestration of iron through importers that depend on diffusion can occur even slowly, whereas at 0.1 µM the amount of ions is too low to be effectively acquired through mechanisms that depend on passive transport. By contrast, at these lower iron concentration, active iron acquisition through the T6SS of the wild-type strain appears to be the only mechanism that allows growth, al-

beit at lower levels, enabling this bacterium to potentially hang on until better growth conditions arise.

Chapter 6

Further investigation of the T6SS apparatus of *R. sphaeroides* WS8N

6.1 Introduction

The results presented in chapter 5 suggest that the *R. sphaeroides* T6SS has a role in ferrous and ferric iron acquisition under iron-limited growth conditions. This chapter aims to develop genetic and biochemical tools to further explore the expression of the *R. sphaeroides* T6SS under low iron conditions using Western blotting and fluorescence microscopy. A mutant of *R. sphaeroides* WS8N, where the endogenous *hcp* gene was replaced with a copy of *hcp* that is C-terminally tagged with a Flag tag (Hcp-FLAG) was constructed, and whole-cell lysates were probed for Hcp expression under conditions where a growth defect was observed for the ΔT6SS mutant. A secretion assay was also performed using the same mutant strain to determine whether Hcp secretion occurs under these conditions. Moreover, a strain where the endogenous *tssB* gene was replaced with a copy of *tssB* that is C-terminally tagged with a fluorophore appropriate for anaerobically grown bacteria was constructed, and fluorescence microscopy was employed to visualise the *R. sphaeroides* WS8N T6SS *in vivo*. Finally, in the absence of a putative metal binding effector in the T6SS cluster of *R. sphaeroides* WS8N the C-terminus of VgrG was investigated for its iron binding capacity. The C-terminal portion of VgrG was expressed heterologously in *E. coli* and purified. Preliminary iron binding assays were performed to begin to explore whether this domain is capable of binding iron and, thus could be a candidate for the secreted effector that mediates iron acquisition.

6.2 Hcp is expressed under both low- and high-iron conditions

When compared to wild-type *R. sphaeroides* WS8N, the ΔT6SS mutant demonstrated a severe growth phenotype under iron limitation suggesting *R. sphaeroides* WS8N requires its T6SS for iron acquisition and photoheterotrophic growth under iron limitation (figure 5.14). To verify that T6SS is expressed in *R. sphaeroides* WS8N, and in accordance with other studies[**Brunet2015**, 56, 134], a Flag tag was introduced at the C-terminus of the native copy of *hcp*. To do this, the *hcp* gene (RSWS8N_RS18730) was fused with a Flag tag DNA sequence into the pK18mobsacB plasmid, and the fusion was then used to replace the native *hcp* locus of the *R. sphaeroides* WS8N chromosome, as described in detail in 4.2. The primers used for the generation of this construct are displayed in table 2.14. Cells were grown as per the protocol optimised in chapter 4 in low-iron succinate media or high-iron succinate media (see 2.2.6) in 1.5 mL tubes with minimal airspace and incubated under constant illumination (light intensity of ˜10 W/m^2) at 30°C. Cells were harvested after 48 h. Western blot analysis (see methods section 2.5) of OD-normalised cell lysates with anti-Flag antibody confirmed expression of Hcp, when cells were grown photoheterotrophically under low iron conditions (lane 1; figure 6.1). Unexpectedly, expression of Hcp was also detected for lysates from cells grown at high-iron conditions. In fact, the amount of Hcp-FLAG detected in this case is considerably higher than that detected in low-iron media (lane 2; figure 6.1). This is contrasting other studies describing metal-acquiring T6SSs, whereby metal starvation increases the expression of the T6SS apparatus[44, 46].

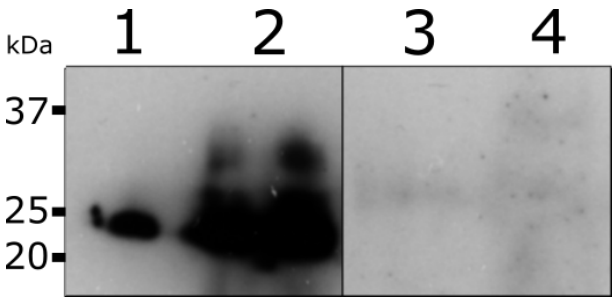


Figure 6.1: **Detection of Hcp-FLAG in whole-cell lysates of *R. sphaeroides* grown under low- and high-iron conditions.** Whole-cell lysate samples of *R. sphaeroides* WS8N and *R. sphaeroides* WS8N Hcp-FLAG strains were prepared using cells grown in low- and high-iron succinate media for 48 h. Samples were analysed with SDS-PAGE and Western blotting with an anti-FLAG antibody. Molecular weight marker are shown on the left. **Lane 1.** Hcp-FLAG mutant grown in low iron; **lane 2.** Hcp-FLAG mutant grown in high iron; **lane 3.** wild-type strain grown in low iron; **lane 4.** wild-type strain grown in high iron.

6.3 The T6SS hallmark protein Hcp can be detected in the cellular but not extracellular fraction of *R. sphaeroides* WS8N cultures

In order to perform a secretion assay, a cell-lysis control is necessary to ensure that detection of proteins in the supernatant media is not due to cell lysis and cytoplasmic contamination during the sample preparation. For this, traditionally a endogenous protein that is constitutively expressed is chosen to be detected using a specific antibody. Such tools are limited for *R. sphaeroides*. The Armitage lab (Biochemistry Department, University of Oxford) had raised a polyclonal antibody against transducer-like protein T (TlpT), which is a cytoplasmic chemoreceptor. Detection of this protein was tested in low- and high-iron conditions to see if it can be used as a lysis control. Western blot analysis of cell lysates normalised to OD_{700} 0.5 with anti-TlpT showed clear expression of TlpT under high-iron conditions, but TlpT expression could not be detected under low iron (figure 6.2). This is not entirely surprising as TlpT

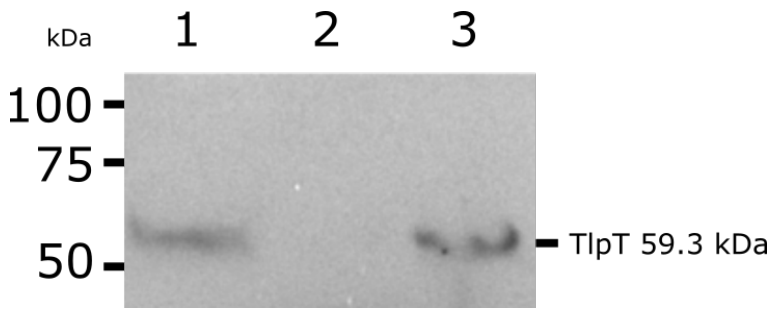


Figure 6.2: **Anti-TlpT Western blot.** *R. sphaeroides* WS8N and *R. sphaeroides* WS8N Hcp-FLAG strains were grown in low- and high-iron succinate media and probed with an anti-TlpT antibody. The molecular weight of TlpT is indicated to the right of the blot and molecular weight marker are shown on the left. **Lane 1.** wild-type strain grown in high iron; **lane 2.** Hcp-FLAG mutant grown in low iron; **lane 3.** Hcp-FLAG mutant grown in high iron. n=1.

s

is involved in the network controlling the flagellar motility of *R. sphaeroides* and could be affected by metal starvation. While not having a lysis control for low-iron conditions, was not ideal, anti-TlpT could at least be used to assess whether our secretion assay samples were free of cytoplasmic contamination when originating from cells grown in high iron.

Wild-type *R. sphaeroides* WS8N and the Hcp-FLAG mutant were grown as per the protocol optimised in chapter 4 in low-iron succinate media or high-iron succinate media (see 2.2.6) in 1.5 mL tubes with minimal airspace and incubated under constant illumination (light intensity of ˜10 W/m^2) at 30°C. Cells were harvested after 48 h. Supernatant samples were prepared as described in section 2.5. Total cell lysates and processed culture supernatants were probed for the presence of the Hcp-FLAG fusion protein as described in section 2.5. Cytosolic TlpT was only detected in the cell lysates of cultures grown in high iron, making us confident that our secretion assay technique is not flawed (see figure 6.3; bottom panel). As shown in figure 6.1, Hcp was

detected in the whole-cell lysates of the Hcp-FLAG mutant strain when grown under both low- and high-iron conditions, with more Hcp being detected under high-iron conditions. However, Hcp could not be detected in any of the culture supernatants that were probed (see figure 6.3; top panel).

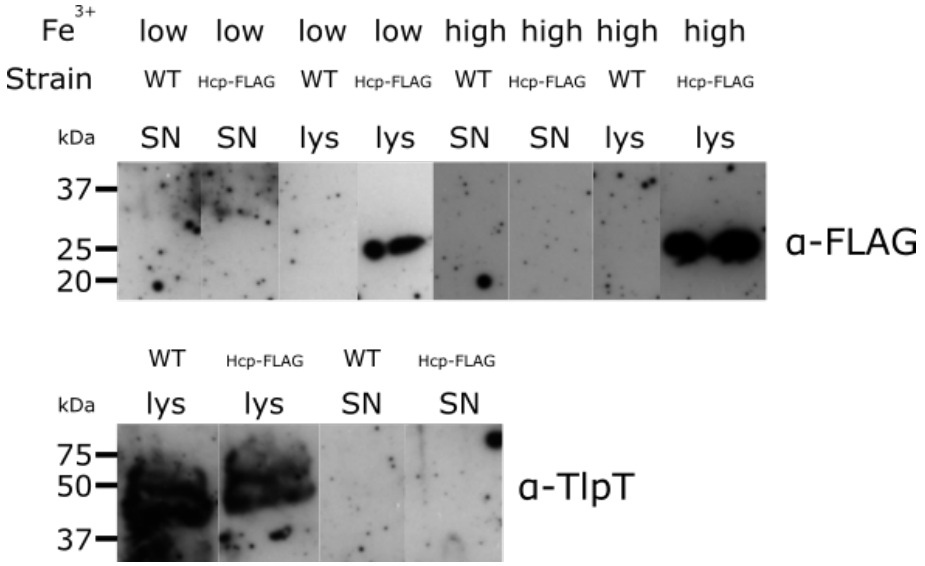


Figure 6.3: **Hcp cannot be detected in culture supernatants after photoheterotrophic growth.** *R. sphaeroides* WS8N (WT) and *R. sphaeroides* WS8N Hcp-FLAG (HCP-FLAG) strains were grown in low- and high-iron succinate media. **(Top panel)** OD-normalized lysates (lys), and culture supernatants (SN) and were probed with an anti-FLAG antibody for Hcp secretion. **(Bottom panel)** TlpT was detected in OD-normalized lysates (lys), and culture supernatants (SN) of cells grown in high iron only. This blot is included as a lysis control.

6.4 T6SS could not be observed *in vivo* under low or high iron conditions

Since a T6SS mutant phenotype is only observed under anaerobic growth conditions, and the maturation of green fluorescence protein (GFP) strictly requires the presence of molecular oxygen, an alternative fluorophore to GFP was chosen to attempt to visualise the *R. sphaeroides* T6SS apparatus *in vivo*. PpFbFP is a flavin mononucleotide (FMN)-based fluorescent protein (FbFP)

engineered from bacterial blue-light photoreceptors that allows *in vivo* labelling and detection of proteins in the absence of oxygen[135]. PpFbFP has been used successfully for labelling entire cells in anaerobically grown *Rhodobacter*, something that failed when YFP fluorescence was used instead[135]. We attempted to visualise the *R. sphaeroides* WS8N T6SS apparatus *in vivo* under low-iron conditions. A *R. sphaeroides* WS8N strain that expressed TssB fused to PpFbFP from the native *tssB* locus was first engineered; PpFbFP was introduced at the C-terminus of the TssB using an Ala-Ala-Ala-Gly-Gly-Gly linker in accordance with current T6SS literature[32]. *R. sphaeroides* WS8N TssB-PpFbFP and wild-type *R. sphaeroides* WS8N were grown as detailed in sections 5.3 and 2.2.6. Cells were then harvested and visualised using fluorescence microscopy. No sheaths were detected in either low-iron media or high-iron media (figure 6.4).

6.5 The C-terminus of VgrG shows preliminary evidence of iron-binding capacity

A VgrG trimer topped by a PAAR domain-containing tip form the puncturing spike of the T6SS. In addition to its structural role, VgrG has a functional role, which it fulfils either by proxy through the binding of effector proteins which it transports out of the cell or by directly encoding an effector domain at its C-terminus. In the case of *B. thailandensis* T6SS-4, which has been shown to function in the acquisition of Mn^{2+} and Zn^{2+} ions, the effectors, TseM and TseZ, respectively, are located within the T6SS cluster. In the absence of a putative metal-ion binding effector in the T6SS cluster of *R. sphaeroides* WS8N, the C-terminus of VgrG, which contains a serine-rich domain, was investigated

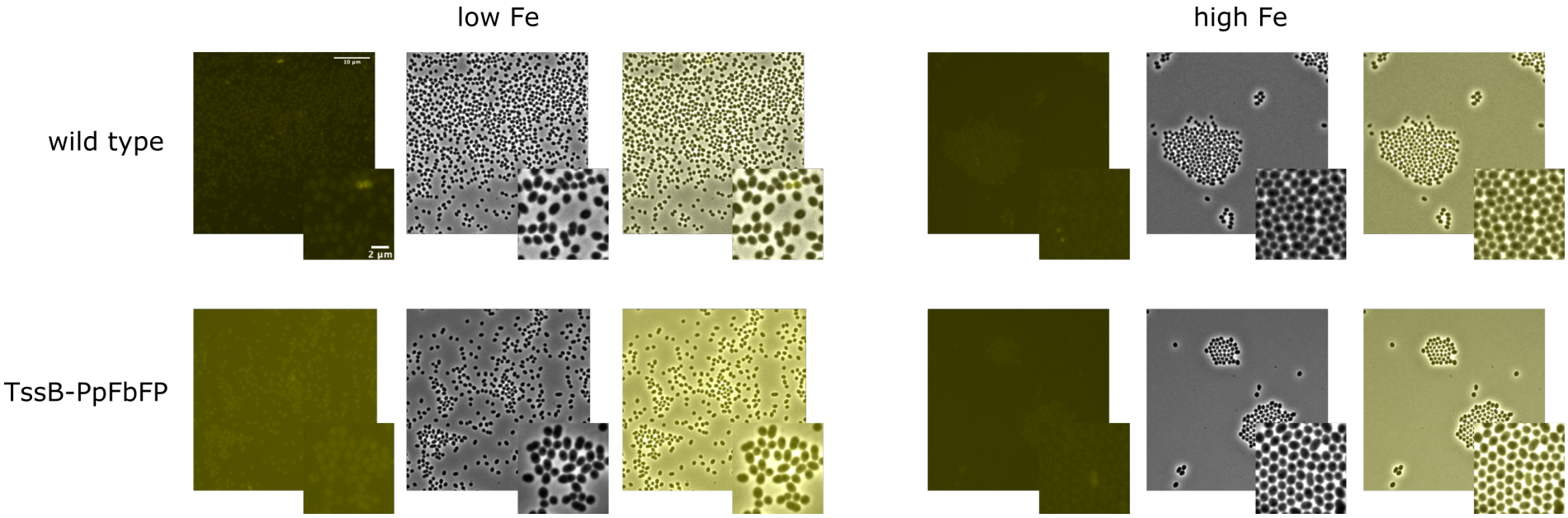


Figure 6.4: ***R. sphaeroides* WS8N T6SS sheaths could not be observed under low- or high-iron conditions.** Wild-type *R. sphaeroides* WS8N and *R. sphaeroides* WS8N TssB-PpFbFP strains were grown in low- and high-iron succinate media and visualised using fluorescence time-lapse microscopy. Panels show representative selected images. Phase contrast channel, TaCFP channel and the composite of both channels are shown for each strain and iron condition. Scale bars indicated on the first panel apply to all panels.

for its iron binding capacity. The C-terminus of *R. sphaeroides* WS8N VgrG (residues 1501-2304), termed hereafter VgrGTer, was cloned into the expression plasmid pET21a under the control of an IPTG-inducible promoter. A twin StrepII tag was introduced at the C-terminus of VgrGCTer and transformed into *E. coli* BL21(DE3). Robust expression of this protein was confirmed by Western blotting (figure 6.5; panel **a**).

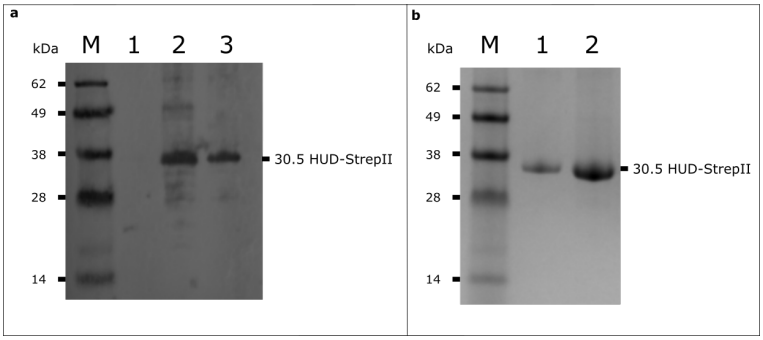


Figure 6.5: **Expression and purification of VgrGCTer-StrepII.** (**a**) Anti-StrepII Western blot of VgrGCTer-StrepII. The C-terminus of VgrG was cloned into the expression plasmid pET21a under the control of an IPTG inducible promoter. The resultant construct was expressed in *E. coli* BL21(DE3). **M.** SeeBlue Plus2 pre-stained protein standard; **lane 1.** uninduced culture; **lane 2**. IPTG-induced culture; **lane 3.** IPTG-induced culture, spun to remove membrane fraction post-lysis. (**b**) SDS-PAGE of purified VgrGCTer-StrepII. **M.** SeeBlue Plus2 pre-stained protein standard; lane 1. 1 4.88 µg of pure VgrGCTer-StrepII; lane 2. 12.3 µg of pure VgrGCTer-StrepII. The molecular weight of VgrGCTer-StrepII is indicated to the right of the blot.

We wanted to perform preliminary tests to examine whether the C-terminal domain of VgrG is an Fe^{2+}-binding protein. To do so, VgrGCTer-StrepII was purified (figure 6.5; panel **b**), yielding 80 µM of total protein. Excess $FeSO_4.7H_2O$ and purified VgrGCTer-StrepII were added to 7 mL of 50 mM Tris-HCl pH 7.5, 150 mM NaCl, to a final concentration of 430 µM and 8.4 µM, respectively. $FeSO_4.7H_2O$ was also added to buffer only, as a control. Samples were concentrated down to 1 mL using a concentrating device. Excess iron,

which in its ferrous form is prone to oxidation (rust formation), seemed to precipitate onto the filter of the concentrating device for both solution, but interestingly this happened more readily when no protein was present in the sample (figure 6.6; panel **a**). Samples were subsequently washed washed with 14 mL of the same buffer and concentrated down to 0.75 mL. The resultant concentrated sample was yellow in colour when VgrGCTer-StrepII is present (figure 6.6, panel **b**), whereas the sample containing buffer only was colourless. This further suggested that the colour is likely not due to free $FeSO_4.7H_2O$, since this was also added to the buffer control. Taken together, these data indicate that the presence of VgrGCTer-StrepII prevents iron from rusting likely through binding. 150 uL of the concentrated samples were left to aerate at room temperature with gentle agitation overnight. The VgrGCTer-StrepII sample remained yellow in colour (figure 6.6; panel **c**), and no further precipitation was observed following centrifugation at 10000 rpm (figure 6.6; panel **d**), indicating the iron remained bound to the protein.

To investigate this further, the experiment was repeated with VgrGCTer-StrepII and a protein known to possess no metal ion binding capacity, the C-terminal domain of the redox protein DsbD (cDsbD) that has a typical thioredoxin fold. Excess $FeSO_4.7H_2O$ and purified cDsbD or VgrGCTer-StrepII were added to 7 mL of buffer as above, to a final concentration of 430 µM and 8.4 µM, respectively. As before, both samples were concentrated to 1 mL and washed with an additional 14 mL of buffer before being concentrated down to 0.75 mL. In the case of both VgrGCTer-StrepII and cDsbD, adding excess $FeSO_4.7H_2O$ in the presence of buffer, washing and concentrating resulted in

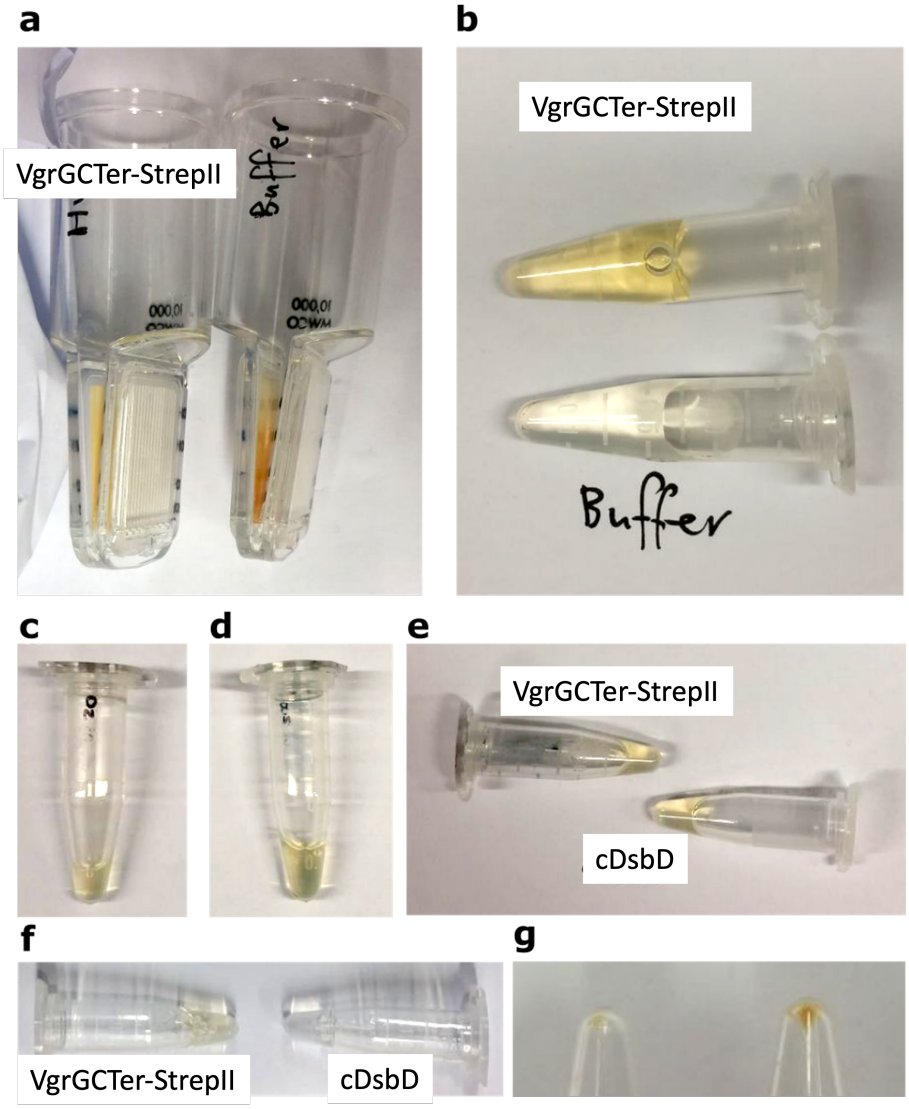


Figure 6.6: **The C-terminal domain of VgrG has putative iron-binding capacity.** **a** $FeSO_4.7H_2O$ precipitates less when VgrGCTer-StrepII (left) is present. **b** VgrGCTer-StrepII retains $FeSO_4.7H_2O$ in solution (top). **c** VgrGCTer-StrepII retains $FeSO_4.7H_2O$ following aeration overnight and **d** centrifugation at 10000 rpm. **e** VgrGCTer-StrepII (left) and cDsbD (right) in the presence of excess $FeSO_4.7H_2O$ are pale yellow in colour following washing and concentration. **f** VgrGCTer-StrepII (left) retains pale yellow colour after aeration overnight, cDsbD (right) becomes colourless owing to precipitation of the iron out of solution, **g** evident after centrifugation at 10000 rpm (right). All samples are in 50 mM Tris-HCl pH 7.5, 150 mM NaCl.

samples that were pale yellow in colour (figure 6.6; panel **e**). Samples were aerated overnight and centrifuged at 10000 rpm, as before. Following aeration overnight, the cDsbD sample became colourless, whilst the VgrGCTer-StrepII sample remained pale yellow in colour (figure 6.6, panel **f**). At the same time, rust-coloured precipitate was clearly visible after centrifugation in the case of cDsbD, but very little material was present in the tube containing VgrGCTer-StrepII (figure 6.6, panel **g**). All these observations, while preliminary, suggest that VgrGCTer-StrepII interacts with iron ions and protects them from oxidation.

6.6 Discussion

This chapter sought to further explore the activity of the *R. sphaeroides* WS8N under low-iron conditions with the aim to validate its role in iron acquisition. While the experiments conducted do not provide conclusive evidence, some of them indicate that this T6SS apparatus might indeed be involved in iron sequestration.

Hcp expression was detected both under low- and high-iron conditions as demonstrated in sections 6.2 and 6.3. Notably, the amount of Hcp detected under high-iron conditions seems to be consistently higher than that under low iron. This was unexpected because in several cases of metal-sequestering T6SSs, expression of the apparatus is minimal when the metal that is sequestered is abundant[44, 46, 47, 61]. Nonetheless, this result does not necessarily disprove the involvement of the *R. sphaeroides* T6SS in metal acquisition. It is possible that the reason cells that have grown in media that are

rich in iron show elevated expression of Hcp is because while the T6SS components are expressed the system is not yet assembled. Assembly or even firing of the system would be regulated to only happen under the right conditions, for example under iron starvation. This is not unheard of in T6SS regulation. For example the*P. aeruginosa* H1-T6SS is known to be primed for firing in a stepwise process, encompassing transcriptional and post-transcriptional control[36, 136]. The last activation step involves sensing of membrane perturbations caused by T6SS attacks of competitors, via the TagQRST signalling cascade[32]. Another explanation for this result could be that the *R. sphaeroides* T6SS is also active at high cell density, where it could perform a different function, for example bacterial killing. T6SSs commonly possess multiple effector proteins [16, 137] and bioinformatic analysis of the *R. sphaeroides* WS8N T6SS cluster revealed a putative metallopeptidase, encoded in the same operon as VgrG. Such effectors have been reported for other T6SS apparatuses, for example the H2-T6SS of *P. aeruginosa* PAO1, where the C-terminal domain of VgrG2b is a member of a widespread family of metallopeptidases. The VgrG2b C-terminal domain possesses antibacterial activity, causing blebbing of the target bacterial membrane[107].

Expression of Hcp was detected in cell lysates, grown under both low- and high-iron conditions, but Hcp was not detected in culture supernatants. While for high-iron this could be because the T6SS does not fire under these conditions, it is possible that for low-iron further optimisation of the secretion assay protocol may be necessary. If firing of the T6SS for iron acquisition happens too infrequently, then the amount of Hcp secreted might be too low to be

readily detected. The expression of Hcp2 in *P. aeruginosa* was shown to be induced under low copper concentrations[47]. In this case, Hcp2-FLAG was expressed from a mini-CTX plasmid along with the native copy of Hcp2. Another explanation for the fact that we could not detect Hcp in *R. sphaeroides* culture supernatants even under low-iron conditions could be that replacing the native copy of Hcp with Hcp-FLAG disrupted the assembly of the apparatus. One can imagine that multiple copies of Hcp bearing a tag might not fit in the lumen of the TssBC sheath, where native Hcp already fits snugly. Future work should involve exogenously expressing Hcp-FLAG in the presence of the native copy of *hcp* and repeating the Hcp secretion assay described in section **??** to assess whether Hcp secretion is induced by low-iron concentrations.

An unsuccessful attempt was made to visualise the *R. sphaeroides* T6SS *in vivo* using fluorescence microscopy. It is possible that the settings of the microscope needed to be optimised further. The fluorophore we used had not previously been tested in *R. sphaeroides*, and there is only one successful example of its use in the literature, whereby it was cytoplasmically expressed to label *R. capsulatus* cells[135]. Time limitations prevented testing whether cytoplasmic PpFbFP expression in *R. sphaeroides* WS8N would result in fluorescent labelling like it did in *R. capsulatus*. It should be noted that even if a *R. sphaeroides* strain expressing PpFbFP could have been used to optimise the microscopy settings, if firing of the*R. sphaeroides* T6SS is too rare an event, then *in vivo* imaging of this system would likely still be challenging.

The data described in section 6.5 provided preliminary evidence towards

an iron-binding C-terminal domain of VgrG (VgrGCTer). Unlike when buffer alone or the binding control protein, cDsbD, were used, VgrGCTer prevents rust from forming when excess of $FeSO_4.7H_2O$ is present; no precautions were taken to prevent the oxidation of $FeSO_4.7H_2O$ in these experiments, thus iron likely was in a ferric state. With data in chapter 5 suggesting a role for the T6SS in the acquisition of both Fe^{2+} and Fe^{3+}, interaction of VgrGCTer with Fe^{3+} is fitting.

Further characterisation of the interaction of VgrGCTer with iron is necessary to confirm its iron-binding activity. The iron-binding experiments described above were performed using $FeSO_4.7H_2O$ in excess; any further experiments would need to use an equal or higher molar ratio of protein to iron, to provide more conclusive results. UV-visible spectral analysis of purified VgrGCTer to which iron would be gradually added in sub-stoichiometric amounts would be first carried out. It is expected that a peak between 300 and 700 nm would be observed if iron is bound to VgrGCTer. Size-exclusion chromatography could also be conducted to determine the oligomeric state of the protein in the absence of iron, before adding iron in a defined oxidation state and subjecting the VgrGCTer-Fe complex to gel filtration to assess whether binding of iron induces any changes. Finally, VgrGCTer is a small protein, well expressed and quite pure (figure 6.5), and thus a good candidate for X-ray crystallography. Crystallising VgrGCTer in the presence of iron and solving its crystal structure would be the most conclusive way to show that VgrGCTer is an iron-binding effector.

Chapter 7

Discussion

This thesis reported and began to describe a yet uncharacterised T6SS apparatus. At the time of writing there was no existing bioinformatic or experimental characterisation of the *R. sphaeroides* WS8N T6SS. Chapter 3 sought to present an initial bioinformatic analysis of the *R. sphaeroides* WS8N T6SS and position it in relation to experimentally characterised T6SS described in the literature. Bioinformatics analysis revealed a T6SS cluster belonging to the plylogenetic group i3 and encoding all thirteen core T6SS components (TssA-M), four regulatory proteins (TagE-H), the tip sharpening protein PAAR, the peptidoglycan-binding protein TagL and an additional seven hypothetical proteins. Further bioinformatic analysis of all currently available Rhodobacteraceae whole genome sequences revealed possession of a T6SS apparatus to be strain- and not species-specific.

The principle aim of this project was to elucidate a function of the T6SS of *R. sphaeroides* WS8N. Preliminary experiments conducted under crude metal-limited growth conditions revealed an informative mutant phenotype under iron limitation. The growth conditions that would allow this phenotype to be further explored required extensive testing and optimisation (Chapter 4). After designing a reliable and reproducible growth assay, we proceeded to use this to test the role of the *R. sphaeroides* WS8NT6SS in metal acquisition (Chapter 5). Our results showed that this T6SS apparatus is necessary for photoheterotrophic growth under iron-limited conditions.

In the first decade of its study, the T6SS was proposed to be a contact-dependent molecular weapon, be it anti-eukaryotic or anti-bacterial, deployed

to promote virulence in the host environment or interbacterial competition. More recently, T6SS with roles in the scavenging and sequestration of metal ions have been described. Bacterial survival in adverse conditions necessitates a repertoire of means by which essential nutrients can be acquired. Although requiring further experimental validation to confirm T6SS-dependent iron acquisition, it is conceivable that the T6SS of *R. sphaeroides* functions similarly to those described in section 1.3.

Bioinformatic analysis failed to identify any compelling metal binding effectors in the *R. sphaeroides* T6SS operon. That said, in the case of the *B. thailandensis* T6SS-4 which has been shown to function in the acquisition of Mn^{2+} and Zn^{2+} ions, *in silico* analysis of its putative effector proteins also does not identify any conserved domains that could have metal-binding capacity. All six T6SS-dependent metal ion acquisition systems described to date deploy a cargo effector to sequester the metal in question. Since an initial bioinformatic analysis of the VgrG protein of *R. sphaeroides* WS8N revealed a putative heme utilisation domain, we were compelled to investigate the C-terminus of VgrG as a potential iron-binding domain, despite no current examples of T6SS-dependent metal ion uptake systems using a specialised VgrG effector described in the literature.

Preliminary data gathered in chapter 6 suggest that the C-terminal domain of VgrG (VgrGCTer) binds iron, although further studies would be is required to confirm the role of VgrG as an iron-binding protein. In addition to solving an iron-bound crystal structure of the C-terminal domain of the *R. sphaeroides*

VgrG protein, isothermal titration calorimetry could be employed to examine the binding of the protein to iron, while using the iron-binding proteins transferrin and Fur as positive controls for Fe^{3+} and Fe^{2+}, respectively. In addition to this we would like to investigate whether the growth of the ΔT6SS mutant under low-iron conditions would be restored if purified VgrGCTer was exogenously added.

How iron bound to VgrG is delivered into the cell remains unanswered. We hypothesise that following secretion of VgrG by the T6SS, VgrGCTer is cleaved from VgrG by a metalloprotease. Subsequently iron-bound VgrGCTer would interact with a TonB-dependent outer membrane transporter to deliver the metal ion to the interior of the cell. To identify such putative receptors, we could perform affinity chromatography with StepII-VgrGCTer-coated beads against total cell lysates of *R. sphaeroides*. Proteins retained by StepII-VgrGCTer could be then identified by mass spectrometry. For such experiments, appropriate negative controls using Strep-II tagged proteins that should not interact with the *R. sphaeroides* proteome would also be performed.

The best-studied function of the T6SS is its role in inter-bacterial warfare as a redoubtable contact-dependent machine for the secretion of anti-bacterial effector proteins into competing neighbouring cells[138]. The question as to why bacteria would deploy such a costly and elaborate apparatus for metal acquisition remains. Perhaps from a survival point of view, the use of such an energetically costly macromolecular machine is not excessive for an element as critical to survival as iron, especially to an organisms like *R. sphaeroides* that

so heavily depends on iron to grow photoheterotrophically.

Bacteria have evolved iron uptake systems for both the ferrous and ferric forms of elemental iron, iron scavenging pathways via siderophores and heme transportation systems that are all under tight regulation owing to the toxicity of excess intracellular iron[77]. It is known that the T6SS is tightly regulated, with regulation spanning transcriptional, post-transcriptional and post-translational mechanisms[139]. Perhaps T6SS-dependent iron acquisition is a variation on the siderophore system that *R. sphaeroides* WS8N does not possess. Owing to the necessity of metal homeostasis being tightly regulated in bacteria, it makes sense to couple iron uptake to an already tightly regulated system. Whilst it is unclear how ubiquitous metal scavenging T6SS are, this function indirectly promotes interbacterial competition as it allows bacteria to cope with environmental nutrient scarcity and thus increases their chances of survival. Although the reasons for using such a system for metal uptake remain obscure, this function really emphasises the versatility of the T6SS.

Two lines of evidence indicate that the T6SS is being used to sequester iron during low iron conditions; the abrogated growth phenotype of the ΔT6SS mutant under iron limitation and the expression of Hcp under iron limitation. However, Hcp is expressed under both low and high iron conditions suggesting *R. sphaeroides* WS8N may use its T6SS for more than just iron acquisition. Competition experiments with a bacteria with a similar growth rate, possibly from the same environmental niche, should be conducted to determine whether *R. sphaeroides* WS8N also deploys its T6SS in bacterial warfare. A possibility

would be to use the ΔT6SS mutant as prey in this case, as this strain would grow if iron was not limited. The six currently described T6SS-dependent metal ion uptake systems also participate in antibacterial combat via the secretion of alternative effectors. Antibacterial effectors with peptidase activity are common[121]. As such, the putative peptidase effector RSWS8N_RS18790 (see section 3.10) should be further investigated for its role in interbacterial competition. Mass spectrometric analysis of T6SS-dependent secretomes should also be conducted to identify additional putative effector proteins that are possibly not encoded in or near the T6SS operon.

Bacteria have evolved a plethora of macromolecular nanomachines that secrete a variety of substrates from small molecules to proteins. These systems enable microorganisms to respond to stresses, by adapting efficiently to their ever-changing environment. T6SS-dependent metal ion scavenging and sequestration is a recently discovered means that bacteria use to respond to environmental nutrient scarcity. Although probably many T6SS-mediated metal acquisition mechanisms remain to be elucidated, this study revealed the involvement of yet another one of these systems in iron acquisition under photoheterotrophic conditions. As such it has expanded our understanding of a metabolically diverse bacterium and further highlighted the versatility of the T6SS.

Chapter 8

Appendix

8.1 Media and reagents

All media and reagents were made up to 1 L with MilliQ water unless otherwise stated.

8.1.1 Luria broth

Ingredient	Quantity per litre
Yeast extract	5 g
Tryptone	10 g
NaCl	5 g

Adjusted to pH 7.0 and autoclaved.

8.1.2 Succinate media

Ingredient	Quantity per litre
1 M Phosphate buffer	20 mL
Concentrated base (see below)	20 mL
Growth factor (see below)	2 mL
(NH4)2SO4	0.5 g
NaCl	0.5 g
Sodium succinate	2 g
Casaminoacids	1 g

Adjusted to pH 7.2 and autoclaved.

8.1.3 1 M Phosphate buffer

Ingredient	Quantity per litre
K2HPO4 1M	174.18 g
KH2PO4 1M	136.09 g

Adjusted to pH 7.0 with KOH, autoclaved and stored at 4°C.

8.1.4 Concentrated base

Ingredient	Quantity per litre
Nitrilotriacetic acid (diNa salt)	5.94 g
Metals 44 solution	25 mL
MgSO4.7H2O	14.5 g
CaCl2.2H2O	1.67 g
FeSO4.7H2O	50 mg
Ammonium molybdate 4H2O	4.6 mg

diNa salt dissolved first and pH adjusted to 5.0 with H2SO4 to allow FeSO4.7H2O to dissolve. Final pH adjusted to 6.8 with KOH. Autoclaved

and stored at 4°C.

8.1.5 Metals 44 solution

Ingredient	Quantity per litre
Ethylenediaminetetraacetic acid (EDTA)	2.5 g
ZnSO4.7H2O	11 g
FeSO4.7H2O	5 g
3M sulphuric acid	1.5 mL
MnSO4.4H2O	3 g
CuSO4.5H2O	0.39 g
H3BO3	0.12 g
CoCl2.6H2O	0.2 g

Filter sterilised and stored at 4°C.

8.1.6 Growth factor

Ingredient	Quantity per litre
Biotin	20 mg
NaHCO3	500 mg
Niacin	1 g
Thiamine HCL	500 mg

Autoclaved and stored at 4°C.

8.1.7 5X Amino Acid Supplement

Stock solution	Quantity per 100 mL
800 mM Alanine (free)	0.5
400 mM Arginine (free)	6.5
50 mM Asparagine (free)	4.0
400 mM Aspartic Acid (K salt)	0.5
10 mM Cysteine (HCl H_2O)	5.0
600 mM Glutamic Acid (K salt)	0.5
123 mM Glutamine (free)	2.5
800 mM Glycine (free)	0.5
200 mM Histidine (HCl H_2O)	0.5
200 mM Isoleucine (free)	1.0
50 mM Leucine (free)	8.0
400 mM Lysine (free)	0.5
200 mM Methionine (free)	0.5
50 mM Phenylalanine (free)	4.0
400 mM Proline (free)	0.5
450 mM Serine (free)	12.5
400 mM Threonine (free)	0.5
50 mM Tryptophane (free)	1.0
10 mM Tyrosine (free)	10.0
300 mM Valine (free)	1.0

Filter sterilised and stored at -20°C.

8.1.8 M22

Ingredient	Quantity per litre
1 M phosphate buffer (see 8.1.3)	20 mL
Concentrated base (see8.1.4)	20 mL
Growth factor (see 8.1.6)	2 mL
(NH4)2SO4	0.5 g
NaCl	0.5 g

Adjusted to pH 7.2 and autoclaved.

8.1.9 10X TBE

Ingredient	Quantity per litre
Tris base	108 g
Boric acid	55 g
EDTA	7.4 g

Adjusted to pH 8.3.

8.1.10 10X SDS Running Buffer

Ingredient	Quantity per litre
Tris	30.3 g
Glycine	144 g
SDS	10 g

8.1.11 10X Vogel-Bonner Medium (VBM)

Ingredient	Quantity per litre
$MgSO_4.7H_2O$	2 g
anhydrous citric acid	20 g
K_2HPO_4	100 g
$NaNH_4HPO_4{\cdot}4H_2O$	35 g

Adjusted to pH 7.0 and filter sterilised.

8.2 The complete nucleotide and amino acid sequences of PpFbFP

8.2.1 Nucleotide sequence of PpFbFP (447 bp)

ATGATCAACGCAAAACTCCTGCAACTGATGGTCGAACATTCCAACGA

TGGCATCGTTGTCGCCGAGCAGGAAGGCAATGAGAGCATCCTTATCT

ACGTCAACCCGGCCTTCGAGCGCCTGACCGGCTACTGCGCCGACGAT

ATTCTCTATCAGGACGCACGTTTTCTTCAGGGCGAGGATCACGACCA

GCCGGGCATCGCAATTATCCGCGAGGCGATCCGCGAAGGCCGCCCCT

GCTGCCAGGTGCTGCGCAACTACCGCAAAGACGGCAGCCTGTTCTGG

AACGAGTTGTCCATCACACCGGTGCACAACGAGGCGGACCAGCTGAC

CTACTACATCGGCATCCAGCGCGATGTCACAGCGCAAGTATTCGCCG

AGGAAAGGGTTCGCGAGCTGGAGGCTGAAGTGGCGGAACTGCGCCGG

CAGCAGGGCCAGGCCAAGCACTGA

8.2.2 Amino acid sequence of PpFbFP(148 aa)

MINAKLLQLMVEHSNDGIVVAEQEGNESILIYVNPAFERLTGYCADD ILYQ-

DARFLQGEDHDQPGIAIIREAIREGRPCCQVLRNYRKDGSLFW NELSIT-

PVHNEADQLTYYIGIQRDVTAQVFAEERVRELEAEVAELRR QQGQAKH

Bibliography

1. Costa, T. R. *et al.* Secretion systems in Gram-negative bacteria: Structural and mechanistic insights. *Nature Reviews Microbiology* **13,** 343–359 (2015).
2. Green, E. R. & Mecsas, J. Bacterial Secretion Systems: An Overview. *Microbiology Spectrum* **4** (2016).
3. Burdette, L. A., Leach, S. A., Wong, H. T. & Tullman-Ercek, D. Developing Gram-negative bacteria for the secretion of heterologous proteins. *Microbial Cell Factories* **17** (2018).
4. Lasica, A. M., Ksiazek, M., Madej, M. & Potempa, J. The Type IX Secretion System (T9SS): Highlights and Recent Insights into Its Structure and Function. *Frontiers in Cellular and Infection Microbiology* **7** (2017).
5. Palmer, T., Finney, A., Saha, C. K., Atkinson, G. C. & Sargent, F. A holin/peptidoglycan hydrolase-dependent protein secretion system. *Journal of Substance Abuse Treatment* **13,** 287–288 (May 1996).
6. Williams, S. G., Varcoe, L. T., Attridge, S. R. & Manning, P. A. Vibrio cholerae Hcp, a secreted protein coregulated with HlyA. *Infection and Immunity* **64,** 283–289 (1996).
7. Pukatzki, S. *et al.* Identification of a conserved bacterial protein secretion system in Vibrio cholerae using the Dictyostelium host model system. *Proceedings of the National Academy of Sciences of the United States of America* **103,** 1528–1533 (2006).
8. Mougous, J. D. *et al.* A virulence locus of Pseudomonas aeruginosa encodes a protein secretion apparatus. *Science* (2006).
9. Bingle, L. E., Bailey, C. M. & Pallen, M. J. Type VI secretion: a beginner's guide. *Current Opinion in Microbiology* **11,** 3–8 (2008).
10. Basler, M. Type VI secretion system: Secretion by a contractile nanomachine. *Philosophical Transactions of the Royal Society B: Biological Sciences* **370** (2015).
11. Leiman, P. G. *et al.* Type VI secretion apparatus and phage tail-associated protein complexes share a common evolutionary origin. *Proceedings of the National Academy of Sciences of the United States of America* **106,** 4154–4159 (2009).

12. Boyer, F., Fichant, G., Berthod, J., Vandenbrouck, Y. & Attree, I. Dissecting the bacterial type VI secretion system by a genome wide in silico analysis: What can be learned from available microbial genomic resources? *BMC Genomics* **10,** 104 (2009).

13. Barret, M., Egan, F., Fargier, E., Morrissey, J. P. & O'Gara, F. Genomic analysis of the type VI secretion systems in Pseudomonas spp.: Novel clusters and putative effectors uncovered. *Microbiology* **157** (2011).

14. Russell, A. B. *et al.* A type VI secretion-related pathway in bacteroidetes mediates interbacterial antagonism. *Cell Host and Microbe* **16** (2014).

15. Clemens, D. L., Ge, P., Lee, B. Y., Horwitz, M. A. & Zhou, Z. H. Atomic structure of T6SS reveals interlaced array essential to function. *Cell* **160** (2015).

16. Coulthurst, S. The Type VI secretion system: A versatile bacterial weapon. *Microbiology* **165,** 503–515 (2019).

17. Bladergroen, M. R., Badelt, K. & Spaink, H. P. Infection-blocking genes of a symbiotic Rhizobium leguminosarum strain that are involved in temperature-dependent protein secretion. *Molecular Plant-Microbe Interactions* **16,** 53–64 (2003).

18. Silverman, J. M., Brunet, Y. R., Cascales, E. & Mougous, J. D. Structure and regulation of the type VI secretion system. *Annual Review of Microbiology* **66** (2012).

19. Aschtgen, M. S., Thomas, M. S. & Cascales, E. Anchoring the type VI secretion system to the peptidoglycan TssL, TagL, TagP,... what else? *Virulence* **1** (2010).

20. Felisberto-Rodrigues, C. *et al.* Towards a structural comprehension of bacterial type vi secretion systems: Characterization of the TssJ-TssM complex of an escherichia coli pathovar. *PLoS Pathogens* **7** (2011).

21. Durand, E. *et al.* Biogenesis and structure of a type VI secretion membrane core complex. *Nature* **523** (2015).

22. Brunet, Y. R., Zoued, A., Boyer, F., Douzi, B. & Cascales, E. The Type VI Secretion TssEFGK-VgrG Phage-Like Baseplate Is Recruited to the TssJLM Membrane Complex via Multiple Contacts and Serves As Assembly Platform for Tail Tube/Sheath Polymerization. *PLoS Genetics* **11** (2015).

23. Cherrak, Y. *et al.* Biogenesis and structure of a type VI secretion baseplate. *Nature Microbiology* **3** (2018).

24. Nazarov, S. *et al.* Cryo- EM reconstruction of Type VI secretion system baseplate and sheath distal end. *The EMBO Journal* **37** (2018).

25. Wu, C. *et al.* Effector loading onto the VgrG carrier activates type VI secretion system assembly. *EMBO reports* **21** (2020).

26. Bernal, P. *et al.* A novel stabilization mechanism for the type VI secretion system sheath. *Proceedings of the National Academy of Sciences of the United States of America* **118** (2021).

27. Planamente, S. *et al.* TssA forms a gp6-like ring attached to the type VI secretion sheath. *The EMBO Journal* **35** (2016).

28. Zoued, A. *et al.* Priming and polymerization of a bacterial contractile tail structure. *Nature* **531,** 59–63 (Feb. 2016).

29. Schneider, J. P. *et al.* Diverse roles of TssA-like proteins in the assembly of bacterial type VI secretion systems. *The EMBO Journal* **38** (2019).

30. Santin, Y. G. *et al.* In vivo TssA proximity labelling during type VI secretion biogenesis reveals TagA as a protein that stops and holds the sheath. *Nature Microbiology* **3** (2018).

31. Salih, O. *et al.* Atomic Structure of Type VI Contractile Sheath from Pseudomonas aeruginosa. *Structure* **26** (2018).

32. Basler, M., Pilhofer, M., Henderson, G. P., Jensen, G. J. & Mekalanos, J. J. Type VI secretion requires a dynamic contractile phage tail-like structure. *Nature* **483,** 182–186 (2012).

33. Kapitein, N. *et al.* ClpV recycles VipA/VipB tubules and prevents non-productive tubule formation to ensure efficient type VI protein secretion. *Molecular Microbiology* **87** (2013).

34. Durand, E., Cambillau, C., Cascales, E. & Journet, L. VgrG, Tae, Tle, and beyond: The versatile arsenal of Type VI secretion effectors. *Trends in Microbiology* **22,** 498–507 (2014).

35. Hernandez, R. E., Gallegos-Monterrosa, R. & Coulthurst, S. J. Type VI secretion system effector proteins: Effective weapons for bacterial competitiveness. *Cellular Microbiology* **22** (2020).

36. Hood, R. D. *et al.* A Type VI Secretion System of Pseudomonas aeruginosa Targets a Toxin to Bacteria. *Cell Host and Microbe* **7** (2010).

37. LaCourse, K. D. *et al.* Conditional toxicity and synergy drive diversity among antibacterial effectors. *Nature Microbiology* **3** (2018).

38. Bondage, D. D., Lin, J. S., Ma, L. S., Kuo, C. H. & Lai, E. M. VgrG C terminus confers the type VI effector transport specificity and is required for binding with PAAR and adaptor-effector complex. *Proceedings of the National Academy of Sciences of the United States of America* **113,** E3931–E3940 (2016).

39. Liang, X. *et al.* Identification of divergent type VI secretion effectors using a conserved chaperone domain. *Proceedings of the National Academy of Sciences of the United States of America* **112,** 9106–9111 (July 2015).

40. Unterweger, D. *et al.* Chimeric adaptor proteins translocate diverse type VI secretion system effectors in Vibrio cholerae. *The EMBO Journal* **34** (2015).

41. Berni, B., Soscia, C., Djermoun, S., Ize, B. & Bleves, S. A type VI secretion system trans-kingdom effector is required for the delivery of a novel antibacterial toxin in Pseudomonas aeruginosa. *Frontiers in Microbiology* **10** (2019).

42. Whitney, J. C. *et al.* An Interbacterial NAD(P)+ Glycohydrolase Toxin Requires Elongation Factor Tu for Delivery to Target Cells. *Cell* **163** (2015).

43. Wang, T. *et al.* Type VI Secretion System Transports Zn2+ to Combat Multiple Stresses and Host Immunity. *PLoS Pathogens* **11** (2015).

44. Si, M. *et al.* Manganese scavenging and oxidative stress response mediated by type VI secretion system in Burkholderia thailandensis. *Proceedings of the National Academy of Sciences of the United States of America* **114,** E2233–E2242 (2017).

45. Lin, J. *et al.* A Pseudomonas T6SS effector recruits PQS-containing outer membrane vesicles for iron acquisition. *Nature Communications* **8,** 1–12 (2017).

46. Si, M. *et al.* The Type VI Secretion System Engages a Redox-Regulated Dual-Functional Heme Transporter for Zinc Acquisition. *Cell Reports* **20,** 949–959 (2017).

47. Han, Y. *et al.* A Pseudomonas aeruginosa type VI secretion system regulated by CueR facilitates copper acquisition. *PLoS Pathogens* **15,** 1–25 (2019).

48. Hachani, A., Wood, T. E. & Filloux, A. Type VI secretion and anti-host effectors. *Current Opinion in Microbiology* **29,** 81–93 (2016).

49. Heisler, D. B. *et al.* ACD toxin-produced actin oligomers poison formin-controlled actin polymerization. *Science* **349** (2015).

50. Schwarz, S. *et al.* VgrG-5 is a Burkholderia type VI secretion system-exported protein required for multinucleated giant cell formation and virulence. *Infection and Immunity* **82** (2014).

51. Chen, H. *et al.* The Bacterial T6SS Effector EvpP Prevents NLRP3 Inflammasome Activation by Inhibiting the Ca2+-Dependent MAPK-Jnk Pathway. *Cell Host and Microbe* **21** (2017).

52. Dong, T. G., Ho, B. T., Yoder-Himes, D. R. & Mekalanos, J. J. Identification of T6SS-dependent effector and immunity proteins by Tn-seq in Vibrio cholerae. *Proceedings of the National Academy of Sciences of the United States of America* **110,** 2623–2628 (2013).

53. Trunk, K. *et al.* The type VI secretion system deploys antifungal effectors against microbial competitors. *Nature Microbiology* **3** (2018).

54. Miyata, S. T., Unterweger, D., Rudko, S. P. & Pukatzki, S. Dual Expression Profile of Type VI Secretion System Immunity Genes Protects Pandemic Vibrio cholerae. *PLoS Pathogens* **9** (2013).

55. Koskiniemi, S. *et al.* Rhs proteins from diverse bacteria mediate intercellular competition. *Proceedings of the National Academy of Sciences of the United States of America* **110** (2013).

56. Pissaridou, P. *et al.* The Pseudomonas aeruginosa T6SS-VgrG1b spike is topped by a PAAR protein eliciting DNA damage to bacterial competitors. *Proceedings of the National Academy of Sciences of the United States of America* **115,** 12519–12524 (2018).

57. Yadav, S. K. *et al.* Immunity proteins of dual nuclease T6SS effectors function as transcriptional repressors. *EMBO reports* **22** (2021).

58. Ting, S. Y. *et al.* Bifunctional Immunity Proteins Protect Bacteria against FtsZ-Targeting ADP-Ribosylating Toxins. *Cell* **175** (2018).

59. Tang, J. Y., Bullen, N. P., Ahmad, S. & Whitney, J. C. Diverse NADase effector families mediate interbacterial antagonism via the type VI secretion system. *Journal of Biological Chemistry* **293** (2018).

60. Nolan, L. M. *et al.* Identification of Tse8 as a Type VI secretion system toxin from Pseudomonas aeruginosa that targets the bacterial transamidosome to inhibit protein synthesis in prey cells. *Nature Microbiology* **6** (2021).

61. Wang, T. *et al.* Pseudomonas aeruginosa T6SS-mediated molybdate transport contributes to bacterial competition during anaerobiosis. *Cell Reports* **35,** 108957 (2021).

62. Cornelis, P., Wei, Q., Andrews, S. C. & Vinckx, T. Iron homeostasis and management of oxidative stress response in bacteria. *Metallomics* **3** (2011).

63. Gaballa, A. & Helmann, J. D. A peroxide-induced zinc uptake system plays an important role in protection against oxidative stress in Bacillus subtilis. *Molecular Microbiology* **45** (2002).

64. Aguirre, J. D. & Culotta, V. C. Battles with iron: Manganese in oxidative stress protection. *Journal of Biological Chemistry* **287** (2012).

65. Argüello, J. M., Raimunda, D. & Padilla-Benavides, T. Mechanisms of copper homeostasis in bacteria. *Frontiers in Cellular and Infection Microbiology* **4** (2013).

66. Grunden, A. M. & Shanmugam, K. T. Molybdate transport and regulation in bacteria. *Archives of Microbiology* **168** (1997).

67. Iobbi-Nivol, C. & Leimkühler, S. Molybdenum enzymes, their maturation and molybdenum cofactor biosynthesis in Escherichia coli. *Biochimica et Biophysica Acta - Bioenergetics* **1827** (2013).

68. Pederick, V. G. *et al.* Acquisition and role of molybdate in Pseudomonas aeruginosa. *Applied and Environmental Microbiology* **80** (2014).

69. Self, W. T., Grunden, A. M., Hasona, A. & Shanmugam, K. T. Molybdate transport. *Research in Microbiology* **152** (Apr. 2001).

70. Ankenbauer, R. G. & Quan, H. N. FptA, the Fe(III)-pyochelin receptor of Pseudomonas aeruginosa: A phenolate siderophore receptor homologous to hydroxamate siderophore receptors. *Journal of Bacteriology* **176** (1994).

71. Sugawara, E., Nagano, K. & Nikaido, H. Alternative folding pathways of the major porin OprF of Pseudomonas aeruginosa. *FEBS Journal* **279** (2012).

72. Hood, M. I. & Skaar, E. P. Nutritional immunity: Transition metals at the pathogen-host interface. *Nature Reviews Microbiology* **10** (2012).

73. Finney, L. A. & O'Halloran, T. V. Transition metal speciation in the cell: Insights from the chemistry of metal ion receptors. *Science* **300** (2003).

74. Miethke, M. & Marahiel, M. A. Siderophore-Based Iron Acquisition and Pathogen Control. *Microbiology and Molecular Biology Reviews* **71** (2007).

75. Porcheron, G., Garénaux, A., Proulx, J., Sabri, M. & Dozois, C. M. Iron, copper, zinc, and manganese transport and regulation in pathogenic Enterobacteria: Correlations between strains, site of infection and the relative importance of the different metal transport systems for virulence. *Frontiers in Cellular and Infection Microbiology* **3** (2013).

76. Hohle, T. H., Franck, W. L., Stacey, G. & O'Brian, M. R. Bacterial outer membrane channel for divalent metal ion acquisition. *Proceedings of the National Academy of Sciences of the United States of America* **108,** 15390–15395 (2011).

77. Zappa, S. & Bauer, C. E. in *Advances in Botanical Research* 289–326 (2013).

78. Braun, V. & Hantke, K. Recent insights into iron import by bacteria. *Current Opinion in Chemical Biology* **15,** 328–334 (2011).

79. Kiley, P. J. & Kaplan, S. Molecular genetics of photosynthetic membrane biosynthesis in Rhodobacter sphaeroides. *Microbiological reviews* **52** (1988).

80. Mackenzie, C. *et al.* Postgenomic adventures with Rhodobacter sphaeroides. *Annual Review of Microbiology* **61** (2007).

81. Naylor, G. W., Addlesee, H. A., Gibson, L. C. D. & Hunter, C. N. The photosynthesis gene cluster of Rhodobacter sphaeroides. *Photosynthesis Research* **62** (1999).

82. Gregor, J. & Klug, G. Regulation of bacterial photosynthesis genes by oxygen and light. *FEMS Microbiology Letters* **179** (1999).

83. Yiğit, D. Ö., Gündüz, U., Türker, L., Yücel, M. & Eroğlu, n. Identification of by-products in hydrogen producing bacteria; Rhodobacter sphaeroides O.U. 001 grown in the waste water of a sugar refinery. *Progress in Industrial Microbiology* **35** (1999).

84. Orsi, E. *et al.* Characterization of heterotrophic growth and sesquiterpene production by Rhodobacter sphaeroides on a defined medium. *Journal of Industrial Microbiology and Biotechnology* **46** (2019).

85. Orsi, E., Beekwilder, J., Eggink, G., Kengen, S. W. & Weusthuis, R. A. The transition of Rhodobacter sphaeroides into a microbial cell factory. *Biotechnology and Bioengineering* **118** (2021).

86. Armitage, J., Havelka, W. & Sockett, R. Methylation-independent taxis in bacteria. *Biology of the Chemotactic Response* **46,** 177–198 (1990).

87. Armitage, J. P. Behavioral responses in bacteria. *Annual Review of Physiology* **54** (1992).

88. Armitage, J. P. & Schmitt, R. Bacterial chemotaxis: Rhodobacter sphaeroides and Sinorhizobium meliloti - Variations on a theme? *Microbiology* **143** (1997).

89. Armitage, J. P., Pitta, T. P., Vigeant, M. A., Packer, H. L. & Ford, R. M. Transformations in flagellar structure of Rhodobacter sphaeroides and possible relationship to changes in swimming speed. *Journal of Bacteriology* **181** (1999).

90. Sirijovski, N., Mamedov, F., Olsson, U., Styring, S. & Hansson, M. Rhodobacter capsulatus magnesium chelatase subunit BchH contains an oxygen sensitive iron-sulfur cluster. *Archives of Microbiology* **188** (2007).

91. Sestok, A. E., Linkous, R. O. & Smith, A. T. Toward a mechanistic understanding of Feo-mediated ferrous iron uptake. *Metallomics* **10** (2018).

92. Andrews, S. C., Robinson, A. K. & Rodríguez-Quiñones, F. Bacterial iron homeostasis. *FEMS Microbiology Reviews* **27** (2003).

93. Celia, H. *et al.* Cryo-EM structure of the bacterial Ton motor subcomplex ExbB–ExbD provides information on structure and stoichiometry. *Communications Biology* **2** (2019).

94. D'Onofrio, A. *et al.* Siderophores from Neighboring Organisms Promote the Growth of Uncultured Bacteria. *Chemistry and Biology* **17** (2010).

95. Rodionov, D. A., Gelfand, M. S., Todd, J. D., Curson, A. R. & Johnston, A. W. Computational reconstruction of iron- and manganese-responsive transcriptional networks in α-proteobacteria. *PLoS Computational Biology* **2** (2006).

96. Peuser, V., Remes, B. & Klug, G. Role of the Irr protein in the regulation of iron metabolism in Rhodobacter sphaeroides. *PLoS ONE* **7** (2012).

97. Sockett, R. E. & Armitage, J. P. Isolation, characterization, and complementation of a paralyzed flagellar mutant of Rhodobacter sphaeroides WS8. *Journal of Bacteriology* **173,** 2786–2790 (1991).

98. Penfold, R. J. & Pemberton, J. M. An improved suicide vector for construction of chromosomal insertion mutations in bacteria. *Gene* **118,** 145–146 (Sept. 1992).

99. Porter, S. L. *et al.* Genome sequence of Rhodobacter sphaeroides strain WS8N. *Journal of Bacteriology* **193,** 4027–4028 (2011).

100. Repizo, G. D., Espariz, M., Seravalle, J. L. & Salcedo, S. P. Bioinformatic Analysis of the Type VI Secretion System and Its Potential Toxins in the Acinetobacter Genus. *Frontiers in Microbiology* **10** (2019).

101. Li, J. *et al.* SecReT6: A web-based resource for type VI secretion systems found in bacteria. *Environmental Microbiology* **17** (2015).

102. Shalom, G., Shaw, J. G. & Thomas, M. S. In vivo expression technology identifies a type VI secretion system locus in Burkholderia pseudomallei that is induced upon invasion of macrophages. *Microbiology* **153** (2007).

103. Barret, M., Egan, F. & O'Gara, F. Distribution and diversity of bacterial secretion systems across metagenomic datasets. *Environmental Microbiology Reports* **5** (2013).

104. Altschul, S. F., Gish, W., Miller, W., Myers, E. W. & Lipman, D. J. Basic local alignment search tool. *Journal of Molecular Biology* **215** (1990).

105. Ma, A. T. & Mekalanos, J. J. In vivo actin cross-linking induced by Vibrio cholerae type VI secretion system is associated with intestinal inflammation. *Proceedings of the National Academy of Sciences of the United States of America* **107** (2010).

106. Brooks, T. M., Unterweger, D., Bachmann, V., Kostiuk, B. & Pukatzki, S. Lytic activity of the Vibrio cholerae type VI secretion toxin VgrG-3 is inhibited by the antitoxin TsaB. *Journal of Biological Chemistry* **288** (2013).

107. Wood, T. E. *et al.* The Pseudomonas aeruginosa T6SS Delivers a Periplasmic Toxin that Disrupts Bacterial Cell Morphology. *Cell Reports* **29** (2019).

108. Suarez, G. *et al.* A type VI secretion system effector protein, VgrG1, from Aeromonas hydrophila that induces host cell toxicity by ADP ribosylation of actin. *Journal of Bacteriology* **192** (2010).

109. Corpet, F. Multiple sequence alignment with hierarchical clustering. *Nucleic Acids Research* **16** (1988).

110. Liu, W. *et al.* IBS: An illustrator for the presentation and visualization of biological sequences. *Bioinformatics* **31** (2015).

111. Ma, L. S., Narberhaus, F. & Lai, E. M. IcmF family protein TssM exhibits ATPase activity and energizes type VI secretion. *Journal of Biological Chemistry* (2012).

112. Toesca, I. J., French, C. T. & Miller, J. F. The type VI secretion system spike protein VgrG5 mediates membrane fusion during intercellular spread by pseudomallei group Burkholderia species. *Infection and Immunity* **82** (2014).

113. Wettstadt, S. & Filloux, A. Manipulating the type VI secretion system spike to shuttle passenger proteins. *PLoS ONE* **15,** 1–20 (2020).

114. Marchler-Bauer, A. & Bryant, S. H. CD-Search: Protein domain annotations on the fly. *Nucleic Acids Research* **32** (2004).

115. Kelley, L. A., Mezulis, S., Yates, C. M., Wass, M. N. & Sternberg, M. J. The Phyre2 web portal for protein modeling, prediction and analysis. *Nature Protocols* **10** (2015).

116. Lu, S. *et al.* CDD/SPARCLE: The conserved domain database in 2020. *Nucleic Acids Research* **48** (2020).

117. Madeira, F. *et al.* The EMBL-EBI search and sequence analysis tools APIs in 2019. *Nucleic Acids Research* **47** (2019).

118. Shneider, M. M. *et al.* PAAR-repeat proteins sharpen and diversify the type VI secretion system spike. *Nature* **500,** 350–353 (Aug. 2013).

119. Liu, Y., Zhang, Z., Wang, F., Li, D. d. & Li, Y. z. Identification of type VI secretion system toxic effectors using adaptors as markers. *Computational and Structural Biotechnology Journal* **18** (2020).

120. Ringel, P. D., Hu, D. & Basler, M. The Role of Type VI Secretion System Effectors in Target Cell Lysis and Subsequent Horizontal Gene Transfer. *Cell Reports* **21** (2017).

121. Sibinelli-Sousa, S. *et al.* A Family of T6SS Antibacterial Effectors Related to L,D-Transpeptidases Targets the Peptidoglycan. *Cell Reports* **31** (2020).

122. Price, M. N. *et al.* Mutant phenotypes for thousands of bacterial genes of unknown function. *Nature* **557,** 503–509 (2018).

123. Nichols, R. J. *et al.* Phenotypic landscape of a bacterial cell. *Cell* **144,** 143–156 (2011).

124. Deutschbauer, A. *et al.* Evidence-based annotation of gene function in Shewanella oneidensis MR-1 using genome-wide fitness profiling across 121 conditions. *PLoS Genetics* **7** (2011).

125. Armitage, J. P. & Macnab, R. M. Unidirectional, intermittent rotation of the flagellum of Rhodobacter sphaeroides. *Journal of Bacteriology* **169,** 514–518 (1987).

126. De la Mora, J. *et al.* Structural characterization of the Fla2 flagellum of Rhodobacter sphaeroides. *Journal of Bacteriology* **197,** 2859–2866 (2015).

127. Mackenzie, C. *et al.* The home stretch, a first analysis of the nearly completed genome of Rhodobacter sphaeroides 2.4.1. *Photosynthesis Research* **70,** 19–41 (2001).

128. Poggio, S. *et al.* A complete set of flagellar genes acquired by horizontal transfer coexists with the endogenous flagellar system in Rhodobacter sphaeroides. *Journal of Bacteriology* **189,** 3208–3216 (2007).

129. Förster, A. *et al.* Coevolution of the ATPase ClpV, the sheath proteins TssB and TssC, and the accessory protein TagJ/HsiE1 distinguishes type VI secretion classes. *Journal of Biological Chemistry* **289,** 33032–33043 (2014).

130. Zeilstra-Ryalls, J. H. & Kaplan, S. Aerobic and anaerobic regulation in Rhodobacter sphaeroides 2.4.1: The role of the fnrL gene. *Journal of Bacteriology* **177** (1995).

131. Jones, C. W. *Dynamics, formation and segregation of the cytoplasmic chemoreceptor cluster in Rhodobacter sphaeroides* eng. PhD thesis (2013).

132. Arai, H., Jung, H. R. & Kaplan, S. Transcriptome dynamics during the transition from anaerobic photosynthesis to aerobic respiration in Rhodobacter sphaeroides 2.4.1. *Journal of Bacteriology* **190** (2008).

133. Nie, X., Jäger, A., Börner, J. & Klug, G. Interplay between formation of photosynthetic complexes and expression of genes for iron–sulfur cluster assembly in Rhodobacter sphaeroides? *Photosynthesis Research* **147** (2021).

134. Santin, Y. G., Doan, T., Journet, L. & Cascales, E. Cell Width Dictates Type VI Secretion Tail Length. *Current Biology* **29** (2019).

135. Drepper, T. *et al.* Reporter proteins for in vivo fluorescence without oxygen. *Nature Biotechnology* **25** (2007).

136. Lesic, B., Starkey, M., He, J., Hazan, R. & Rahme, L. G. Quorum sensing differentially regulates Pseudomonas aeruginosa type VI secretion locus I and homologous loci II and III, which are required for pathogenesis. *Microbiology* **155,** 2845–2855 (2009).

137. Sana, T. G., Berni, B. & Bleves, S. The T6SSs of Pseudomonas aeruginosa strain pao1 and their effectors: Beyond bacterial-cell targeting. *Frontiers in Cellular and Infection Microbiology* **6** (2016).

138. Russell, A. B., Peterson, S. B. & Mougous, J. D. Type VI secretion system effectors: Poisons with a purpose. *Nature Reviews Microbiology* **12** (2014).

139. Chen, L., Zou, Y., She, P. & Wu, Y. Composition, function, and regulation of T6SS in Pseudomonas aeruginosa. *Microbiological Research* **172,** 19–25 (2015).